

The Messenger



No. 126 – December 2006



Mapping the Properties of SDSS Galaxies with the VIMOS IFU

Joris Gerssen¹
Lise Christensen²
David Wilman³
Richard Bower⁴

¹ Astrophysikalisches Institut Potsdam, Germany

² ESO

³ Max-Planck-Institut für Extraterrestrische Physik, Garching, Germany

⁴ Durham University, United Kingdom

We present initial results from our VIMOS IFU study of galaxies selected from the Sloan Digital Sky Survey. Large fibre-based surveys like SDSS have made a major contribution to our understanding of processes that shape galaxies. The SDSS results, however, are derived from integrated properties over the area of the fibre. As the angular extent of galaxies is usually considerably larger than the fibre diameter, the SDSS results are biased toward the nuclear properties of galaxies. By contrast, data obtained with an Integral Field Unit (IFU) are free of aperture bias.

In the increasingly well-defined cosmological framework, the broad outline of galaxy formation is thought to be well understood. Briefly, galaxies form in the gravitational wells of dark matter halos from gas that got trapped there after losing kinetic energy through cooling or dissipative shocks. However, galaxy-formation models generally overpredict the fraction of gas that is locked up by a factor of about five compared to observations. To overcome this problem a feedback mechanism is needed to remove gas from galaxies. The detailed physical processes that govern this are not well known and are at present hard to constrain observationally (Wilman et al. 2005, Bower et al. 2006).

The vast database accumulated by the SDSS survey (York et al. 2000) is ideally suited to constrain many of the fundamental physical processes that drive galaxy evolution. For example, Tremonti et al. (2004) find evidence for stellar-wind feedback in the SDSS data from the observed mass – metallicity relations. Unfor-

tunately, mass cannot be measured directly from the SDSS data and the derived metallicities could be affected by aperture bias.

Another essential ingredient of galaxy evolution, intimately connected to feedback, is the star-formation history. Quantifying the star-formation rate from the past to the present is therefore an active area of research. The largest study to date (Brinchmann et al. 2004) uses $\sim 10^5$ galaxies in the SDSS database. They conclude that the present-day star-formation rate is now at about a third of the average value over the lifetime of the Universe. As the SDSS apertures typically sample less than half of a galaxy's size, they need to correct their results for this missing information using resolved images and procedures based on nuclear correlations between SFR and colour.

Aperture bias

Large surveys such as the SDSS provide the statistically most complete samples of fundamental galaxy properties. However, the SDSS properties represent integrated quantities derived over the central three arcsec only. Consequently, the results suffer from highly significant aperture effects (Brinchmann et al. 2004, Wilman et al. 2005, Kewley et al. 2005) that bias the results toward the bulge and nuclear emission properties. Galaxies, however, can exhibit strong colour gradients. Correcting emission line strengths for aperture effects when gradients are present is uncertain at best, and compounded by unknown contributions from variations in metallicity and age. With IFU observations the bright emission lines are spatially resolved and can be traced over the whole galaxy. These data are therefore free of aperture effects.

This project

To quantify internal variations in the emission line properties of SDSS galaxies we have begun a project to map a number of them with the VIMOS IFU. In order to build up a sample of galaxies in a modest amount of observing time we selected galaxies from the SDSS database with moderately strong H α emission (min-

imum equivalent widths of 2 nm). This could potentially bias us toward selecting objects with strong nuclear emission such as AGN. However, it ensures that each galaxy requires only 60 minutes of observing time to build a detailed map of spatially resolved star formation and metal abundance. We use the MR mode of VIMOS as its wavelength coverage (~ 450 to 900 nm) and spectral resolution closely match the SDSS fibre observations.

The sample was constructed to uniformly cover the redshift range up to 0.1. Above these redshifts aperture effects become less important. We visually inspected the SDSS images of candidates to assess their morphology and inclination and selected a total of 24 galaxies to guarantee that after binning the data in a variety of ways (in redshift, size, or luminosity) we still obtain statistically significant results for each bin.

The selected galaxies are all at intermediate inclination. While not the main goal of our project, this allows us to constrain the velocity fields and, hence, the enclosed mass profiles of the galaxies in our sample. The mass distribution as a function of radius is a key prediction of hierarchical galaxy formation scenarios. Observational constraints on velocity fields are scarce even in the local Universe. The SDSS database itself contains no kinematical information other than the recessional velocity of a system. The total masses of SDSS galaxies are normally estimated indirectly, usually from their total magnitude.

In Period 76 we obtained data for 12 of the galaxies in our sample. A further 12 systems are scheduled for observation in Period 78. The VIMOS IFU provides data sets of the form (RA, DEC, λ). Four examples of our data are shown in Figure 1. For each galaxy we show an image slice (i.e. a cut in λ through a data set) in the light of H α and a composite broadband image.

Preliminary results

The emission line properties are derived by fitting Gaussian profiles simultaneously to the Balmer lines (H α , H β) and strong

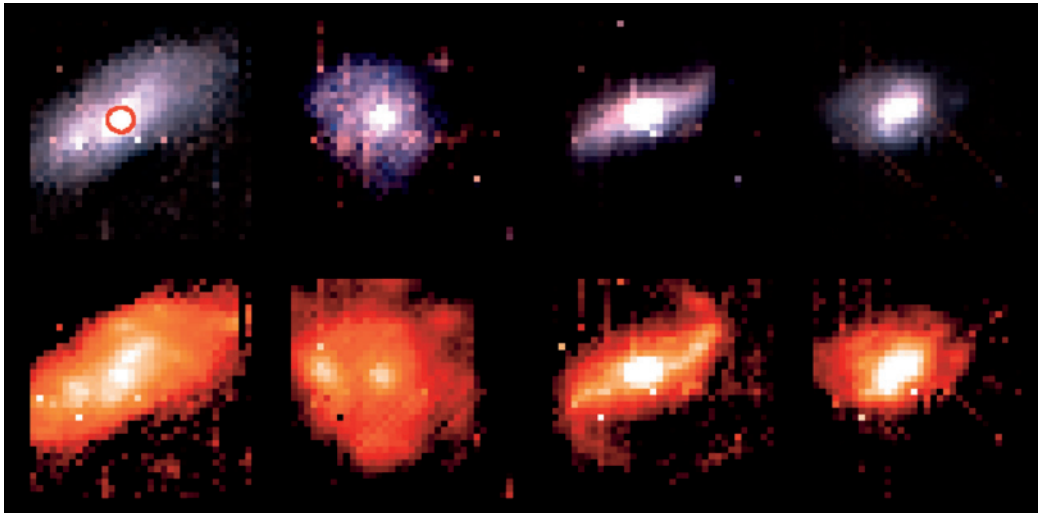


Figure 1: Examples from our sample of SDSS galaxies observed with the VIMOS IFU. Shown from left to right in ascending redshift order are sdss6, sdss13, sdss22 and sdss9 (the names simply reflect the RA ordering in our selected sample) at redshifts of 0.028, 0.034, 0.074 and 0.106 respectively. In the top panels composite colour images derived from the VIMOS IFU data extracted over the SDSS *r* and *i* bands are shown. The corresponding H α images are shown in the bottom panels. Panels measure 27 by 27 arcsec and each pixel is 0.67 arcsec. For comparison the SDSS fibre size is indicated by the red circle in the top left panel.

forbidden transition lines ([O III], [N II]) after removing the continuum using a sliding median. In our full analysis we will follow Tremonti et al. (2004) and fit the continuum with an optimal stellar template model. Subtracting this model will correctly take any underlying absorption into account that may otherwise significantly affect our results (in this article we assume an average correction for absorption of $EW = 0.2$ nm). This model also provides a handle on the stellar kinematics.

To quantify aperture effects we examine the cumulative line flux and line strength of the H α lines in the four galaxies used in this article (Figure 2) as a function of aperture size. Not surprisingly, the cumulative flux grows systematically beyond the radius of the SDSS aperture. When extrapolating to larger radii it is frequently assumed that the line flux and continuum properties follow the same trend. But as the bottom panel illustrates the line-flux to continuum-flux ratio (that is, equivalent width or line strength) is not always constant. Extrapolating quantities derived from the SDSS database to larger radii is therefore fraught with difficulties.

Systems harbouring an AGN such as sdss22 display the strongest variation in cumulative line strength. A useful way to classify the activity level of a galaxy is by determining its location in a diagnostic BPT diagram (Baldwin, Phillips and Terlevich 1981). In Figure 3 we reproduce the BPT diagram derived by Brinchmann et al. (2004) using $\sim 10^5$ SDSS galaxies. This diagram of emission line ratios has a

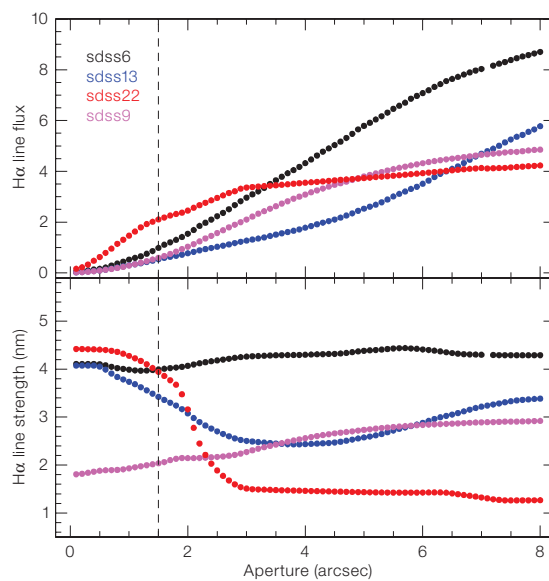


Figure 2: Cumulative quantities derived using a software aperture with increasing radius and centred on the nucleus of each galaxy. The cumulative H α line flux (arbitrarily normalised) shown in the top panel grows monotonically as the galaxies in our sample are larger than the radius of the SDSS fibre (dashed line). The continuum flux does not necessarily follow the same trend. This is illustrated in the bottom panels where the cumulative line strength of the H α emission line is shown. This can lead to strong aperture bias when extrapolating the SDSS results to larger radii.

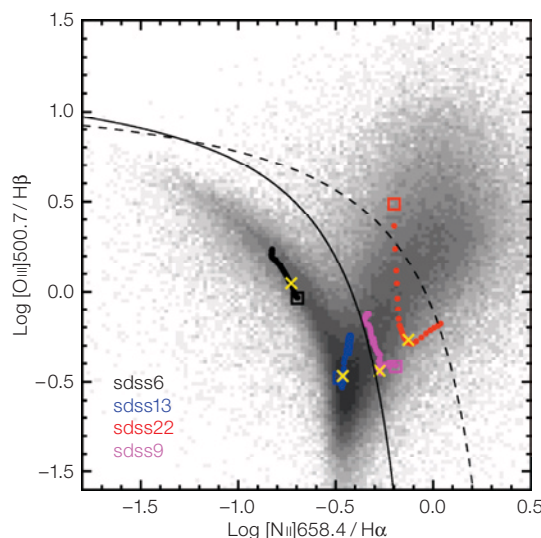


Figure 3: To quantify the effect of varying aperture size on the derived metallicities we plot the VIMOS IFU results as 'tracks' in a BPT diagram. The starting point (i.e. smallest radius) of each track is highlighted by the open squares. The crosses mark where the radius is equal to the SDSS fibre radius. The underlying gray-scale image shows the 'raw' emission line measurements by Brinchmann et al. (2004, see also <http://www.mpa-garching.mpg.de/SDSS/#dataprod>) of some 500 000 SDSS galaxies. The lines divide the sample into star forming (left), hybrid (centre) and AGN (right).

characteristic ‘double-wing’ shape. Normal galaxies are found on the left branch while active systems occupy the top right part. Overplotted on this diagram are the results of our cumulative emission line analysis. Varying the size of the aperture can have an impact on the location of a galaxy within this diagram. But, as the four examples used here show, it would not necessarily change the classification of a system.

Apart from the large variation in the single AGN system, all systems show at least 0.2 dex change in their line ratios as a function of radius. This translates roughly into 0.1 dex in metallicity, a value that is not inconsistent with the 0.13 dex average difference of Kewley et al. (2005) for large galaxies and which they claim is substantial. At this preliminary stage it should be kept in mind that different methods to estimate metallicities from strong emission lines can yield values that differ considerably.

Our project aims to quantify the internal variations of emission line properties in a self-consistent manner. A by-product of these observations are emission line velocity fields. The data analysis yields mean line positions for every spatial location in our data sets. An example is shown in Figure 4 where the velocities are derived from the mean positions of the H α and [NII] lines.

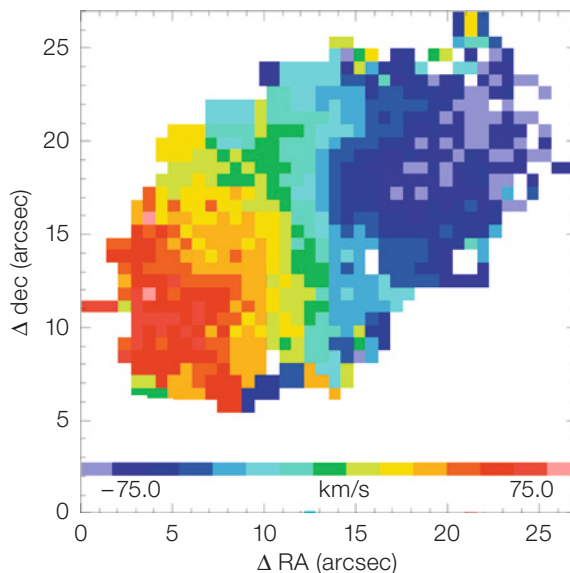


Figure 4: Together with metallicity, mass is another key observable used to quantify galaxy evolution. However, it can only be estimated indirectly from the SDSS database using magnitude as a proxy. Our VIMOS IFU data analysis yields emission line velocity maps with which the circular velocity, and hence the enclosed mass, can be constrained accurately. In the preliminary example shown here the velocity field is derived from a three-component Gaussian fit to the H α + [NII] lines.

Flores et al. (2006) recently demonstrated the power of IFU observations to constrain internal kinematics at intermediate redshifts. They used the Flames IFU buttons to reach the striking conclusion that only one in three galaxies is dynamically unperturbed at redshifts of ~ 0.5 and thus presumably undergoing rapid evolution. It will be very interesting to compare this to the kinematical properties derived from our lower redshift galaxies.

Aperture effects are important. To investigate the accuracy of the various correction methods we are observing a small sample of SDSS galaxies. To fully probe

the data-space covered by SDSS requires a much larger sample. As our results show, such a sample can be obtained efficiently with the VIMOS IFU even in relatively poor atmospheric conditions.

References

Baldwin J. A., Phillips M. M. and Terlevich R. 1981, PASP 93, 5
 Bower R. et al. 2006, MNRAS 370, 645
 Brinchmann J. et al. 2004, MNRAS 351, 1151
 Flores H. et al. 2006, A&A 455, 107
 Kewley L. J. et al. 2005, PASP 117, 227
 Tremonti C. A. et al. 2004, ApJ 613, 898
 Wilman D. et al. 2005, MNRAS 358, 88
 Wilman R. et al. 2005, Nature 436, 227
 York D. G. et al. 2000, AJ 120, 1579



The barred spiral galaxy NGC 613 was imaged with the FORS1 and FORS2 multi-mode instruments (at VLT MELIPAL and YEPUN, respectively) in December 2001. The images were taken by Mark Neeser (Universitäts-Sternwarte München, Germany) and Peter Barthel (Kapteyn Astronomical Institute, the Netherlands) during twilight. The galaxy was observed in three different wavebands for up to 300 seconds per waveband, and the image obtained in each waveband was associated to a colour: B (blue), V (green) and R (red). The full-resolution version of this photo retains the original pixels. Note the many arms and the pronounced dust bands. North is up and East is left. Neeser and Barthel also performed the first stage of the image processing; further processing and colour-encoding was made by Hans Hermann Heyer and Henri Boffin (ESO).

(From ESO Press Photo 33a/03)

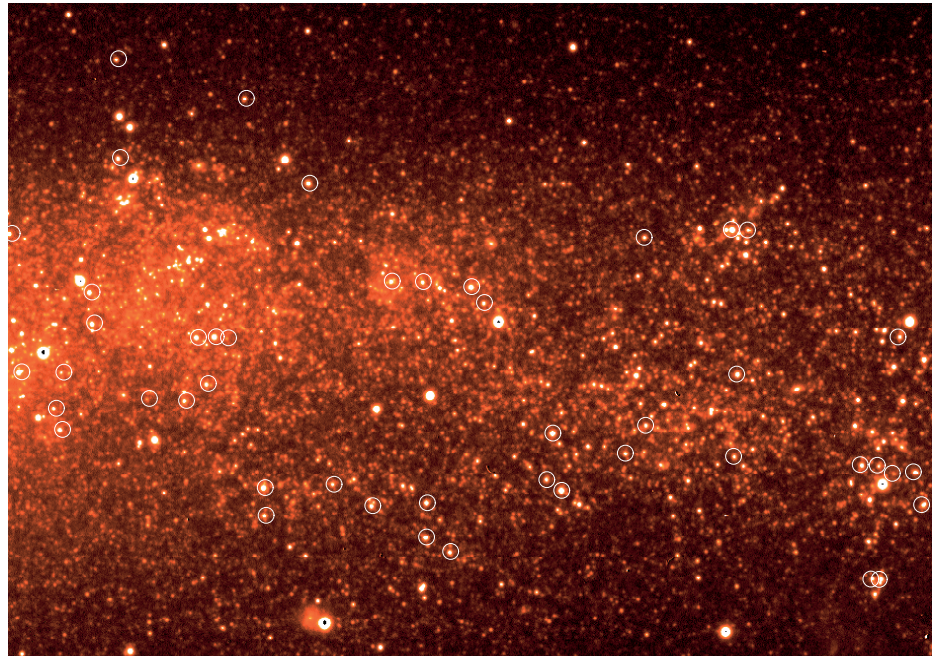
The ARAUCARIA Project – First Observations of Blue Supergiants in NGC 3109

Chris Evans¹
 Fabio Bresolin²
 Miguel Urbaneja²
 Grzegorz Pietrzyński^{3,4}
 Wolfgang Gieren³
 Rolf-Peter Kudritzki²

¹ United Kingdom Astronomy Technology Centre, Edinburgh, United Kingdom
² Institute for Astronomy, University of Hawaii, USA
³ Universidad de Concepción, Chile
⁴ Warsaw University Observatory, Poland

NGC 3109 is an irregular galaxy at the edge of the Local Group at a distance of 1.3 Mpc. Here we present new VLT observations of its young, massive star population, which have allowed us to probe stellar abundances and kinematics for the first time. The mean oxygen abundance obtained from early B-type supergiants confirms suggestions that NGC 3109 is very metal poor. In this context we advocate studies of the stellar population of NGC 3109 as a compelling target for future Extremely Large Telescopes (ELTs).

The ARAUCARIA Project is an ESO Large Programme using FORS2 on the VLT. Its principal motivation is to provide improved distances to galaxies in the Local and Sculptor Groups, via the period-luminosity relationship of Cepheid variables (Gieren et al. 2005). A secondary component of the project is to characterise tens of blue supergiants (typically B- and A-type stars) in each of the target galaxies. Blue supergiants are the most visually luminous ‘normal’ stars, thereby enabling direct studies of stellar populations in galaxies that are otherwise unreachable with 8-m telescopes. From comparisons with theoretical spectra, we can investigate physical parameters such as temperatures and chemical abundances of our targets, obtaining estimates of the metallicity of the host systems. Moreover, blue supergiants have also been advanced as an alternative method of distance determination via the flux-weighted gravity luminosity relationship (Kudritzki et al. 2003).



NGC 3109 is a large Magellanic Irregular at 1.3 Mpc, which puts it at the outer edge of the Local Group. Using FORS2 in the configurable MOS (multi-object spectroscopy) mode, we have observed 91 stars in NGC 3109. These were observed in 4 MOS configurations, using the 600 B grism (giving a common wavelength coverage of λ 3900 to λ 4750 Å). The cumulative exposure time for each field was roughly 3 hours. Part of our most western field is shown in the FORS pre-image in Figure 1, with our targets encircled. From published photometry it has been suggested that red giants in NGC 3109 have metal abundances that are similar to those found in stars in the Small Magellanic Cloud (SMC), i.e. very metal poor when compared to the solar neighbourhood. With this in mind, we classified the FORS spectra using criteria that have already tackled the issue of low metallicity (e.g. Evans et al. 2004). Our sample is primarily composed of late-O, B and A spectral types – this is the first spectral exploration of this galaxy. As an aside, we note that the first large-scale CCD survey of NGC 3109 was reported in this publication by Bresolin et al. (1990) – the acquisition of high-quality spectroscopy in this galaxy some 16 years later illustrates the considerable advancement in studies of extragalactic stellar populations over that period.

Figure 1: Part of the V-band FORS pre-image of our most western field, with the targets encircled. NGC 3109 is approximately edge-on and the FORS targets are well sampled along both the major and minor axes.

Example spectra are shown in Figure 2. Of our 91 targets, 12 are late O-type stars, ranging from O8 to O9.5 – such high-quality observations of resolved O-type stars (note the He II emission ‘bump’ at λ 4686 Å in the spectrum of star #33) beyond 1 Mpc are really quite remarkable.

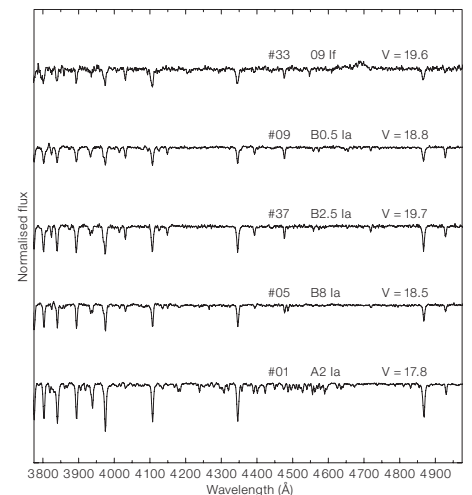


Figure 2: FORS spectra of five of our targets in NGC 3109. The quality of the data is particularly impressive when one remembers that the stars are at distances of over 1 Mpc.

However, in terms of quantitative analysis, the early B-type supergiants in our sample are of more immediate interest – these stars have a wide variety of strong metallic lines in their absorption spectra, providing an excellent tool for investigating chemical abundances of young stellar populations.

We have analysed a subset of eight of our early B-type spectra using the FASTWIND model atmosphere code (Puls et al. 2005). From comparisons with theoretical spectra we can obtain physical parameters such as temperatures, gravities, and, of most interest in a broader context, chemical abundances. An example FASTWIND model matched to one of the observed spectra is shown in Figure 3. The mean oxygen abundance in our eight stars is found to be $\log(\text{O}/\text{H}) + 12 = 7.76 \pm 0.07$, in excellent agreement with results from HII regions. This is only $\sim 12\%$ of the oxygen abundance found in the solar neighbourhood, and is lower than the oxygen abundances found in the SMC (cf. $\log(\text{O}/\text{H}) + 12 = 8.13$, Trundle and Lennon, 2005). We also obtain upper limits to the magnesium and silicon abundances, which are comparable to those found for stars in the SMC – the exact abundance of the alpha-elements will require higher-resolution spectroscopy, but it is clear that stars in NGC 3109 have metal abundances that are very deficient when compared to the solar neighbourhood, and likely even lower than in the SMC.

We have also used our FORS spectra to investigate the stellar rotation curve of NGC 3109. H α observations suggest a dominant dark-matter halo (Jobin and Carignan 1990), that cosmological N-body cold dark matter simulations have struggled to reproduce (Navarro et al. 1996). The spectral resolution from FORS ($R \sim 1,000$) is somewhat limiting for studies of stellar kinematics, but from simple measurements of line-centres of hydrogen and helium lines, we estimated radial velocities for the majority (84) of our stars. The mean 1-sigma (internal) uncertainty is of order 20 km/s. Figure 4 shows differential radial velocities for each of our stars, compared with published results from H α radio maps and H α imaging (Jobin and Carignan 1990, Blais-Ouellette et al. 2001). As one might expect, the

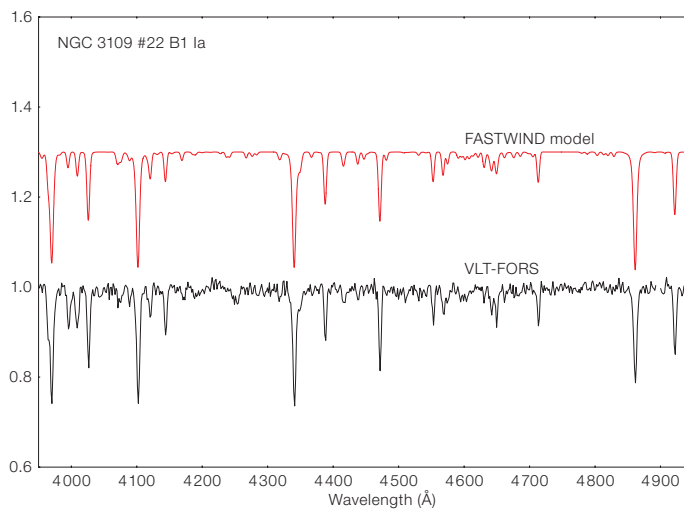


Figure 3: FORS spectrum (black line) of star #22, classified as B1 Ia. A FASTWIND model spectrum ($T_{\text{eff}} = 22,000$ K, $\log g = 2.60$) is shown above in red, smoothed to the same resolution as the FORS data.

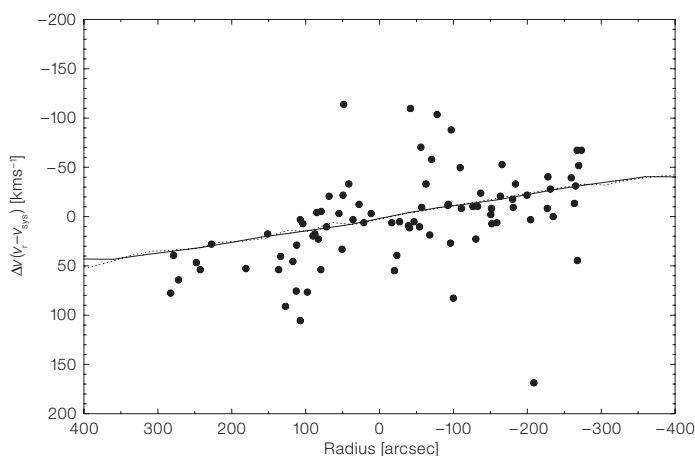


Figure 4: Differential radial velocities as a function of radius along the major axis of NGC 3109 – typical uncertainties are of order ± 20 km/s. Also shown are rotation curves from H α (solid line) and H α (dotted line).

velocities of the young population largely trace those of the gas, with a fair amount of scatter. Further observations of this sort would be of value to ascertain whether the stellar results are revealing genuine sub-structures in the disc, or whether we are simply limited by the small sample/spectral resolution.

Plans for the next generation of large ground-based telescopes, the so-called Extremely Large Telescopes (ELTs), are now gaining momentum. In this context we suggest NGC 3109 as an exciting opportunity to study many stages of stellar evolution in a very metal poor environment. A large primary aperture would enable high-resolution spectroscopy of the young, massive population, and of stars on the asymptotic giant branch.

Meanwhile, lower-resolution spectroscopy could trace the kinematics of the non-supergiant population (e.g. via the Calcium Triplet), probing the outer structure of this dark-matter dominated dwarf and providing crucial input for cosmological simulations.

References

- Blais-Ouellette S., Amram P. and Carignan C. 2001, AJ 121, 1952
- Bresolin F., Capaccioli M. and Pliotto G. 1990, The Messenger 60, 36
- Evans C. J. et al. 2004, MNRAS 353, 601
- Gieren W. et al. 2005, The Messenger 121, 23
- Jobin M. and Carignan C. 1990, AJ 100, 648
- Kudritzki R.-P., Bresolin F. and Przybilla N. 2003, ApJ 582, 83L
- Navarro J. F. et al. 1996, ApJ 462, 563
- Puls J. et al. 2005, A&A 435, 669
- Trundle C. and Lennon D. J. 2005, A&A 434, 677

Early Science Results from the UKIDSS ESO Public Survey

Steve Warren¹
 Andy Lawrence²
 Omar Almaini³
 Michele Cirasuolo²
 Sebastien Foucaud³
 Nigel Hambly²
 Paul Hewett⁴
 Richard Jameson⁵
 Sandy Leggett⁶
 Nicolas Lodieu⁷
 Phil Lucas⁸
 Ross McLure²
 Richard McMahan⁴
 Daniel Mortlock¹
 David Pinfield⁸
 Bram Venemans⁴

¹ Imperial College, London, United Kingdom

² University of Edinburgh, United Kingdom

³ University of Nottingham, United Kingdom

⁴ Institute of Astronomy, Cambridge, United Kingdom

⁵ University of Leicester, United Kingdom

⁶ Gemini North, Hawaii, USA

⁷ Instituto de Astrofísica de Canarias, Tenerife, Spain

⁸ University of Hertfordshire, Hatfield, United Kingdom

The first large release of data from the UKIDSS ESO public survey took place in July 2006. The size of the data set is about 7% of the size of the final survey data set. Early science results are presented here, ranging from the nearest coolest brown dwarfs, to the most luminous, rarest, galaxies at $5 < z < 6$. Progress on the headline science goals of UKIDSS, such as the determination of the faint end of the stellar IMF, and the discovery of quasars beyond $z = 6$, is in line with expectation at this stage of the surveys.

The UKIDSS First Data Release (DR1) took place on 21 July 2006 (as announced on the ESO web pages), following on from the small Early Data Release (EDR), in February (The Messenger 123, 67). DR1 is a much larger data set than the EDR, and marks completion of 7% of the survey programme. The programme and the goals of UKIDSS are set out in

Lawrence et al. (2006). This first release is an important milestone on the route to completion of UKIDSS, as it marks the point where the survey surpassed 2MASS as the largest near-infrared survey, quantified by the product $P = A\Omega t$. Here A is the telescope collecting area, Ω is the solid angle of the camera field, and t is the summed integration time. The symbol P stands for photons, since, for the same field, and other things being equal (such as camera throughput), the quantity P is proportional to the number of source photons collected.

UKIDSS is an ESO public survey (see The Messenger 108, 31), with equal data access rights to all astronomers at institutions in ESO member states. The data are available from the WFCAM Science Archive at <http://surveys.roe.ac.uk/wsa/index.html>. The procedure for archive registration is described in a previous article (see The Messenger 119, 56), as well as on the UKIDSS web site (at <http://www.ukidss.org>). The UKIDSS programme comprises five surveys covering complementary combinations of area, depth, Galactic latitude, and filter coverage, from the full ZYJHK set of the camera.

Table 1 summarises the contents of DR1 for each of the five surveys, in terms of area and depth over regions with coverage by the full filter set for that survey. DR1 contains substantial additional data in fields where the filter coverage is so far incomplete. The contents of DR1, including maps of the areas surveyed, are detailed in a submitted paper (Warren et al. 2006). The median seeing across the data set is 0.82 arcsec.

Although DR1 only appeared at the end of July, some interesting science is already emerging. In this article we publicise some of the early results of which we are aware. The authors of this article are members of the UKIDSS Consortium, which designed and is implementing the surveys. This explains the UK bias, but we emphasise that we have no

Survey	Area deg ²	Filters	K 5 σ depth (Vega)
Large Area Survey	190	YJHK	18.2
Galactic Clusters Survey	52	ZYJHK	18.2
Galactic Plane Survey	77	JHK (+ H ₂)	18.1
Deep ExtraGalactic Survey	3.1	JK	20.7
Ultra Deep Survey	0.8	JK	21.6

priority access to the data. The science described here is some of the work with which we have been involved. We look forward to hearing about work being undertaken by other ESO astronomers who have not been involved in the implementation of the surveys.

High-redshift galaxies in the Ultra Deep Survey

The deepest, and narrowest, element of UKIDSS is the Ultra Deep Survey (UDS). The final goal of the UDS is to cover 0.8 deg² to 5 σ depths of $K = 23.0$, $H = 23.8$, $J = 24.6$. The aim of the UDS is to produce a deep, large-scale map of a representative volume of the distant Universe, $1 < z < 6$, providing large samples with which to directly test models for galaxy formation and evolution. The depths reached in DR1 are $K \approx 21.6$ and $J \approx 22.7$, over the full field, based on 86 hours of observations (the results reported here in fact use the shallower EDR data set). The area also benefits from public deep optical data obtained with the Subaru instrument SuprimeCam.

Although the UDS campaign is in its infancy, the DR1 data set is already the largest existing near-infrared survey to these depths. This enables surveys for rare objects. For example, McLure et al. (2006) have reported the discovery of nine of the most luminous candidate Lyman-break galaxies at redshifts $5 < z < 6$. These appear to be relatively massive stellar systems ($M_{stars} > 5 \times 10^{10} M_{\odot}$) already in place < 1.2 Gyr after the Big Bang. Because they are so rare, these luminous objects are particularly useful for testing theories of galaxy formation. Another galaxy population of current interest are the Distant Red Galaxies (DRGs), objects selected with $(J - K)_{AB} > 1.3$, which are believed to be the most massive galaxies at $z \sim 2$. Foucaud et al. (2006) used the UDS EDR to produce a sample of 239 bright DRGs. This sample is an order of

Table 1: Depth and coverage in fields with the filter complement in UKIDSS DR1.

magnitude larger than existing samples of bright DRGs, allowing a first look at their clustering properties. The computed 2-point angular correlation function is reproduced in Figure 1. Full circles represent DRGs, while open circles mark the correlation function for the parent sample of K -selected field galaxies, from which the DRG sample is drawn. The inferred correlation length of $r_0 \sim 12 \text{ h}^{-1} \text{ Mpc}$, confirms that DRGs are hosted by massive dark matter halos.

At somewhat lower redshifts, Cirasuolo et al. (2006) have used the UDS EDR to chart the evolution of the K -band luminosity function (LF) over the redshift range $0.25 < z < 2.25$; the first time this has been achieved to such high statistical accuracy. Galaxy colours were also used to separate systems with blue/red rest-frame optical colours. The results are illustrated in Figure 2. It was found that red galaxies dominate the bright end of the LF at $z < 1$, with bright blue galaxies dominating at $z > 1$.

Rare objects in the Large Area Survey I: High-redshift quasars

One of the main factors that influenced the design of the LAS was the opportunity to search for rare objects, extending the work of 2MASS in finding very cool brown dwarfs, and of SDSS in finding quasars of very high redshifts, as well as cool brown dwarfs. These goals are described in Lawrence et al. (2006), and Hewett et al. (2006). UKIDSS DR1 provides the first opportunity for teams to exploit a data set sufficiently large to be of interest.

SDSS has been highly successful in discovering quasars beyond $z = 6$. The most distant quasar at $z = 6.4$, found by SDSS, lies near the observable limit of the survey. Due to absorption by intervening neutral hydrogen, at higher redshifts a quasar would be extremely faint in z , the longest-wavelength SDSS band. Yet analysis of the very strong absorption in the $\text{Ly}\alpha$ forest of the highest redshift quasars has yielded tantalising evidence that at $z = 6$ we have reached the tail-end of the epoch when the Universe was reionised. Therefore there is strong motivation for extending the redshift limit of quasar surveys.

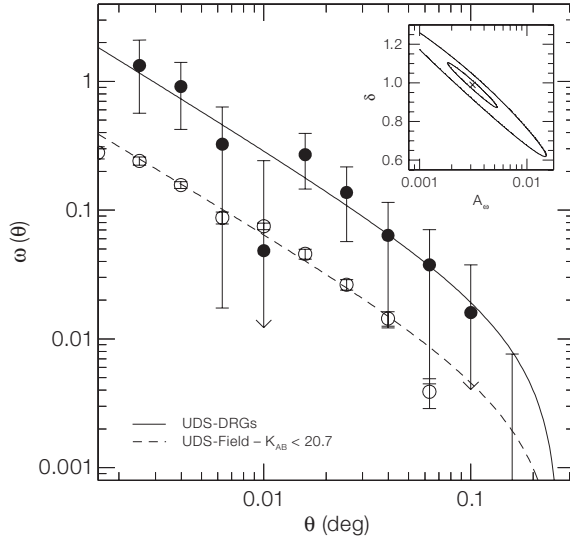


Figure 1: The 2-point angular correlation function determined for a sample of bright Distant Red Galaxies (DRGs), measured by Foucaud et al. (2006) from the UDS EDR.

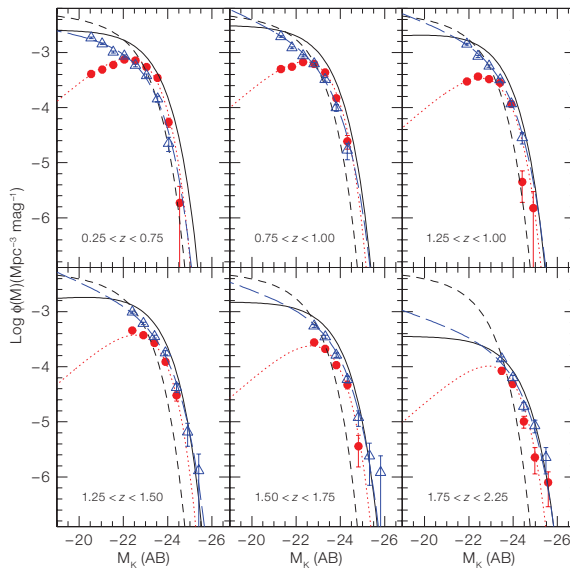


Figure 2: Rest-frame K -band luminosity function from Cirasuolo et al. (2006), based on the UDS EDR. The red and blue symbols and lines plot the LF for galaxies with red/blue rest-frame optical colours. The solid line is the LF fitted to the combined sample. For reference the dashed line shows the local K -band LF from Kochanek et al. (2001).

The search for high-redshift quasars exploits the UKIDSS Y -band ($0.97\text{--}1.07 \mu\text{m}$). Quasars at $z > 6.4$ will be very red in $i\text{-}Y$ or $z\text{-}Y$, but bluer in $Y\text{-}J$ than the more common L and T brown dwarfs, and therefore distinguishable from them. So far we have searched some 140 deg^2 , and have found a single high-redshift quasar, at $z = 5.86$. The spectrum is shown in Figure 3, and shows the characteristic very strong break in the continuum across $\text{Ly}\alpha$. To a limit $Y = 19.5$ we expect to find about one quasar $z > 6.0$ in 150 deg^2 , so our results so far are consistent with this expectation. The discovery of this high-redshift quasar is extremely encouraging for the future of the search, as the LAS database expands.

Rare objects in the Large Area Survey II: Cool brown dwarfs

The coolest brown dwarfs are the T dwarfs, of which 99 are known, all discovered since 1995. The main samples have come from SDSS and 2MASS. The classification scheme of Burgasser et al. (2006) defines nine spectral classes from T0 to T8. The primary spectral standard for the coolest class, T8, is the object 2MASS 0415-09. There are only six T8 dwarfs known. These are the coolest brown dwarfs and have temperatures $\sim 700 \text{ K}$. Jupiter has a temperature $\sim 150 \text{ K}$. What lies in between? One of the goals of UKIDSS is to explore this temperature range. Ultracool dwarfs are

expected to be extremely red in z - J , and so difficult to detect in z . Therefore the Y -filter is again expected to play an important role. At some point a new spectral feature is expected to emerge, possibly NH_3 absorption, defining a new spectral class, for which (coincidentally) the letter Y has been suggested.

One brown dwarf discovered in DR1, ULAS J0034, is extremely cool, and has proven particularly interesting. The spectrum is plotted in Figure 4, where it is compared against the T8 standard 2MASS 0415-09. There are some minor differences, for example, the suggestion of excess absorption in the blue wing of the 1.5–1.6 μm emission peak – a wavelength region where NH_3 may appear – as well as the enhanced flux in the Y -band. These hint that ULAS J0034 may be even cooler than 2MASS 0415-09, and they warrant deeper spectroscopy. Nevertheless, because the principal molecular absorption bands, due to water and methane, are practically saturated at these cool temperatures, it may be that it will become necessary to obtain photometry and spectroscopy at mid-infrared wavelengths of candidates such as this, in order to delineate the development of the spectral sequence beyond T8.

The substellar initial mass function below 30 Jupiter masses, from the Galactic Clusters Survey

The aim of the Galactic Clusters Survey (GCS) is to investigate the substellar initial mass function (IMF) in a number of open clusters and star-forming regions, to shed light on the formation of brown dwarfs. The survey will cover 1000 deg^2 in $ZYJHK$, in 10 clusters, to uncover low-mass brown dwarfs. A second epoch coverage will be conducted in a few years time to derive proper motions over a large mass range. One of the regions covered in DR1 is the young (age = 5 Myr) and nearby ($d = 145$ pc) OB association Upper Scorpius. Over 6 deg^2 have been covered in the central part of the association. The Z - J versus J colour-magnitude diagram for stellar sources is striking (Figure 5). The cluster sequence stands out clearly from the field stars over the 0.3–0.01 M_\odot mass range, i.e. right down to 10 Jupiter masses (M_J), and the selection of clus-

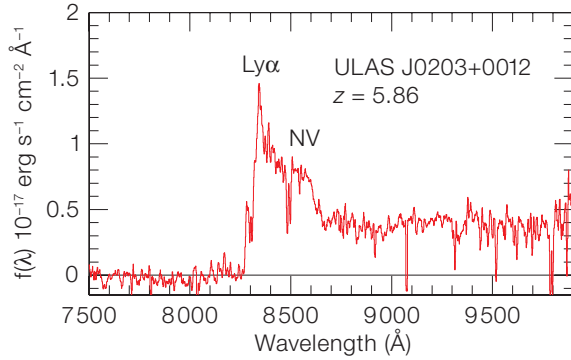


Figure 3: The discovery spectrum of the first very high redshift quasar from UKIDSS (from Venemans et al., in prep.). This 1200 sec spectrum was taken on the night of 1 September 2006, with FORS2 on the VLT.

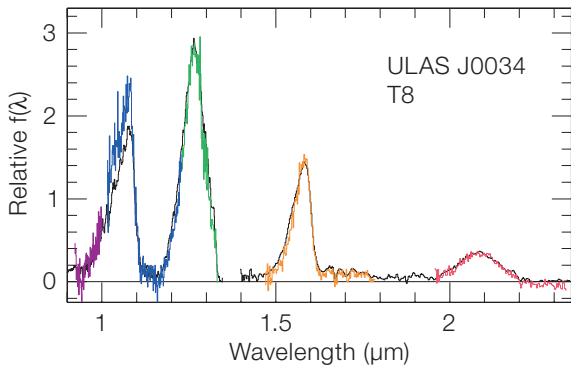


Figure 4: Spectrum of the cool T dwarf ULAS J0034, the coolest brown dwarf found so far in DR1. The colours correspond to different orders of this cross-dispersed spectrum which was a 60 min exposure taken with GNIRS on Gemini South. The black line plots the spectrum of the T8 standard 2MASS 0415-09, the coolest T dwarf known, for comparison.

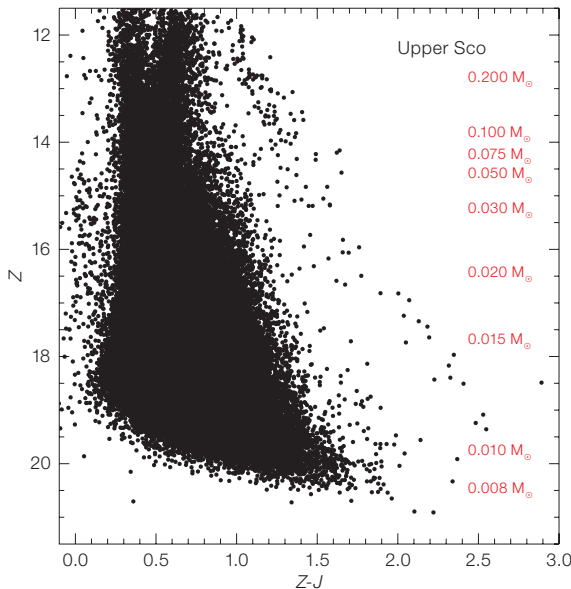


Figure 5: Z - J versus Z colour-magnitude diagram for 6 deg^2 in the Upper Scorpius association. The cluster sequence stands out clearly from field stars all the way down to 10 M_J , according to theoretical models.

ter members is straightforward. We have increased significantly the number of known substellar members in Upper Scorpius, and uncovered over a dozen new brown dwarfs below 20 M_J , the limit of previous studies in the region. Furthermore, we have confirmed all candidates more massive than 15 M_J as proper motion members using the 2MASS database

as first epoch. Preliminary optical spectroscopy of the bright members reveals signs of chromospheric activity and weak gravity features, characteristics of young stars. The inferred cluster IMF keeps rising across the hydrogen-burning limit and is best fit by a single power law index $\alpha = 0.6 \pm 0.1$ down to 10 M_J . This result is in agreement with previous IMF estimates

Figure 6: The synergy of UKIDSS-GPS and Spitzer-GLIMPSE data. **Upper:** *K*-band image of the central parts of a star-formation region in the mid-plane: G28.983-0.603 from Bica et al. (2003). **Lower left:** The *J-H* versus *H-K* two-colour diagram, used to establish $A(V)$. **Lower right:** The *K-4.5* μm versus $A(V)$ diagram, combining UKIDSS and Spitzer data,

for sources with GLIMPSE 4.5 μm detections. Candidate YSOs are sources with *K-4.5* μm excess, and are clearly separated in this diagram. In the *K*-band image, black triangles mark GLIMPSE mid-IR detections, and red squares mark candidate YSOs.

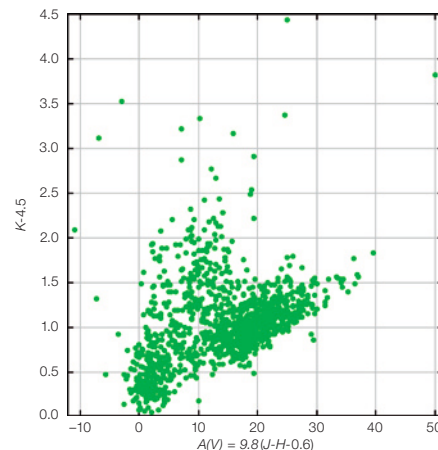
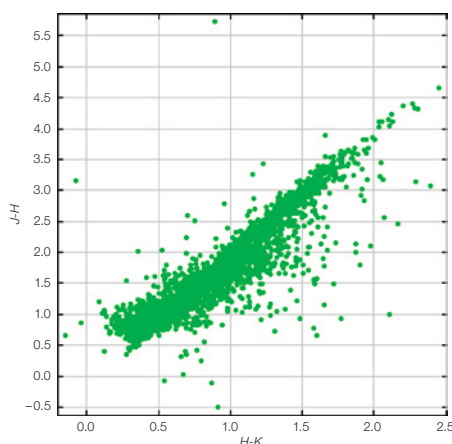
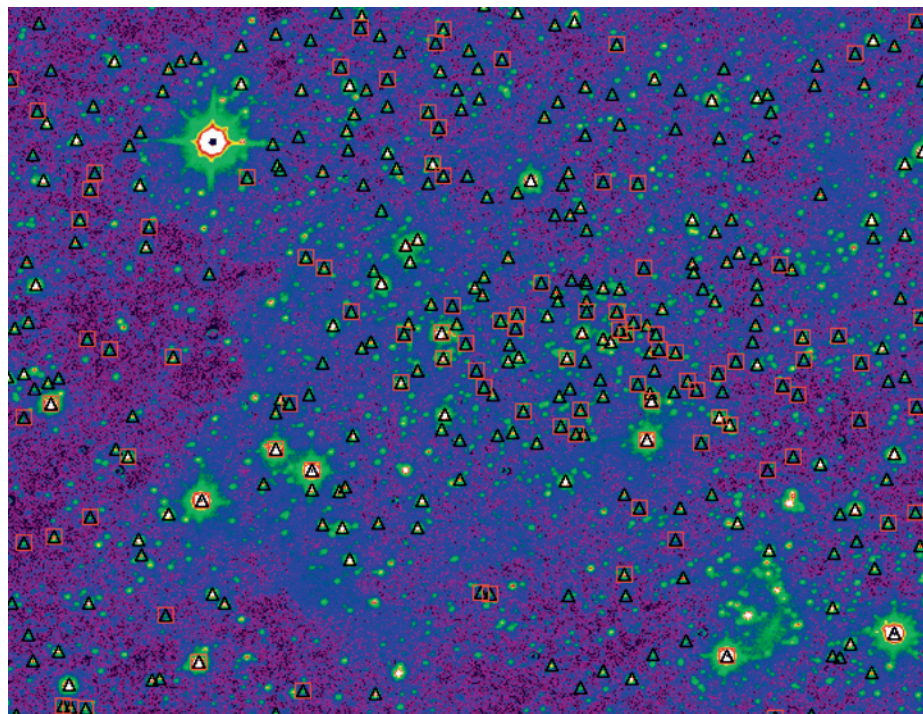
in open clusters but extends our knowledge to lower masses.

Stellar clusters in the Galactic Plane Survey

The Galactic Plane Survey is a legacy survey designed to be useful for all areas of Galactic astronomy. It consists of a first epoch of *JHK* photometry at longitudes $l = -2^\circ$ to 107° and $l = 142^\circ$ to 230° , and latitudes $|b| < 5$ degrees, followed by two additional epochs of *K*-band photometry to provide proper motion data and to detect rare, high amplitude variable stars.

One of the principal science goals is to search for any variation of the IMF over different star-forming environments, by studying a larger sample of young clusters than any previous survey. To detect Young Stellar Objects (YSOs), the combination of Spitzer-GLIMPSE mid-IR data with UKIRT *JHK* is much more effective than the use of the mid-IR or near-IR data alone. This is illustrated in Figure 6. The image at the top shows a UKIDSS *K*-band image covering $3' \times 3'$, of a star-formation region in the mid plane. The GLIMPSE data on its own in this region can be used to identify YSOs – but there are only 128 four-band IRAC detections, and nine YSOs identified in a (3.6–4.5) versus (5.8–8.0) μm two-colour diagram for the field. Alternatively the UKIDSS data alone may be used to select YSOs. The lower-left diagram plots *J-H* versus *H-K* for 2326 sources, with uncertainties < 0.1 mag on each axis, in the field. We see a well-defined reddening sequence from lower left to upper right. Candidate YSOs are objects with infrared excess to the right of this sequence.

Combining the UKIDSS and GLIMPSE data gives a much cleaner separation. The lower left-hand diagram may be used to estimate $A(V)$. In the lower right-hand diagram the *K-4.5* μm colour is plotted against $A(V)$ for the 1084 sources with GLIMPSE 4.5 μm detections. Candidate YSOs are identified by their *K-4.5* μm colour excess. These are plotted as red open squares in the upper figure, and show a concentration towards the cluster centre.



Timetable for future releases

The next release, DR2, is planned for the end of February 2007, and will include new data obtained in the period May to July 2006. Note that the UDS was not observable in this block. A new very large WFCAM block began at the end of October 2006, and runs through to mid-May 2007. By the end of this block UKIDSS will be about 20% complete. These data will be released in DR3, intended to take place late in 2007.

References

- Bica E. et al. 2003, A&A 404, 223
- Burgasser A. et al. 2006, ApJ 637, 1067
- Cirasuolo M. et al. 2006, MNRAS, submitted, astro-ph/0609287
- Foucaud S. et al. 2006, MNRAS, submitted, astro-ph/0606386
- Hewett P. et al. 2006, MNRAS 367, 454
- Kochanek C. et al. 2001, ApJ 560, 566
- Lawrence A. et al. 2006, MNRAS, submitted, astro-ph/0604426
- Lodieu N. et al. 2006, MNRAS, in press, astro-ph/0610140
- McLure R. et al. 2006, MNRAS 372, 357
- Warren S. et al. 2006, MNRAS, submitted, astro-ph/0610191

Starburst Galaxies Under the Microscope: High-Resolution Observations with VISIR and SINFONI

Paul P. van der Werf, Leonie Snijders, Liesbeth Vermaas, Juha Reunanen and Marten Hamelink (Leiden Observatory, the Netherlands)

Infrared observations of starburst galaxies not only enable penetration of the obscuring veil of dust, but also provide unique diagnostics in the form of nebular emission lines and emission from dust and polycyclic aromatic hydrocarbons (PAHs). Here we describe some first results of our ongoing study of starburst galaxies with VISIR and SINFONI at the VLT.

Starburst galaxies

Starburst galaxies are unique laboratories. Starburst episodes are phases in the evolution of galaxies that are by definition transient, and during which they convert a significant fraction of their gas reservoirs into stars. During a starburst phase a galaxy thus evolves rapidly in stellar, gas, dust and metal content, colour, luminosity and morphology. Starburst galaxies also cover an enormous range in luminosity. At the low luminosity end the small star-forming dwarf galaxies such as the Small and Large Magellanic Clouds have infrared luminosities $L_{\text{IR}} = 7 \cdot 10^7 L_{\odot}$ and $L_{\text{IR}} = 7 \cdot 10^8 L_{\odot}$. More distant infrared-bright dwarf galaxies typically have $L_{\text{IR}} = 3 \cdot 10^9 L_{\odot}$. Well-studied nearby starbursts such as NGC 253 and M82 have $L_{\text{IR}} = 3 \cdot 10^{10} L_{\odot}$ and $6 \cdot 10^{10} L_{\odot}$. At higher luminosities, we have the luminous infrared galaxies (LIRGs) with $L_{\text{IR}} > 10^{11} L_{\odot}$. (e.g., the Antennae, NGC 4038/4039), the ultraluminous infrared galaxies (ULIRGs) with $L_{\text{IR}} > 10^{12} L_{\odot}$ (e.g. Arp 220), and the hyperluminous infrared Galaxies (HyLIRGs) with $L_{\text{IR}} > 10^{13} L_{\odot}$. While the luminosity range spanned is more than five decades, the starbursts that are most amenable to detailed study are obviously the nearest ones, which have only moderate luminosity. It is therefore important to understand how these nearby starbursts relate to their more distant and spectacular cousins.

Since stars form in dusty molecular clouds, it is no surprise that (most) starbursts are also dusty. The study of starburst galaxies has therefore received

an enormous boost from technical developments in ground-based and space-based infrared astronomy. The infrared regime in fact offers two advantages. In the first place, reduced extinction offers the opportunity to see through the obscuring dust, and to probe the active star-forming complexes directly. Secondly, a number of unique diagnostics are available in the infrared in the form of highly diagnostic nebular emission lines, H_2 vibrational lines which provide a kinematic probe of the molecular gas at high spatial resolution, and emission and absorption features of the dust itself, including those attributed to polycyclic aromatic hydrocarbons (PAHs).

We have recently embarked on an observational study of nearby starbursts with two new VLT instruments: SINFONI and VISIR, and here report some first results.

The importance of spatial resolution

The study of starburst galaxies through infrared techniques has benefited significantly from observations with the Infrared Space Observatory (ISO) and the Spitzer Space Telescope. Yet, while these space-based observations have provided unmatched sensitivity and wavelength coverage, they cannot provide the spatial resolution enabled by ground-based telescopes. VISIR at the VLT has opened up the ground-based mid-infrared (mid-IR) spectral region for routine imaging and spectroscopy at an angular resolution of $0.3''$ (essentially the diffraction limit of the VLT). For comparison, the resolution of Spitzer at $8 \mu\text{m}$ is $2.5''$. Thus VISIR gains over Spitzer in spatial resolution by a factor of eight in two dimensions. As we will show, this gain in spatial resolution is fundamentally important for studying the anatomy of starburst galaxies in detail. The VISIR data are complemented with SINFONI near-infrared (near-IR) integral field spectroscopy at a similar resolution. High spatial resolution allows us to isolate active star-forming regions from diffuse extended emission and thus provides a more secure diagnostic of the conditions in the star-forming regions themselves (e.g., local densities and radiation fields). An application of this is the determination of the mass of the most massive star in a young star-forming re-

gion, for which the youngest regions have to be isolated. A second example is the origin of the PAH emission in starburst galaxies, which can be studied if the emission regions and the local sources of excitation can be spatially resolved. Both of these require high spatial resolution and will be discussed in some detail in the following sections.

A case study: superstarclusters in the Antennae (NGC 4038/4039)

The Antennae system (NGC 4038/4039) is the nearest major merger of two large spiral galaxies. Since the beginning of the interaction the system went through several episodes of violent star formation, of which the last one is probably still ongoing.

The resulting star clusters have been studied extensively. Radio and mid-IR observations show that the region between the two remnant nuclei (usually referred to as the overlap region) hosts spectacular obscured star formation. The brightest mid-IR component produces 15 % of the total $15 \mu\text{m}$ luminosity of the entire system (Mirabel et al. 1998). This region is covered by a prominent dust lane and may be associated with a faint, red source in Hubble Space Telescope (HST) images, illustrating how optical data alone are insufficient to identify and study the youngest star-forming regions. Such superstarclusters are of interest as potentially the youngest simple coeval stellar populations in starbursts and thus furnish excellent tests for the properties of the most massive stars formed in these systems. For sufficiently massive and young superstarclusters, they may offer the opportunity of directly measuring a possible upper mass cutoff of the stellar Initial Mass Function (IMF). Mid-IR nebular fine-structure lines are excellent probes of such systems, since they are relatively unaffected by dust and can be used to measure the temperature of the ionising radiation field, and hence the masses of the most massive stars present.

We used VISIR to study the most prominent clusters at $0.3''$ resolution (30 pc at the assumed distance of 21 Mpc for the Antennae). Our data set consists of

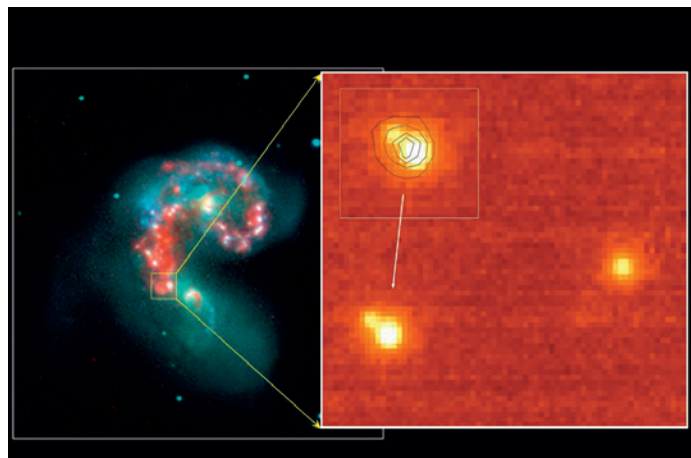
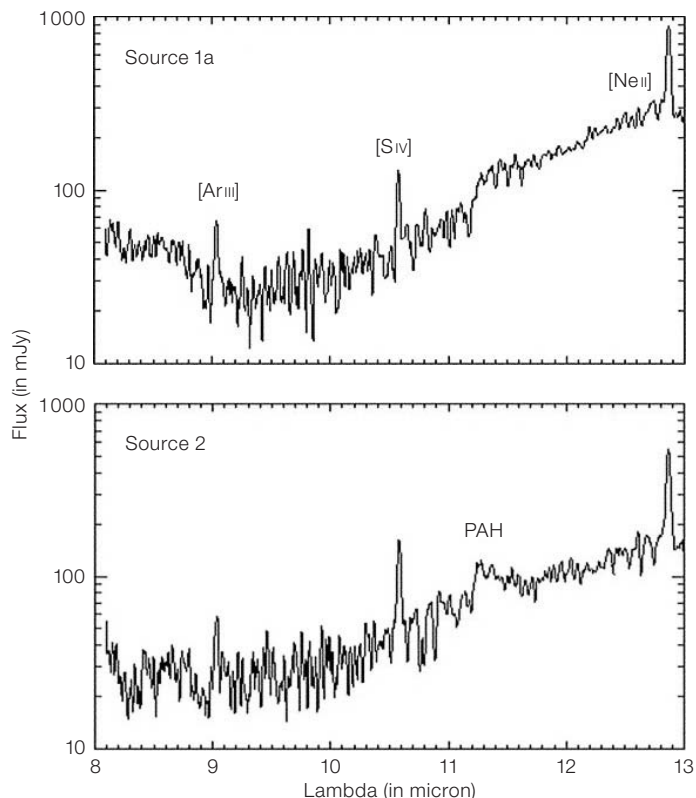


Figure 1 (above): VISIR image of the [Ne II] 12.8 μm emission from the most prominent superstarclusters in the Antennae (right panel). The diameter of the VISIR field shown here is 9". Its location is indicated in the left panel, which shows a composite of data obtained with Spitzer (Wang et al. 2004). The inset in the right panel shows the contours of the dust emission at 11.3 μm overlaid on the [Ne II] image (from Snijders et al. 2006).

Figure 2 (right): VISIR spectra, taken with a 0.75" slit, of the two prominent superstarclusters in the Antennae seen in Figure 1. Source 1a is the brightest part of the Eastern source, while Source 2 is the Western source. The apparently enhanced noise from 9 to 10 μm results from the log scale of these plots (from Snijders et al. 2006).



imaging in a number of narrow-band filters in the N -band, and long-slit spectroscopy with a 0.75" slit, covering the two most prominent clusters. Some key results are shown in Figures 1 and 2 (Snijders et al. 2006), which show a number of surprising results. In the first place, the Eastern cluster is separated into two components, separated by approximately 0.5" (50 pc). The brightest of these two (cluster 1a) is slightly resolved. This result immediately shows that any attempt to model this region as a single coeval stellar population is flawed. Cluster 1b has no counterpart in any other available data set; from the available upper limits, we derive a visual extinction $A_V > 72^m$ towards this cluster. Remarkably, the 11.3 μm emission shows a different morphology, suggesting a common envelope of emission from hot dust and polycyclic aromatic hydrocarbons (PAHs). Cluster 2, which is optically complex, is a simple and compact object at 10 μm ; presumably the N -band emission is dominated by a single (obscured) object within the general complex.

An even more surprising result comes from comparison with Spitzer-IRS spec-

tra (Brandl, priv. comm.) with a 5" slit, revealing that approximately 75 % of the 12 μm continuum is detected in the 0.75" VISIR slit; however, the equivalent width of the 11.3 μm PAH feature in the VISIR data is much smaller than in the larger aperture Spitzer spectra.

Both clusters exhibit emission in the 10.5 μm [S IV] line, an ionisation stage requiring 34.8 eV (while the 12.8 μm [Ne II] line requires only 21.6 eV); in particular in cluster 2 the [S IV]/[Ne II] ratio in our data is higher than in larger aperture Spitzer data, significantly affecting the interpretation of the results, and indicating that VISIR closes in on the regions of most intense star formation, while larger aperture data are significantly affected by more diffuse emission.

A detailed analysis of the fine-structure line ratios in the two clusters indicates conditions similar to those in Galactic ultracompact H II regions (but extended over tens of parsecs). This is an important result, since it would affect the interpretation of results at other wavelengths (from radio to near-IR) as well (Snijders et al., in preparation).

The low equivalent width of the PAH emission indicates that either the PAHs are destroyed in the direct environment of the superstarclusters, or that the PAH emission is not preferentially excited by the superstarclusters, but is dominated by more diffuse emission, excited by the softer UV radiation from more widespread young stars of slightly later type. Understanding which of these explanations is correct is important for the interpretation of the PAH emission. In order to study this issue further, we now turn to a more nearby starburst, where much higher linear resolution is obtained.

The resolved starburst in M83

M83 is a nearby ($D = 4.5$ Mpc) grand-design barred spiral with a nuclear region that is sometimes described as 'amorphous'. It has a prominent optical peak, which is however not at the centre of the fainter isophotes and therefore probably not the dynamical centre. The starburst in M83 is not centred on this optical peak, but displaced significantly towards the West. The situation is illustrated in Figure 3. Here the K -band continuum is

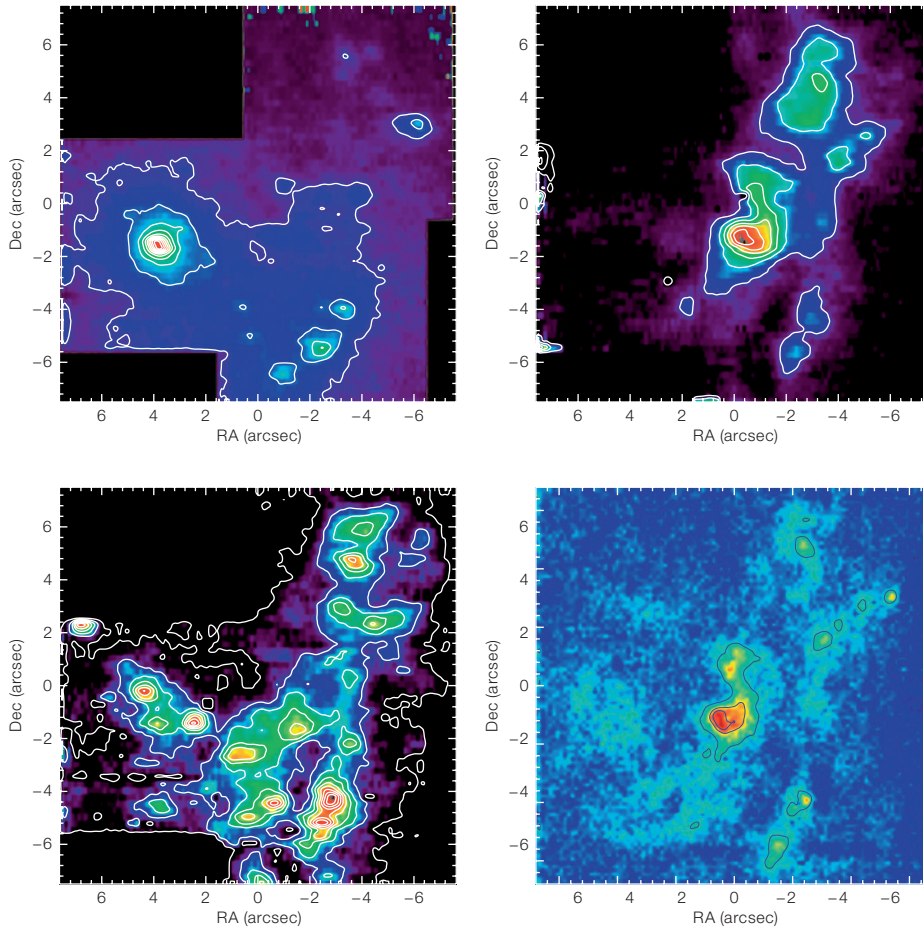


Figure 3: The off-nuclear starburst in M83. Each of these frames shows a $13.6'' \times 13.6''$ (300 pc diameter) region. Top-left panel: K -band continuum (from SINFONI); top-right panel: $\text{Br}\gamma$ $2.17 \mu\text{m}$ (from SINFONI); lower-left panel: $[\text{FeII}]$ $1.26 \mu\text{m}$ (from SINFONI). These data result from three overlapping SINFONI exposures, with on-source integration times of 10 minutes per frame and per spectral band (from Vermaas et al., in preparation); lower-right panel: $11.3 \mu\text{m}$ PAH emission obtained with VISIR (from Snijders et al., in preparation).

dominated by the underlying bulge population, with emission from red supergiants formed in the starburst superimposed. The full spectral data cubes produced by SINFONI provide a wealth of detail on the morphology and spatial and temporal evolution of this starburst, which is illustrated by the spectra shown in Figure 4.

Key spectral features which are evident in these spectra include lines of ionised hydrogen ($\text{Br}\gamma$ $2.17 \mu\text{m}$ in the K -band, the Brackett series in the H -band and $\text{Pa}\beta$ $1.28 \mu\text{m}$ in the J -band). These lines trace the distribution of the young massive stars (spectral types B3 and earlier) and (under the usual assumption of dust-free and ionisation-bounded HII regions) provide a direct measurement of the Lyman continuum output of these stars; in addition, combining these lines gives a direct measurement of the extinction towards the ionised gas. In addition we observe HeI lines (principally the $2.06 \mu\text{m}$ and $1.70 \mu\text{m}$ lines, but also fainter transi-

tions). These lines trace the helium-ionising continuum and therefore the most massive stellar population in the starburst. In principle helium/hydrogen recombination line ratios can be used to measure the relative volumes of the helium and hydrogen Strömgren spheres and thus the hardness of the ionising radiation field. In practice, collisional excitation effects from metastable levels in the helium atom make this procedure complicated, and in particular the use of the bright HeI $2.06 \mu\text{m}$ line is fraught with difficulties; however, the HeI $1.70 \mu\text{m}$ line is quite suitable for this purpose.

In addition we find forbidden fine-structure lines of singly ionised iron, principally the $[\text{FeII}]$ $1.64 \mu\text{m}$ line in the H -band and the $1.26 \mu\text{m}$ line in the J -band. The $[\text{FeII}]$ emission results from strong shocks from supernovae, which destroy the dust grains, thus raising the gas-phase iron abundance by a large factor. The resulting iron atoms are then easily ionised

and excited by the supernova blast wave shock. Since the $[\text{FeII}]$ $1.64 \mu\text{m}$ and $1.26 \mu\text{m}$ lines originate from the same upper level, their intrinsic ratio is fixed and the observed line ratio can thus be used as an independent extinction measurement. Furthermore, fainter $[\text{FeII}]$ lines can be used to constrain temperature and density of the emitting material.

Also commonly detected are the rovibrational lines of H_2 . Arising from levels about 6000 K above the ground state, these lines trace hot molecular gas. While the diagnostic use of these lines is complicated by the fact that multiple excitation mechanisms can play a role (and probably do play a role), such as fluorescence following UV-absorption, shock waves and X-ray excitation, they provide a unique high-resolution probe of molecular gas in galactic nuclei which can often be used for gas-dynamical studies.

In addition to these emission features, there are photospheric absorption features arising in the cool atmospheres of red supergiants created in the starburst. These include the CO first overtone absorption bands at $2.30 \mu\text{m}$ and longer wavelengths, as well the second overtone absorptions in the H -band; there are also atomic absorption lines (e.g., SiII $1.59 \mu\text{m}$, NaI $2.21 \mu\text{m}$ and CaI $2.27 \mu\text{m}$) which together with the CO bands can be used for stellar dynamical studies as well as for spectral typing of the dominant stellar population.

Finally, high-excitation so-called coronal lines (named after their detection from the solar corona) require a hard radiation

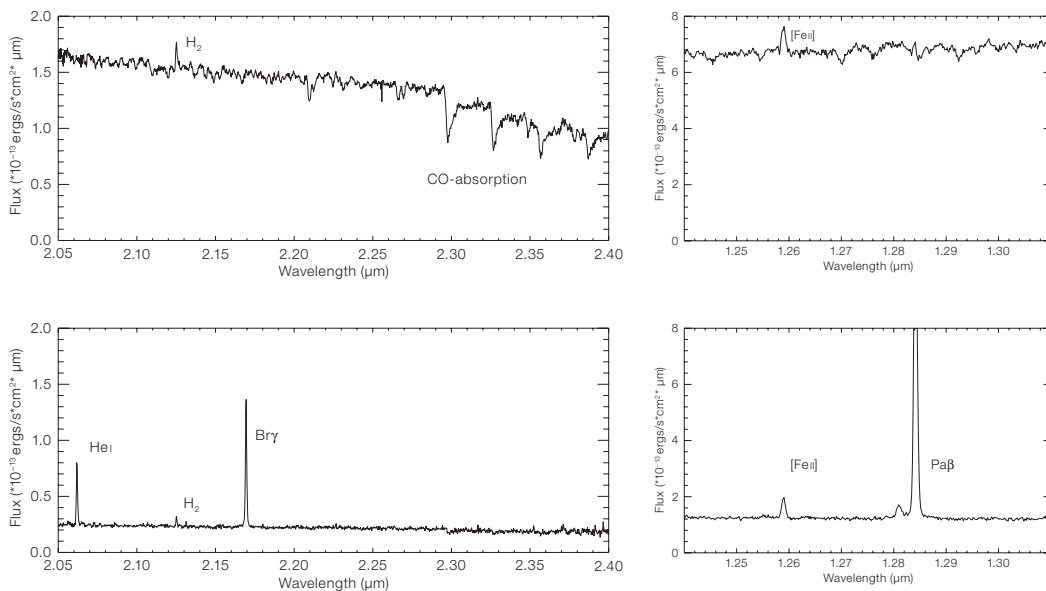


Figure 4: SINFONI spectra taken at two positions in M83. Shown are SINFONI K -band spectra (left column) and partial J -band spectra (right column) on the K -band continuum peak (upper panels), on the peak of the $\text{Br}\gamma$ emission (lower panels). These spectra are from Vermaas et al. (in preparation).

field that cannot be produced by normal young stars and therefore reveal the presence of an active galactic nucleus (AGN); these lines include $[\text{SiVI}]$ 1.96 μm , $[\text{CIV}]$ 2.32 μm and $[\text{SiI}]$ 1.25 μm .

With the exception of the coronal lines, all of these lines are evident in the spectra shown in Figure 4. Given that these tracers probe different temporal phases of the starburst, they can be used as an age indicator. For instance, the $\text{Br}\gamma$ equivalent width $\text{EW}(\text{Br}\gamma)$ can be formed by dividing the $\text{Br}\gamma$ emission by the underlying continuum, thus measuring the relevant importance of young O-stars and their direct descendants, the red supergiants, which is time-dependent and can thus be used to determine the age of the stellar population. Age determinations may also be obtained by comparing $\text{Br}\gamma$ flux to CO absorption bands (again a comparison of O-stars with red supergiants) or $[\text{FeII}]$ flux (O-stars compared to supernova remnants). Turning again to Figures 3 and 4, it is seen that at the K -band nucleus the $\text{EW}(\text{Br}\gamma)$ is very low, but that the CO bands are quite prominent, showing that this region is dominated by an evolved stellar population. In contrast, the bright $\text{Br}\gamma$ region seen in Figure 3 has essentially no counterpart in the K -band continuum and its high $\text{EW}(\text{Br}\gamma)$ thus indicates a very young age. This is also seen in its J -band spectrum, where the $\text{Pa}\beta$ line is much stronger than the $[\text{FeII}]$ line at 1.26 μm .

Since the supernova rate is dominated by stars with a mass of about $8 M_{\odot}$ (the most numerous stars still producing supernovae), which have a lifetime of about $3 \cdot 10^7$ years, the $\text{Br}\gamma$ and $[\text{FeII}]$ emission trace phases of the starbursts that are temporally separated by this amount of time. In principle, one could use these results then to calculate the speed at which the star formation propagates through the nuclear region. Remarkably however, there is no pattern in the derived ages. Instead, the results point to a situation in which a large area becomes globally unstable, after which individual star-forming complexes form stochastically. There is thus no evidence for propagating star formation in this region. However, a *global* trigger is still needed. Presumably this may be found in the accumulation of gas in the barred potential in the M83 nucleus, which continues until a critical value is reached, after which star formation is ignited stochastically.

Inspection of Figure 3 also reveals that the PAH emission traces star formation only approximately. Clearly the brightest PAH emission traces the brightest $\text{Br}\gamma$ emission, and there is therefore no evidence for PAH destruction by the hottest stars. However, diffuse PAH emission is present also where no $\text{Br}\gamma$ emission is found, e.g., in the region of the K -band nucleus. The presence of $[\text{FeII}]$ emission in this area indicates the presence of supernova remnants, but direct excitation

by these is unlikely, given the lack of detailed morphological agreement. The presence of supernova remnants however indicates a radiation field dominated by the most massive stars that do not end as supernovae, i.e., mid-B-type stars or later. This result confirms earlier claims that PAHs can be excited by a fairly soft radiation field (e.g., Li and Draine 2002). A quantitative analysis will be able to show what fraction of the PAH emission is excited by stars of various types, which will ultimately lead to a more secure calibration of PAH emission as a star formation indicator.

Mid-IR emission as a star formation indicator

A fundamental result from Spitzer is the use of 24 μm dust emission (well away from solid state spectral features) as a star-formation indicator (e.g., Calzetti et al. 2005, Pérez-González et al. 2006). Ground-based imaging in the Q-band spectral window (17–26 μm) allows us to examine the dust emission in this spectral region in detail in spatially resolved starbursts.

An example is presented in Figure 5, where we present images of $\text{Br}\gamma$ emission (from SINFONI) together with the Q-band dust emission imaged with VISIR (Snijders et al., in preparation). It is evident that these two match quite well.

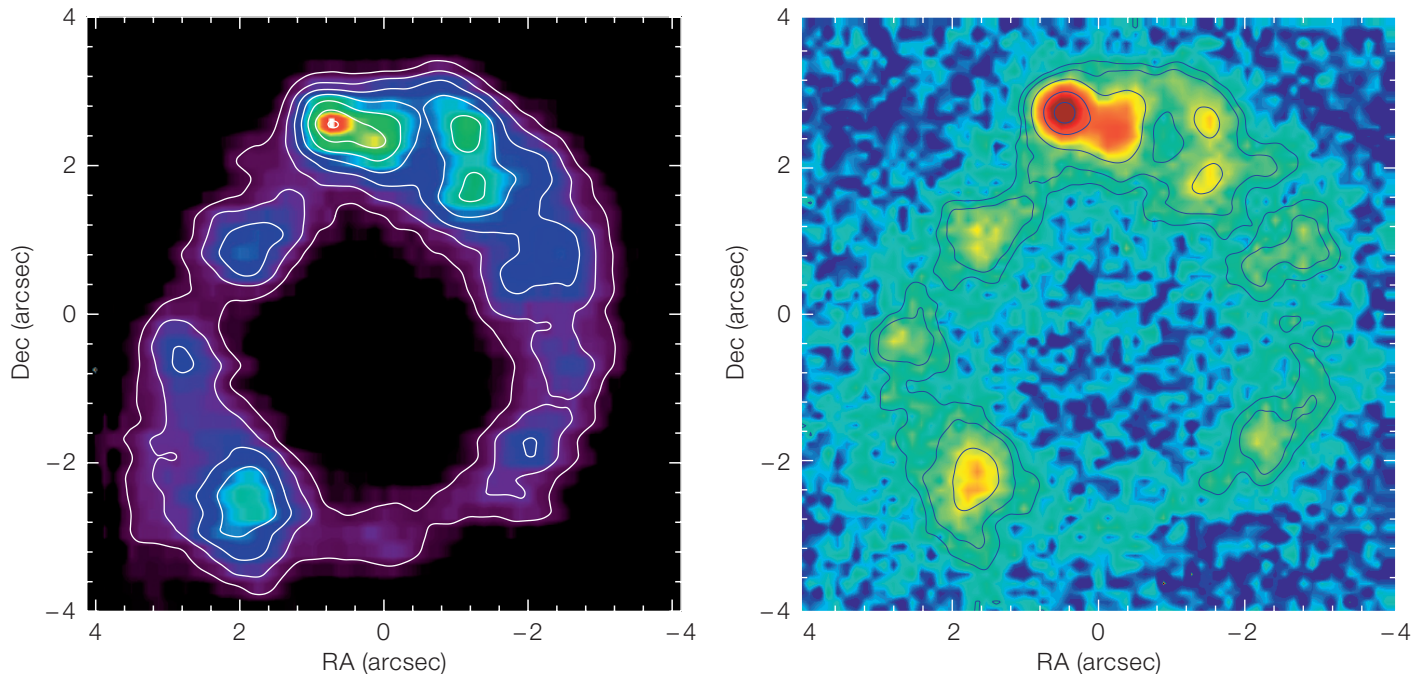


Figure 5: The circumnuclear starburst in NGC 7552. Each of these frames shows an $8'' \times 8''$ (800 pc diameter) region. **Left panel:** Br γ emission (from SINFONI); **right panel:** Q-band dust emission (from VISIR; from Snijders et al., in preparation).

These data will allow us to correlate the extinction-corrected (using the Br γ /Pa β ratio) Br γ emission with the Q-band dust emission at high spatial resolution to study both the correlation and possible deviations from the correlation (Snijders et al., in preparation).

Outlook

In this paper we have only scratched the surface of the possibilities offered by SINFONI and VISIR for ground-based studies of starburst galaxies. We are currently extending this work in two directions.

First, we are including studies of AGNs. In gas-rich galactic nuclei containing a (dormant) supermassive black hole the triggering of activity may be related to the supply of fuel to the very centre. In galaxies with an Inner Lindblad Resonance (ILR) this supply is halted by a torque barrier at the ILR. In other words, under only the effects of gravity the inflowing gas will accumulate at the ILR and form a ring, which, after building up sufficient surface density, will form stars, as observed in NGC 7552 (Figure 5). However, the gas cannot pass the ILR, and any supermassive black hole located at the nucleus remains fuel-starved

and thus dormant. On the other hand, in galaxies with an active AGN, gas emission is observed all the way to the nucleus. This is the case for instance in Cen A, which has no ILR, and where our SINFONI data reveal a warped disc of H $_2$ gas, extending all the way to the nucleus. Kinematic modelling of this disc then provides a new determination of the black hole mass (Neumayer et al., in preparation).

A second avenue for expanding this work is with studies of ULIRGs. Given the now well-documented correlation of (stellar) spheroid mass with mass of the central supermassive black hole for galaxies (e.g., Magorrian et al. 1998), the formation of the bulk of the stellar mass and of the black hole must be related. It is likely that this relation is put into place in high- z ULIRGs, where violent star formation not only builds up significant stellar mass, but where an AGN is often also evident. Local ULIRGs can be studied as analogues of these high- z objects. Again, spatial resolution is essential, and with the Laser Guide Star Facility on UT4 of the VLT, it is likely that SINFONI will play a key role in revealing the nature of the relation between starburst and AGN in these extreme objects.

In summary, it is clear that with SINFONI and VISIR, and with the spatial resolution offered with the VLT and the Laser Guide Star Facility, new territory is being opened for the study of activity (starburst or otherwise) in galactic nuclei, which is not available with present space-based facilities.

References

- Calzetti D. et al. 2005, ApJ 633, 871
- Li A. and Draine B. T. 2002, ApJ 572, 232
- Magorrian J. et al. 1998, AJ 115, 2285
- Mirabel F. et al. 1998, AA 333, L1
- Pérez-González P. G. et al. 2006, ApJ 648, 987
- Snijders L. et al. 2006, ApJ 648, L25
- Wang Z. et al. 2004, ApJS 154, 193

The Short Gamma-Ray Burst Revolution

Jens Hjorth¹
 Andrew Levan^{2,3}
 Nial Tanvir⁴
 Rhaana Starling⁴
 Sylvio Klose⁵
 Chryssa Kouveliotou⁶
 Chloé Féron¹
 Patrizia Ferrero⁵
 Andy Fruchter⁷
 Johan Fynbo¹
 Javier Gorosabel⁸
 Páll Jakobsson²
 David Alexander Kann⁵
 Kristian Pedersen¹
 Enrico Ramirez-Ruiz⁹
 Jesper Sollerman¹
 Christina Thöne¹
 Darach Watson¹
 Klaas Wiersema¹⁰
 Dong Xu¹

¹ Dark Cosmology Centre, Niels Bohr Institute, University of Copenhagen, Denmark

² Centre for Astrophysics Research, University of Hertfordshire, United Kingdom

³ Department of Physics, University of Warwick, United Kingdom

⁴ Department of Physics and Astronomy, University of Leicester, United Kingdom

⁵ Thüringer Landessternwarte Tautenburg, Germany

⁶ NASA Marshall Space Flight Center, Huntsville, Alabama, USA

⁷ Space Telescope Science Institute, Baltimore, Maryland, USA

⁸ Instituto de Astrofísica de Andalucía, Granada, Spain

⁹ Institute for Advanced Study, Princeton, New Jersey, USA

¹⁰ Astronomical Institute, University of Amsterdam, the Netherlands

Swift, a dedicated gamma-ray burst (GRB) satellite with ultrarapid slewing capability, and a suite of ground-based (ESO) telescopes have recently achieved a major breakthrough: detecting the first afterglows of short-duration GRBs. The faintness of these afterglows and the diversity of old and young host galaxies lend support to the emerging 'standard model', in which they are created during the merging of two compact objects. However,

the afterglow light-curve properties and possible high-redshift origin of some short bursts suggests that more than one progenitor type may be involved.

A decade ago studies of gamma-ray bursts (GRBs) were revolutionised by the discovery of long-lived afterglow emission at X-ray, optical and radio wavelengths. The afterglows provided precise positions on the sky, which in turn led to the discovery that GRBs originate at cosmological distances, and are thus the most luminous events known in the Universe. These afterglows also provided essential information for our understanding of what creates these extraordinary explosions. Observations from the VLT finally showed them to be associated with the final, catastrophic collapse of massive stars (Hjorth et al. 2003).

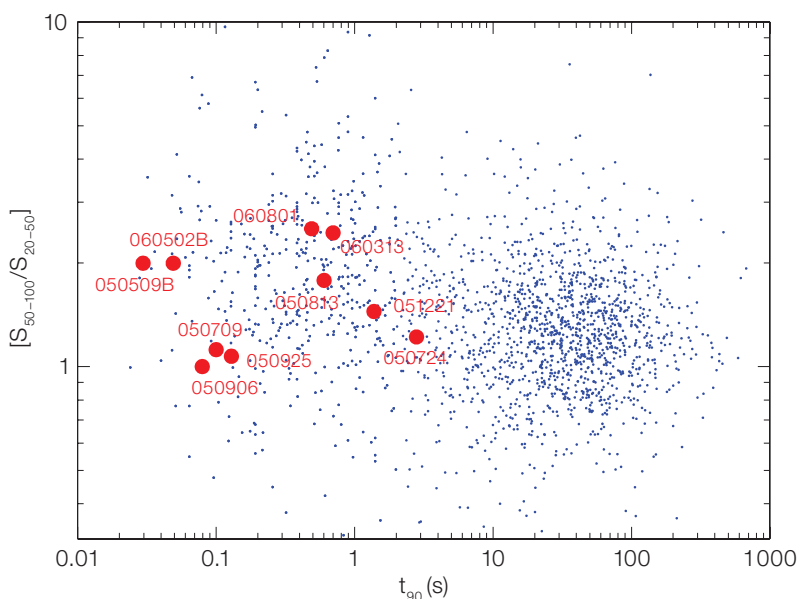
But the picture was not yet complete. In particular, these results applied only to the bursts with durations of > 2 s, while the burst duration distribution was clearly bimodal (Kouveliotou et al. 1993) splitting into long and short GRBs, with the short bursts also exhibiting markedly harder gamma-ray spectra (see Figure 1). The short bursts proved even more elusive than their long-duration cousins, and despite significant effort no afterglows could be found, maintaining our ignorance of their distance scales, energies and, of course, physical origin.

Afterglows – found!

Finally, in May 2005 *Swift* discovered the first X-ray afterglow to a short GRB.

This was made possible because of the rapid ability of *Swift* to slew across the sky, pointing at the approximate location of the burst only a minute after it happened and pinpointing a very faint X-ray afterglow. The afterglow lies close to a massive elliptical galaxy in a cluster of galaxies at $z = 0.225$ (Gehrels et al. 2005; Pedersen et al. 2005; Figure 2). Many extremely deep observations, including those at the VLT, failed to locate either a fading optical afterglow, or a rising supernova component at later times (Hjorth et al. 2005a). The lack of an accompanying supernova (Figure 3), and the purported elliptical host galaxy (Figure 2), strongly suggest that the progenitors for these short bursts are different from those of long bursts. In particular, any radioactive material produced in the explosion must be far less.

Figure 1: The hardness-duration diagram for GRBs. The x-axis shows the duration over which 90% of the observed total flux is detected, while the y-axis shows the ratio of fluxes in the 50–100 keV over the 20–50 keV bands, and is essentially a gamma-ray colour. Two groups (blue points) are seen, those with durations > 2 s and soft gamma-ray spectra and those with durations < 2 s and harder gamma-ray emission. These GRBs are taken from the BATSE catalogue. Also shown (in red) are the short bursts detected by *Swift* and *HETE-2* over the past 18 months.



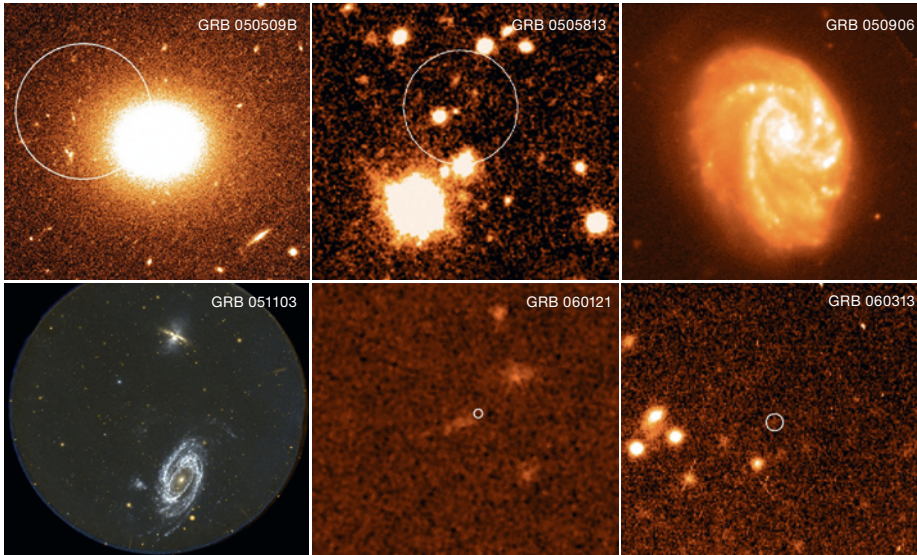


Figure 2: The diverse possible host galaxies of several short duration GRBs. GRB 050509B, the first localised short GRB, had no optical afterglow, no supernova (Figure 3) but was localised to an elliptical galaxy at $z = 0.225$ (image from VLT). GRB 050813 had no optical afterglow. In its error circle several galaxies at $z = 1.72$ were found (image from VLT). GRB 050906 had no afterglow either but inside the error circle (which is much larger than the image shown) the galaxy IC 328 ($z = 0.031$) was present (image from VLT). Inside the large IPN error box of GRB 051103 several galaxies from the nearby M81/M82 group were found (image from GALEX). GRB 060121 had a faint optical afterglow and was localised to a very faint galaxy (image from HST). GRB 060313 had a bright afterglow discovered at ESO and was localised to a very faint galaxy (image from VLT).

Optical emission from a short GRB was finally found for the HETE-2 GRB 050709 (Hjorth et al. 2005b) using the Danish 1.5-m telescope at La Silla. Gemini observations pinpointed the burst to a dwarf galaxy at $z = 0.16$. This emission is likely to be synchrotron emission, just as in long GRBs. Another short burst with an optical afterglow was GRB 051221 at $z = 0.54$. These results firmly place short GRBs at cosmological distances. However, the evidence so far indicates that they are at moderate redshifts, closer than the mean for the long GRBs which now lies at $z = 2.8$ (Jakobsson et al. 2006), a result which in itself relies significantly on ESO efforts.

Host galaxies

One of the striking differences between long and short GRBs is in the properties of their host galaxies. Long GRB hosts are mostly blue, sub-luminous and star-forming, and the GRBs preferentially occur in their brightest regions (Fruchter et al. 2006). In contrast, short GRB host galaxies seem to be a more varied class, and can be red, old and non-star-forming, with the GRBs originating at occasionally large radial separations from the host core. Any model for the origin of the short GRBs must naturally explain these observations; so far the prevailing choice is therefore compact objects – compact object mergers, e.g., neutron star – neutron star (NS-NS) or neutron

star – black hole (NS-BH). These systems merge following orbital decay due to emission of gravitational radiation. Based on observations of known systems in the Milky Way, it is clear that this can take billions of years. Also, on creation, a neutron star obtains a large ‘kick’ from the supernova, removing it from the region of star formation in which it was made, and, potentially pushing the binary far from its host galaxy at the time of the merger. This has made compact binary mergers the most popular model for short GRB origin, yet some observations continue to challenge this suggestion.

Light curves

So far, the optical afterglows of short GRBs have typically been fainter than for long GRBs (Figure 4). This has meant

that the afterglows have been less well sampled and few good spectral energy distributions have been secured. For this work 8-m telescopes are required, even at early times. By far the best early optical light curve for a short GRB comes from GRB 060313, with observations beginning on the ground (from the Danish 1.5-m telescope) only six minutes after the burst and continuing for several hours. At the VLT, following a Rapid Response Mode activation, a total of twenty seven 100-second observations were obtained. These high-S/N and high-cadence observations allowed rapid, small amplitude variability to be seen. This suggests that energy is being input into the afterglow out to late times post-burst. This is problematic for merger models, since the final coalescence should occur very rapidly, with little material remaining to fuel the burst afterwards. One possible

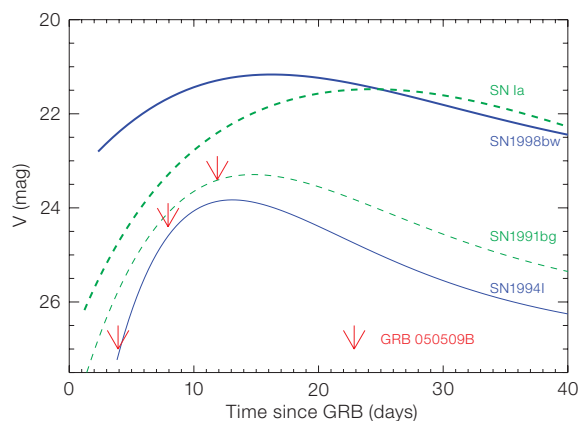


Figure 3: No supernova associated with short GRB 050509B. The upper limits (red arrows) on variable sources inside the GRB 050509B error circle (see Figure 2) compared to the light curves of different SNe redshifted to $z = 0.225$ (blue: Type Ic; green: Type Ia; thick curves: bright supernovae; thin curves: faint supernovae). The stringent upper limits obtained with the VLT rule out the presence of a super-nova accompanying the first localised short burst, GRB 050509B.

solution of this puzzle is that after the merger, a neutron star/magnetar rather than a black hole is formed.

Near and far

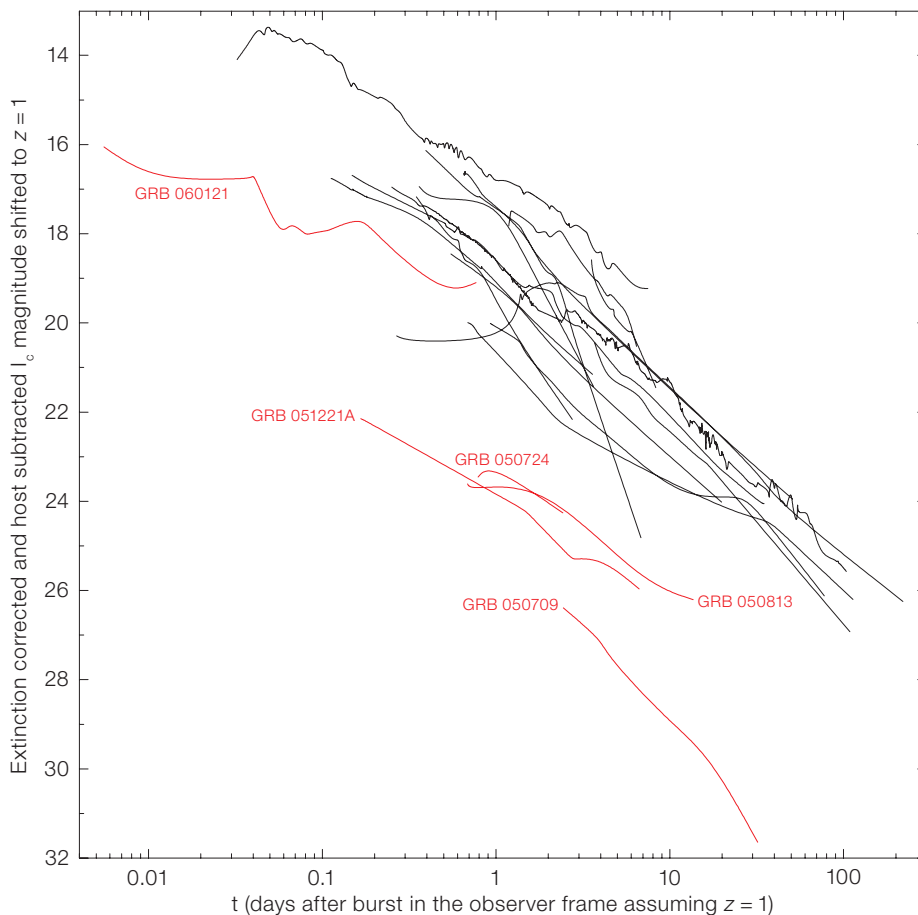
In parallel with these discoveries, other insights into the nature of short bursts were also emerging. At the end of 2004 the Galactic soft gamma repeater SGR 1806–20 underwent a giant flare, re-releasing over 10^{46} ergs of energy in 0.2 s. This event could have been seen from tens of megaparsecs away, and indicated that some short bursts may arise from similar flares (Hurley et al. 2005; Palmer et al. 2005). This being the case it might be expected that GRBs would correlate with large-scale structure in the local universe, and indeed our comparison of the locations of bursts seen by BATSE with the locations of local galaxies revealed that between 10–25% of short bursts might originate from within 100 Mpc (Tanvir et al. 2005). This may be supported by the presence of the bright nearby galaxy IC 328 in the error box of the short GRB 050906 and the short GRB 051103 localised to the M81/M82 galaxy group (Figure 2).

But these nearby short GRBs only represent one extreme of the population. At the other end, the short GRB 060121 (Figures 2 and 4) was found to originate in a very faint and red host galaxy, which may have $z > 4.5$, and therefore a much larger energy budget than previously known short bursts. Similarly, GRB 060313 (Figure 2) also has a faint host, possibly indicative of a higher redshift.

Where next?

Recent progress in understanding short bursts has been both dramatic and yet the picture is far from complete. It would seem hard to explain the full range of behaviour of short bursts with a single progenitor model, and it is likely that more than one progenitor type (e.g. SGR flares, and compact binary mergers) is required. Even allowing for this, the luminosity function and distance range of the two (or more) systems must be extremely broad.

Figure 4: Illustrative light curves of long GRBs (black) and short GRBs (red). The light curves have been interpolated, corrected for extinction and shifted to a common redshift of $z = 1$. The afterglows of short GRBs are much fainter in the mean than those of long GRBs. The curve for GRB 050813 represents an upper limit. The redshift of GRB 060121 has been assumed to be $z = 4.6$.



Fortunately, ESO telescopes are likely to drive further progress. We expect that the continued build-up of light curves (through Rapid Response Mode and Target of Opportunity observations) and host galaxies (through our dedicated Large Programme to study galaxies of long and short GRBs) will allow stronger statements to be made about the progenitors of short GRBs. Detailed modelling of light curves and broadband spectra will allow us to constrain the emission mechanism and physical properties such as the density of the surrounding medium. A statistical study of the galaxies hosting short GRBs should also give clues about formation time scales and environments.

Absorption line spectroscopy, as is routinely obtained on long GRBs for measuring redshifts and probing the environment of the progenitors, has so far not been successful on short GRBs. For GRB 060313 we obtained a spectrum which unfortunately was too noisy to reveal any significant absorption lines.

Another interesting line of research may be to obtain polarimetric observations. In contrast to long GRB afterglows, the ordered, strong magnetic field of a neutron star may imply that NS-NS mergers create highly polarised afterglows.

Whatever else we learn, our experience of attempting to resolve the puzzle of GRBs tells us to expect many further surprises.

References

- Fruchter A. et al. 2006, *Nature* 441, 463
- Gehrels N. et al. 2005, *Nature* 437, 851
- Hjorth J. et al. 2003, *Nature* 423, 847
- Hjorth J. et al. 2005a, *ApJ* 630, L117
- Hjorth J. et al. 2005b, *Nature* 437, 859
- Hurley K. et al. 2005, *Nature* 434, 1098
- Jakobsson P. et al. 2006, *A&A* 447, 897
- Kouveliotou C. et al. 1993, *ApJ* 413, L101
- Palmer D. et al. 2005, *Nature* 434, 1107
- Pedersen K. et al. 2005, *ApJ* 634, L117
- Tanvir N. et al. 2005, *Nature* 438, 991

Probing the Universe Using a Mostly Virtual Survey: The Garching-Bonn Deep Survey

Marco Hetherscheid¹
 Patrick Simon¹
 Thomas Erben¹
 Peter Schneider¹
 Mischa Schirmer²
 Jörg P. Dietrich^{1,8}
 Hendrik Hildebrandt¹
 Oliver Cordes¹
 Tim Schrabback¹
 Lutz Habertzettl^{3,6}
 Olaf Schmithuesen³
 Clemens Trachternach³
 Christian Wolf⁴
 Klaus Meisenheimer⁵
 Alberto Micol⁷
 Francesco Pierfederici⁸

¹ Argelander-Institut für Astronomie, Universität Bonn, Germany

² Isaac Newton Group of Telescopes, Santa Cruz de La Palma, Tenerife, Spain

³ Astronomisches Institut der Ruhr-Universität Bochum, Germany

⁴ Denys Department of Physics, University of Oxford, United Kingdom

⁵ Max-Planck-Institut für Astronomie, Heidelberg, Germany

⁶ Department of Physics and Astronomy, University of Louisville, USA

⁷ ESA/ESO Space Telescope European Coordinating Facility, Garching, Germany

⁸ ESO

We have entered a new era of powerful instruments, enabling high-precision cosmological observations. The Wide-Field-Imager (WFI) at the ESO/MPG 2.2-m telescope is a precursor of them since its field of view is large and of superb image quality. We employed the WFI to compile the *Garching-Bonn Deep Survey* (GaBoDS), where most of the high-quality images are obtained via data mining the ESO archive. This large *virtual* survey is used to determine some of the statistical properties of the Universe utilising weak gravitational lensing.

Gravitational lensing describes the deflection of light from distant objects by intervening mass concentrations in the Universe. Galaxy images which are affected by lensing change their apparent position and flux, but the main observ-

able is a systematic distortion of their shape. Amongst the most prominent examples of gravitational lensing are strongly deformed images of objects behind massive galaxy clusters. They can appear as very elongated, arc-like structures or even as multiple images from a single source as shown in Figure 1.

During the last decade large-format CCD mosaic cameras have been developed which can map up to one square degree of the sky with a single exposure. Furthermore, significant improvements in the image quality of optical observations have been achieved. With these technical developments and expanding data sets, lensing studies have increasingly concentrated on the *weak lensing regime* of field galaxies. Here, the coherent gravitational light deflection of distant galaxies by the tidal gravitational field of the large-scale structure (LSS) in the Universe induces only weak shape distortions of galaxy images. This weak gravitational lensing effect by the LSS is called *cosmic shear* and can only be measured statistically by averaging the distortion signal of many background galaxies.

After its first detection in 2000, cosmic shear has become one of the pillars of our cosmological model. Gravitational

light deflection is independent of any assumptions on the relation between dark and luminous matter. It can therefore explore the statistical properties of the LSS and constrain cosmological parameters. Furthermore, the cosmic shear signal can be used to reconstruct maps of the projected mass density field of the LSS. By cross-correlating these maps with galaxy surveys, one can study galaxy biasing as a function of redshift and angular scale. Here we present a report on our cosmic shear and galaxy biasing analysis of the GaBoDS.

GaBoDS – a mostly virtual survey

In 2002, our group started a weak lensing survey with the WFI at the ESO/MPG 2.2-m telescope. The WFI mosaic camera turned out to be an excellent instrument for weak lensing studies because it has a very well-behaved point spread function (PSF) over the whole field of view (FOV; see Figure 2).

The shape distortion of distant galaxy images induced by the LSS is weak and its measurement very noisy since the images of faint distant galaxies typically comprise only a few CCD pixels. Hence, besides the necessary analysis tech-



Figure 1: The rich lensing cluster RXJ1347-1145 at a redshift $z = 0.45$. It was observed with the ACS on board the HST for a total of nine orbits in the three broad-band colours g , i and z . Image by Thomas Erben and Tim Schrabback.

niques to extract a reliable source catalogue, we need high-quality data to perform a successful cosmic shear analysis:

- The data must be observed under superb seeing conditions in clear, dark nights. This ensures a sufficiently high number density of faint background sources to obtain statistically significant results.
- Weak lensing surveys of at least 10–20 square degrees are necessary to obtain significant cosmological constraints. The fields should be spread over a large fraction of the sky in order to have a statistically representative sample.
- A quantitative analysis of lensing signals requires knowledge of the redshift distribution of the galaxy population which is best obtained from the cosmic shear data itself, for instance in the form of photometric redshifts.

It turns out that a cosmic shear survey of about 10 square degrees is very difficult to execute with regular observing proposals on a short timescale, even with wide-field imaging and Service mode observations which ensure data of high quality. On the other hand, several observing programmes, such as the multi-colour ESO Deep Public Survey¹ (DPS, Hildebrandt et al. 2006a) or the Capodimonte Deep Field², obtained data which are well suited for cosmic shear studies. After a one-year proprietary period (not for the DPS) those data sets became publicly available to the astronomical community via the ESO archive and we could immediately add them to our own observations. Therefore, we initiated a dedicated archive research proposal within the ASTROVIRTEL³ project (ASTROVIRTEL cycle 2: *Gravitational lensing studies in randomly distributed, high galactic latitude fields*; P.I. Thomas Erben) to systematically search the ESO archive for high-quality WFI observations. Our archive query requirements, which aim at observations with a minimum observing time in a given filter configuration, together with constraints on seeing and galactic latitude, needed a substantial extension of the existing archive interface. To this end, the ASTROVIRTEL team de-

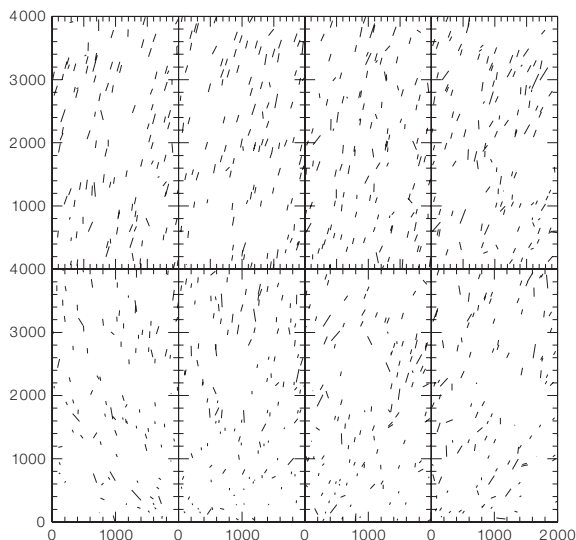


Figure 2: A typical ellipticity distribution of stellar objects for a WFI exposure with a seeing of 1''. WFI is a CCD mosaic camera with 4 × 2 chips each having 2K × 4K image pixels. The total field of view of the camera is 34' × 33'. The sticks indicate the orientation and length of the stellar ellipticity in the field. No stellar image has an ellipticity larger than 2.5% (corresponding to an ellipse with an axis ratio of ~ 0.95) and the PSF is smooth over the whole field of view.

veloped the tool *querator*⁴ which extends the traditional archive query form for telescope, camera, filter configuration and object position by advanced search possibilities for multi-colour observations and our needs. Whereas we obtained one square degree of usable data with our own observations in the first year, the archive search with *querator* provided us, without new observations, with 4.5 square degrees within two months. Together with the previously retrieved archive data, WFI data from the COMBO-17 project (e.g. Wolf et al. 2004) and the EDisCS survey (White et al. 2005), the GaBoDS currently consists of 15 square degrees of high-quality imaging data.

All raw science and calibration frames were reduced and analysed in a homogeneous way, employing the THELI pipeline that we developed and released publicly (Erben et al. 2005). THELI is a stand-alone reduction pipeline based on UNIX scripts which uses only open source software, and which makes heavy use of pre-existing software modules. The pipeline has been developed with weak lensing applications in mind: owing to the stringent requirements posed by weak lensing, the relative astrometric accuracy of the dithered individual exposures must be better than about 1/10 of a pixel to not introduce artificial image ellipticities in the coaddition process.

The GaBoDS is a useful cosmic shear survey due to its field depth (*R*-band limiting magnitude between 25.0 mag and 26.5 mag; 5 σ sky level measured in a circular aperture of 2'' radius) and seeing (between 0.7'' and 1.2''). This yields a large number of faint galaxies that we finally used for our cosmic shear analysis (almost 10⁶ galaxies) and permits a good PSF correction. Furthermore, the images form small patches which are widely separated in the sky, hence they are uncorrelated (Figure 3).

Cosmic shear analysis with GaBoDS

In the weak lensing regime, shape distortions are characterised by a quantity called shear. It quantifies the anisotropic stretching of a source image, where, for example, an intrinsically round object is deformed into an ellipse. The shear can be estimated from the galaxy ellipticity which is directly related to its observable light distribution. Correlations in the *cosmic shear field* (the coherent shear pattern) are connected to the matter density power spectrum and its underlying cosmology. We calculated from the measured correlations the aperture mass dispersion. The aperture mass measures the tangential alignment of galaxy images relative to a chosen reference point, and thus quantifies the local strength of the coherent shear field (just like the tangential stretching of arcs measures the lensing strength of a cluster; see Figure 1). Its dispersion is a powerful cosmic shear

¹ <http://www.eso.org/eis>

² ESO Press Photos 15a-f/01

³ <http://www.euro-vo.org/astrovritel/>

⁴ <http://archive.eso.org/querator/>

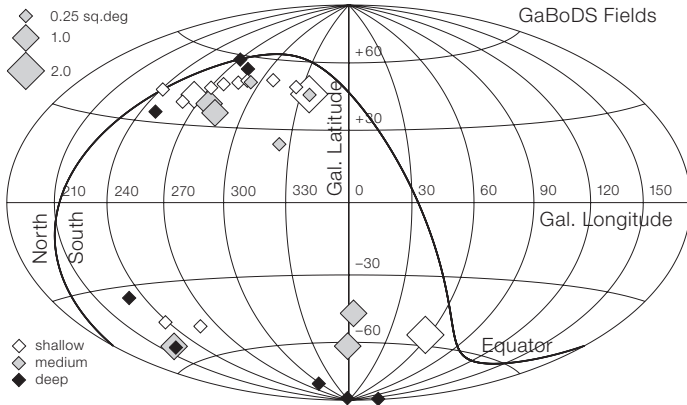


Figure 3: Sky distribution of the GaBoDS fields. The survey has a total area of 15 square degrees and contains 29 different lines of sight, all at high galactic latitude. The different patches comprise areas from 0.25 up to 2 square degrees.

estimated from external redshift surveys covering only a small area in the sky. These DPS fields yield accurate photometric redshift information for about 10% of the galaxies considered for the cosmic shear analysis. To acquire a smooth redshift distribution for all galaxies of the GaBoDS galaxy lensing catalogue, we perform a five-parameter fit to the measured redshift distribution.

Cosmological parameters from cosmic shear

For our cosmic shear analysis of the GaBoDS we calculated the aperture mass dispersion and found no significant systematic errors resulting from the data treatment (e.g. an imperfect PSF-anisotropy correction), see Figure 5. This en-

Figure 4: Example of a PSF anisotropy correction. Upper panels: the uncorrected (e_1 , e_2 , left) and PSF-corrected (e_1' , e_2' , right) stellar ellipticity components. Lower panels: the uncorrected stellar ellipticity (left) and the ellipticity of the interpolation (right) as a function of position. Here, the interpolation is a low-order 2D polynomial fit to the stellar ellipticities.

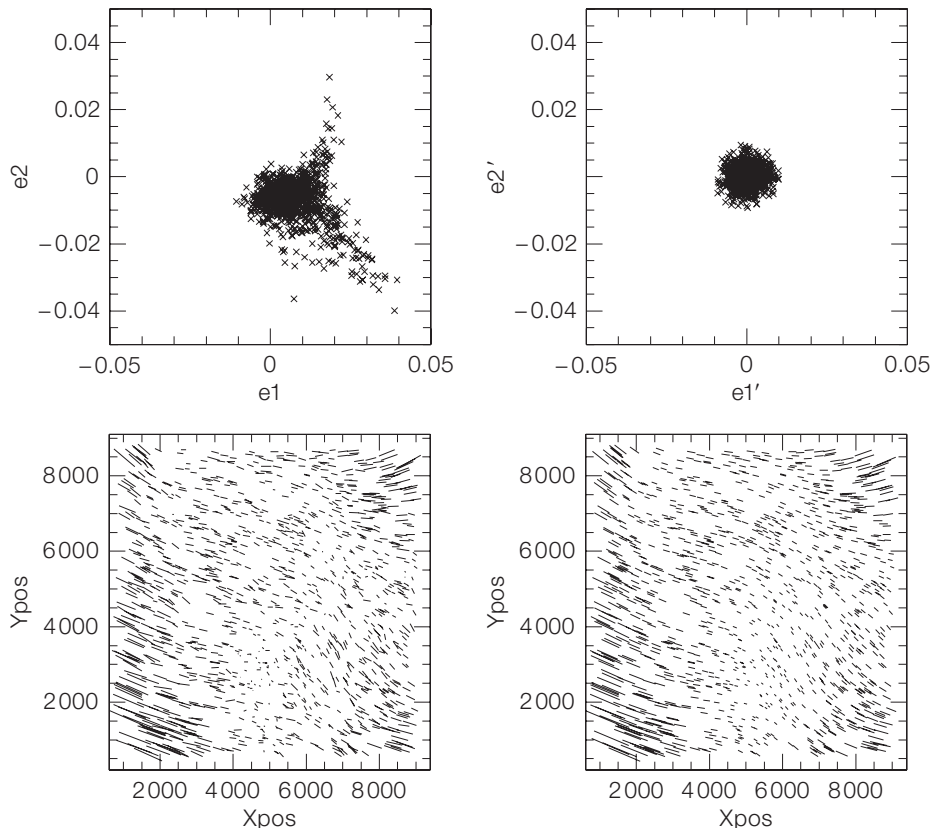
measure since it is a very local measure of the power spectrum of the line-of-sight projected mass density. Moreover, it is a sensitive tool to reveal possible systematic errors in the data.

PSF correction

Cosmic shear induces per-cent level correlations in the ellipticities of distant galaxy images which can be an order of magnitude lower than correlations induced by systematic effects, like the anisotropic PSF. The correction of these systematics is challenging and has to be tested and applied carefully. Therefore, we performed a precise PSF correction method to obtain reliable shear estimates. The correction is done in two steps. One first has to correct the galaxy ellipticities for the effect of an *anisotropic* PSF using a sample of bright, unsaturated stars which are point-like and unaffected by lensing. Measuring their ellipticity yields the PSF anisotropy pattern of the field. Since the PSF anisotropy of the coadded images from the WFI is rather small and varies smoothly over the total FOV, we perform an *interpolation* of the stellar anisotropy over the entire FOV (Figure 4) to estimate the PSF anisotropy at the position of the galaxies. Second, the *isotropic* smearing caused by seeing has to be accounted for. Specialised software for these tasks has been developed independently and thoroughly tested, most recently in a world-wide blind test: the STEP project (Heymans et al. 2006).

Redshift distribution of galaxies

For quantitative cosmic shear analyses not only the observed shape of source galaxies but also their redshift distribution has to be known. This distribution is directly estimated from galaxies of seven statistically independent DPS fields observed in *UBVRi*. In this way, the total error estimate of our redshift distribution includes sampling variance. This is an advantage of the GaBoDS since we do not have to rely on redshift distributions



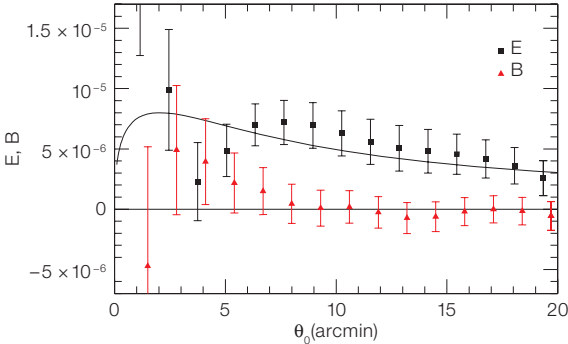


Figure 5: The decomposition of the aperture mass dispersion signal into E- and B-modes of the GaBoDS fields. The E-modes carry the cosmic shear signal, whereas ‘curl-like’ B-modes are not expected from lensing and would indicate remaining systematics. The line is a CDM prediction assuming a flat Universe with $\Omega_m = 0.3$ and $\sigma_8 = 0.9$.

couraged us to perform a cosmological parameter estimate (Hettterscheidt et al. 2006). For this purpose we combine the fit of the redshift distribution with the cosmic shear signal and estimate the total noise covariance matrix in an unbiased way *directly from the data without any further assumptions*, since the observed fields are statistically independent. Our analysis is basically concentrated on the mass power spectrum normalisation, σ_8 , and the total matter density, Ω_m . For this estimate we assume a flat Λ CDM Universe with negligible baryon content. We derive σ_8 and Ω_m while marginalising over the HST Key Project uncertainties in the Hubble parameter and the source redshift distribution. We employ the so-called Monte Carlo Markov Chain, an efficient method to estimate the posterior likelihood in our *eight-dimensional* parameter space (Ω_m , σ_8 , h , and the five fit parameters of the redshift distribution).

As a result we obtain the joint constraints on Ω_m and σ_8 (Figure 6). The confidence contours reveal the typical ‘banana’-like shape reflecting the strong degeneracy between these two parameters, hence they are poorly constrained without further priors: $\sigma_8 = 0.61^{+0.31}_{-0.20}$ and $\Omega_m = 0.46^{+0.30}_{-0.22}$. Measurements of the CMB, however, yield a degeneracy in the Ω_m - σ_8 plane that is almost perpendicular to that of cosmic shear (Figure 6). Combining them would therefore substantially improve the Ω_m , σ_8 estimate.

The GaBoDS data set alone yields a normalisation of $\sigma_8 = 0.80 \pm 0.10$ (1σ statistical error) for a fixed total matter density of $\Omega_m = 0.3$, which is of similar accuracy to those obtained from measurements of the CMB and galaxy clusters.

Probing galaxy bias with GaBoDS

The relation between the spatial distribution of galaxies and the distribution of dark matter is expressed *statistically* by galaxy biasing parameters. Weak gravitational lensing provides a unique method to study the dark-matter distribution independently from the galaxy distribution, and to compare the two in order to measure the galaxy bias. Moreover with lensing, also the smaller, highly non-linear scales can be assessed which is not possible with other methods relying on linear perturbation theory.

In Figure 7 the basic concept of galaxy biasing and its measurement is illustrated. From the statistical point of view, *bias parameters* quantify the auto- and cross-correlation of the matter and galaxy distribution. Observationally, the projected mass distribution is measured

in terms of the shear, whereas the projected galaxy distribution is seen as their distribution in the sky. The bias parameter b is the ratio of rms fluctuations of galaxies and matter, whereas the correlation coefficient r quantifies the correlation of galaxies and matter. Unbiased fields have $b = r = 1$.

Our primary interest is in the *spatial values* of b and r and not their projections in the sky. Therefore, we perform a deprojection of the measurements based on a fiducial cosmology, and the redshift distribution of foreground and background galaxies.

In Simon et al. (2006), we measured the spatial bias parameters b and r on *different scales*. The fluctuations in the projected matter distribution are smoothed using the already mentioned aperture mass; the filter radius determines the scale we are looking at. The aperture mass fluctuations are then compared to the projected number density of (foreground) galaxies, smoothed by using the same aperture filter as the one used for the aperture mass.

We perform the galaxy bias analysis for three different foreground galaxy samples that are selected by R -band magnitude. The redshift distributions of galaxies in the various samples are estimated from the COMBO-17 survey which provides

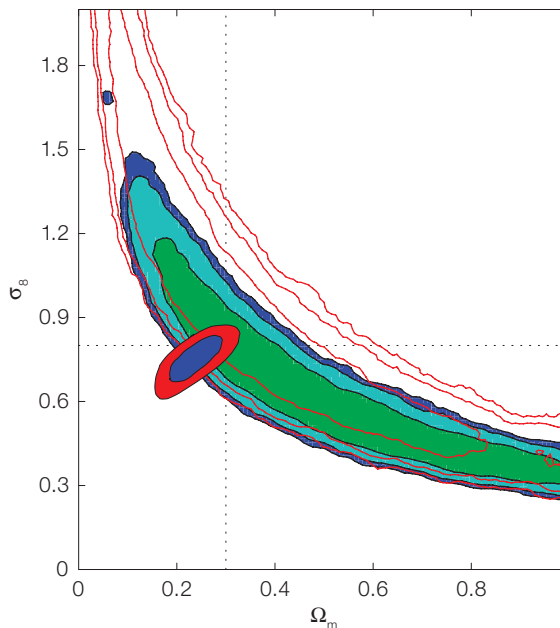
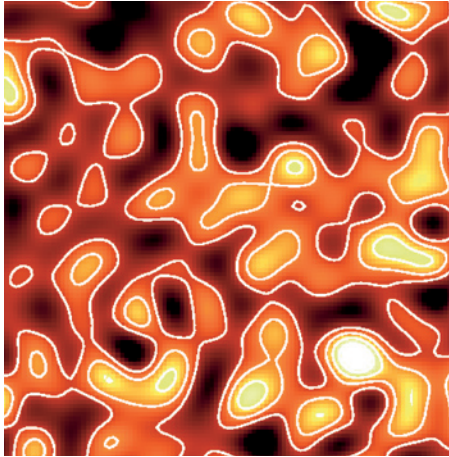
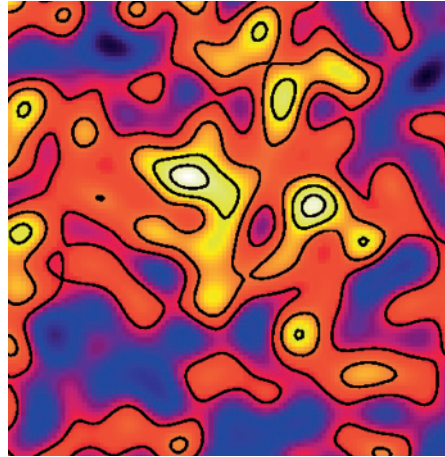


Figure 6: Joint marginalised constraints on σ_8 and Ω_m from our cosmic shear analysis of the GaBoDS data set. The shaded regions and the red contours show 1,2,3 σ significance regions, obtained with two different cosmic shear statistical measures. Overlaid is a sketch of the joint constraint for WMAP only (Spergel et al. 2006, 1 σ and 2 σ contours in blue and red, respectively).

Figure 7: Left: smoothed fluctuations in the number density distribution of ‘foreground’ galaxies in the sky ($21.0 \leq R \leq 23.0$) as observed in the A901 field. Right: projected and smoothed fluctuations in the total matter density obtained from image ellipticities of faint ‘background’ galaxies ($21.5 \leq R \leq 24.0$) within the same field of view. Comparing, in a statistical sense, both maps allows a measurement of (pro-



jected) galaxy bias, thus the relation between the distribution of matter and galaxies. Although galaxies are almost unbiased tracers of the matter distribution at low redshift, both maps appear quite different. This is partly due to overlaid shot-noise patterns, but also partly due to different redshift sensitivities of the projections. We accounted for both in the final analysis.



Outlook

The use of the GaBoDS data is not restricted to lensing analyses, but has already been extended to other projects as well, including Lyman-break galaxies (Hildebrandt et al. 2006b). We have made our reductions and derived products of a large fraction of the GaBoDS data publicly available via the ESO archive, such as the DPS^{5,6}, which includes the ultra-deep WFI image of the Chandra Deep Field South⁷. With its substantial scientific output, the GaBoDS is a good example for the use of the ESO archive. The upcoming public surveys with the new VST and VISTA telescope will provide an enormous increase of such data products, and we foresee a large scientific harvest from these surveys.

References

- Erben T. et al. 2005, AN 326, 432
 Hetherscheidt M. et al. 2006, A&A, submitted
 Heymans C. et al. 2006, MNRAS 368, 1323
 Hildebrandt H. et al. 2006a, A&A 452, 1121
 Hildebrandt H. et al. 2006b, A&A, submitted
 Simon P. et al. 2006, A&A, in press
 Spergel D. N. et al. 2006, ApJ, submitted
 Springel V. et al. 2005, Nature 435, 629
 White S. D. M. et al. 2005, A&A 444, 365
 Wolf C. et al. 2004, A&A 421, 913

⁵http://archive.eso.org/archive/adp/GaBoDS/DPS_stacked_images_v1.0/

⁶<http://marvin.astro.uni-bonn.de/DPS>

⁷ESO press release (14.04.2006): <http://www.eso.org/outreach/press-rel/pr-2006/pr-14-06.html>

accurate photometric redshifts for three of the GaBoDS fields that are thought to represent the whole survey. The samples have a relatively wide distribution with means of $\bar{z} = 0.34 \pm 0.18$, 0.47 ± 0.22 , 0.62 ± 0.27 (‘foreground’) and $\bar{z} = 0.67 \pm 0.29$ for the mean redshift of galaxies inside the lensing catalogue (‘background’); the 1σ -widths of the distributions are also given. Therefore, the three foreground samples represent galaxies at different redshifts, albeit as averages over a quite large range.

The final result was obtained by combining the measurements for all individual GaBoDS fields. The result for the bias parameters is very similar for all three galaxy samples and is shown for the brightest sample in Figure 8. This means that over the observed redshift range, and for the range of scales considered, the bias evolution is relatively mild.

The bias factor shows indications for a scale-dependence with an anti-bias, $b < 1$, at about $3h^{-1}$ Mpc; towards smaller

(and perhaps also larger) scales the bias factor rises again. This behaviour, especially a scale-dependence of b on scales where the structure growth is in the non-linear regime, is expected from cosmological simulations such as in Springel et al. (2005). The average of b between one and eight Mpc/ h , weighted by the statistical uncertainty of our measurement, is $\bar{b} \approx 0.8 \pm 0.1$.

The correlation between the matter and galaxy distributions is measured with larger uncertainties. Still, we find that there is a decorrelation between both in all three samples with an average (over the same range of scales as for \bar{b}) of approximately $\bar{r} \approx 0.6 \pm 0.2$. The fact that this correlation is not perfect, i.e. $r \neq 1$, implies that the biasing of galaxies is either non-linear and/or stochastic. In order to disentangle non-linear and stochastic biasing, a higher-order correlation analysis will be required which is within reach by the upcoming weak lensing surveys.

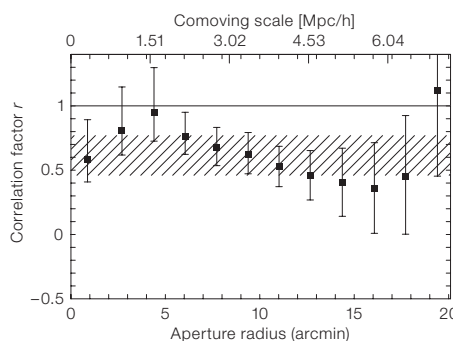
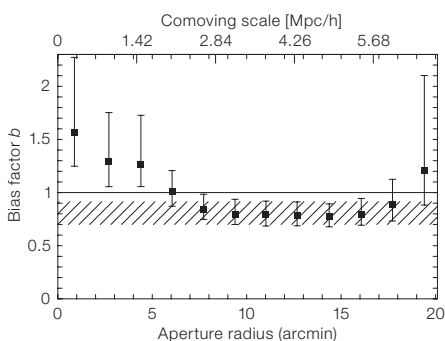


Figure 8: Left: Spatial linear bias factor b of the brightest ‘foreground’ galaxy sample (the effective comoving spatial scale in the top axis is based on the mean redshift of the sample, $\bar{z} \approx 0.34$). Right: Spatial linear correlation r between total matter fluctuations and galaxy number density fluctuations. Shaded areas denote the 1σ -confidence of the average b and r for smoothing scales between $2'$ and $19'$. The results are for a flat Universe with $\Omega_m = 0.3$. Note that the errors of neighbouring bins are strongly correlated.

Burst or Bust: ISAAC at Antu Sets New Standards with Lunar Occultations

Andrea Richichi¹
 Octavi Fors^{2,3}
 Elena Mason¹
 Jörg Stegmeier¹

¹ ESO
² Departament d'Astronomia i Meteorologia, Universitat de Barcelona, Spain
³ Observatori Fabra, Barcelona, Spain

Imagine a car as fast as a Ferrari, and as cheap as a Trabi. Sounds crazy? Maybe it is, but when it comes to high angular resolution in astronomy there is something that comes close to the miracle: lunar occultations. As the Moon moves over a background star, the phenomenon of diffraction causes tenuous, quick fringes to appear in the stellar light just before it vanishes. The fringes carry valuable information on the size of the source, on scales much smaller than possible with even a perfect, extremely large telescope. Paranal is now superbly equipped to perform this kind of observation, and for that matter all sorts of high-speed near-IR photometry. And the results are impressive. Find out more about the ISAAC burst mode, which is now officially supported from Period 79.

The power of lunar occultations

Astronomers are always seeking to resolve the smallest possible angular details of their favourite sources, and for this they are prepared to invest huge amounts of

money and resources. You are certainly familiar already with the wonderful results afforded by adaptive optics and long-baseline interferometry, but no doubt you will have also been struck by their complications. However, there is a way to obtain very high angular resolution, far exceeding the diffraction limit of any telescope, and still keep the whole business simple for the mind and easy on your observatory budget. Even better, it is possible to achieve this under any seeing and with an optical quality of your mirror which would send any self-respecting optician into a rage. How? Well, let us forget about the telescope in the first place. Instead, let us use an entirely different apparatus, namely the Moon. More precisely, its edge. As the lunar limb occults a distant background source, diffraction fringes are generated. From the analysis of these fringes, it is possible to infer the size of the occulted source, and even to reconstruct a precise scan of its brightness profile. Since the diffraction phenomenon takes place in space, the quality of the atmosphere or the optical quality of the telescope we use to look at does not really matter to a first approximation. The fringes have a characteristic size which is determined by the distance to the Moon and the wavelength, and is typically several metres across at the Earth surface. However, they also move rather fast, almost one kilometre per second on average. Therefore, the trick is to measure them fast: in order to achieve a good measurement, sampling rates of about 1 millisecond are required.

To be sure, there are some critical limitations in this technique: for one, you cannot choose which sources in the sky the Moon is going to occult, and when. Other more subtle limitations are that, lunar occultations being fixed-time events, their observation can easily be wiped out by a single cloud in the wrong place at the wrong time. And it might take a long, long time until the next opportunity: the Moon moves across the sky following a so-called Saros cycle, the same as solar eclipses. For the record, it lasts about 18.5 years! Also, a lunar occultation only gives a one-dimensional scan of the source. In spite of these limitations, lunar occultations have represented the main provider of stellar angular diameters for decades. Their typical angular resolution and sensitivity have been only recently reached, and sometimes surpassed, by a few long-baseline interferometers such as the ESO VLTI.

Lunar occultations at Paranal

So if some interferometers can now offer the performance of lunar occultations, why do we still go around bragging about the Moon? There is one good reason: lunar occultations have just added a few more magnitudes to their sensitivity limit, thanks to a mode recently implemented at Paranal. Because occultations require very fast integration times, they have been traditionally observed by photometers, which in turn are usually found at small telescopes. However, clever read-out electronics also exist to read an array detector at a sufficiently fast rate, pro-

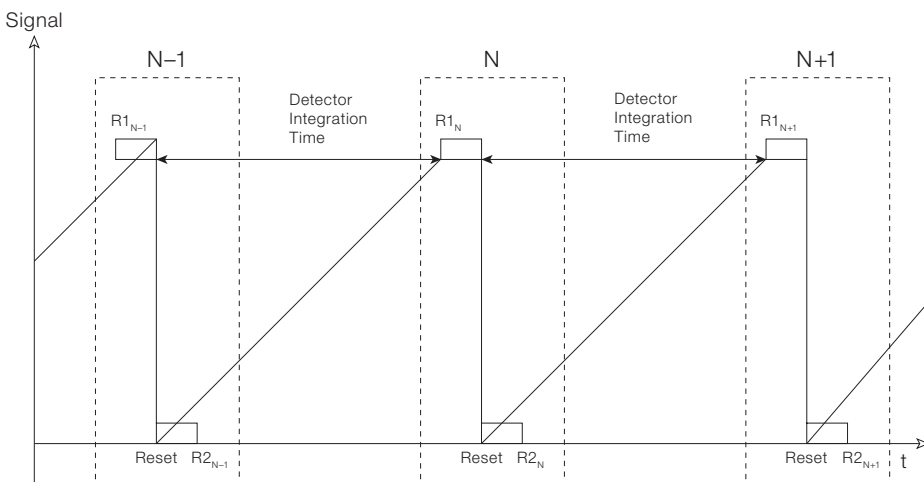
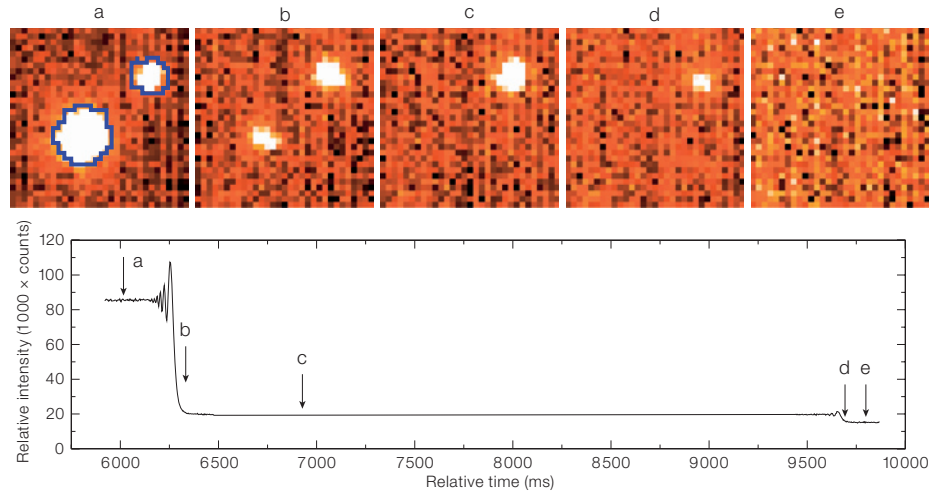


Figure 1: Read-out scheme (Read-Reset-Read). Two lines of the sub-window are read, then reset and read again. This is repeated for the whole sub-window and the result is computed as $R1_N - R2_{N-1}$. This read-out scheme allows a 100% duty cycle for minimum integration time (= read-out time of the sub-window).

Figure 2: The occultation disappearance of 2MASS17560902-2830501. At the top, five frames are shown at arbitrary positions in the data cube (total 6000 frames), as marked by the letters a–e. The light curve at the bottom has been reconstructed by performing a simple aperture photometry on each frame, using a mask shown in blue in the first frame. Two clearly separated stars are visible, giving rise to distinct diffraction patterns. The projected separation is 1423 ± 4 mas, and the brightness ratio $\Delta K = 2.96 \pm 0.02$ mag. This 'binary' is in fact too wide for occultations: not only are the two stars clearly resolved in standard imaging, but the wide separation also implies possibly different slopes of the lunar limb at the contact point.



vided that you are satisfied with a sub-window rather than the whole array, and the ESO IRACE is one of them (see Figure 1). Moreover, for such short integration times, the sensitivity is of course critically dependent on the telescope area.

The combination of Antu, ISAAC and IRACE seemed thus perfect, but we still needed a good justification to try them together in a convincing demonstration, and the opportunity was given by the close approach of the Moon to the Galactic Centre (GC). This is an event which is repeated every 18.5 years (remember, the Saros cycle!), and is observable only a few times from restricted regions on Earth. Due to lunar parallax and the southern location of the Paranal observatory, this time around the Moon would not go exactly over the GC, but still it would traverse a very crowded, very obscured region with literally tens of thousands of largely unknown infrared sources. We obtained time to perform observations

of two such passages, one in March and one in August 2006, for some hours each.

Obviously it was not possible to observe all the occultations: even if each event lasts less than a second, significant chunks of time are required just to point the telescope and to read out the data (refer to the ISAAC web pages for some typical numbers). After some practice, we found a good compromise in which each observation would require about two minutes. Thousands of frames for each cube are analysed and photometry is extracted through software masks that maximise the SNR by sampling as much as possible of the stellar signal and as little as possible of the background. An example of a lunar occultation data cube and the corresponding light curve is given in Figure 2. The analysis of hundreds of light curves is a tedious task, and for this we have developed a data pipeline that creates template files for the initial data reduction, aimed at a prelimi-

nary estimate for each occultation of parameters such as background and stellar intensity, rate of lunar limb motion, time of the occultations. These parameters are subsequently refined in an interactive analysis.

The passages near the Galactic Centre

The reward for these attempts was certainly satisfactory: we could record 53 events on 22 March, and 71 on 6 August. Thanks to the large collecting power of Antu, the quality of the data is unprecedented and it allowed us to reach new standards of sensitivity and precision. The VLT mirror is so large that scintillation is reduced to a very low level, since differences in wavefront amplitude from one turbulence cell in the atmosphere to the next are averaged out. Figure 3 illustrates this quality, by showing the light curves for both an unresolved and a resolved star.

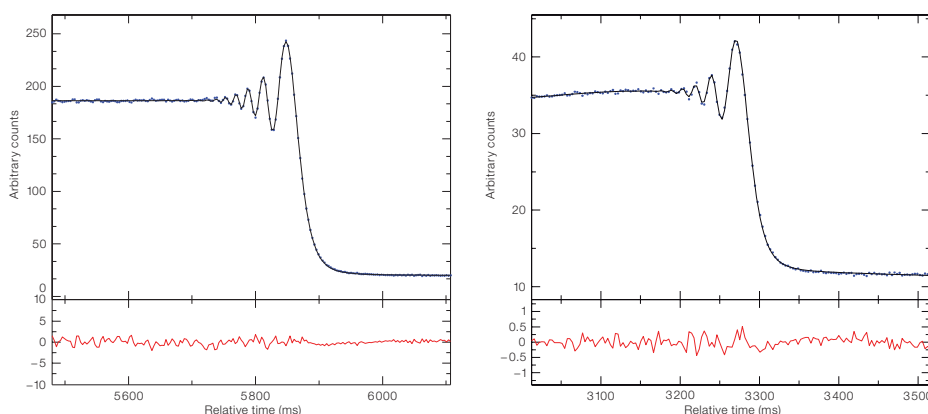


Figure 3: The light curves (top, blue) and best fit models (black) for 2MASS17474895-2835083 and 2MASS17582187-2814522. The bottom panels show the fit residuals (red), enlarged by a factor of four for clarity. The star on the left is unresolved, with an upper limit of the diameter of 0.65 mas. The other one is resolved, with an estimated diameter of 3.67 ± 0.56 mas. The difference between the two cases is in the number and amplitude of the diffraction fringes.

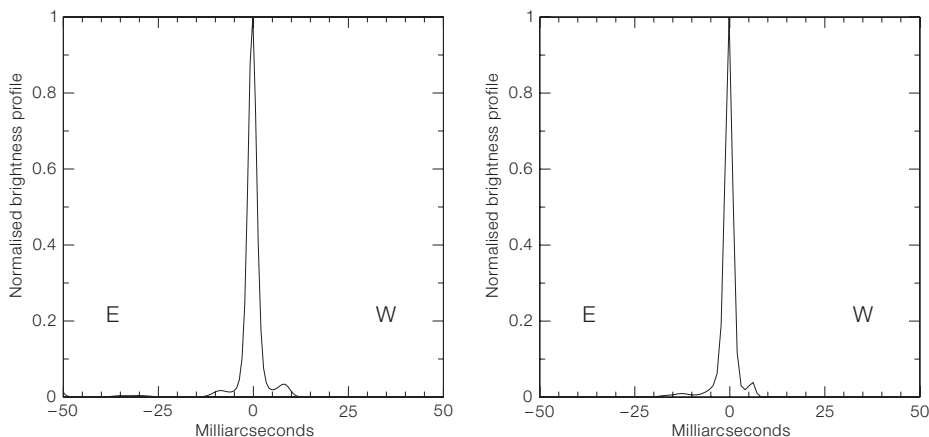


Figure 4: Examples of brightness profiles of stars surrounded by what are presumably compact dust shells. Left, the carbon star C2490 (2MASS17531817-2849492). Right, 2MASS17553507-2841150. In both cases, the inner rims of an optically thin shell are visible, indicating a non-symmetric structure and a characteristic size of about 20 mas.

A detailed analysis of the observations is in preparation, but we can already provide some general results for the August run. We have detected seven binaries, five resolved angular diameters and four stars with extended emission. It should be noted that almost all of our targets have no optical counterpart, and in fact almost no information is known except from that in 2MASS. Colours are very red, as is to be expected from the high interstellar extinction, but extreme cases (*J-K* up to 8 mag) are also present which point to possible strong local reddening. The stars with extended emission are particularly interesting, since this is probably due to the presence of compact circumstellar shells (see Figure 4). We have now submitted a proposal to follow up a selected number of sources by adaptive optics observations with NACO, and for which we hope to derive a fully consistent model of the star and the surrounding

dust from the combination of occultation, AO imaging and photometry.

We also mention that about 50 sources were found to be unresolved. This is also a useful result because it helps to establish a database of stars with high-accuracy upper limits that can be in turn adopted as calibrators for long-baseline interferometry at intermediate and faint magnitudes. We have established upper limits for the diameters of our unresolved sources which vary between 0.5 and 1.5 mas. We have also evaluated the sample in terms of SNR against magnitude, and we can reliably extrapolate to predict that the limiting sensitivity of this method at the VLT would be close to $K = 12.5$ mag, a new record for measurements with milliarcsecond resolution. This is fainter than even the theoretical performance of the VLTI in the combination of 2 UTs. Therefore, occultations with ISAAC at

UT1 represent at the moment the most sensitive technique available for such measurements anywhere in the world.

The way is now paved to observe lunar occultations in a routine fashion from Paranal. In fact, since occultations require a minimum amount of time and can be observed practically at any moment in which the Moon is above the night horizon, they represent an ideal filler programme for those occasional chunks of time when no other programmes are readily available either because of insufficient atmospheric conditions or because of their duration. In addition, the burst mode has many applications other than occultations by the Moon: phenomena that require rapid photometry for sustained periods of time are relatively frequent, and it is now up to the inventiveness and imagination of astronomers to find the best applications.



Gordon Gillet (ESO) captured this stunning photo of a moonset over Paranal. In addition to the four main unit telescopes (UTs), the VLT Survey Telescope (VST) is visible at the far right and the small, white VLTI auxiliary domes can also be seen.

This image was selected as Astronomical Picture of the Day on 4 November 2006; see <http://antwrp.gsfc.nasa.gov/apod/ap061104.html>

Measuring the Masses of Neutron Stars

Lex Kaper¹
 Arjen van der Meer¹
 Marten van Kerkwijk²
 Ed van den Heuvel¹

¹ Astronomical Institute “Anton Pannekoek” and Centre for High Energy Astrophysics, University of Amsterdam, the Netherlands

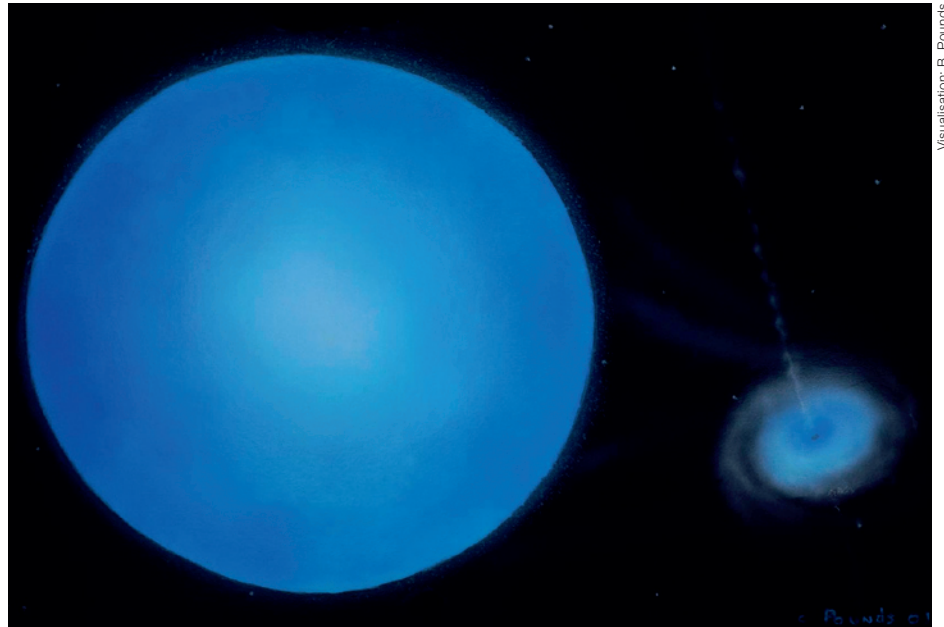
² Department of Astronomy and Astrophysics, University of Toronto, Canada

Until a few years ago the common understanding was that neutron stars, the compact remnants of massive stars, have a canonical mass of about $1.4 M_{\odot}$. Recent observations with VLT/UVES support the view that the neutron stars in high-mass X-ray binaries display a relatively large spread in mass, ranging from the theoretical lower mass limit of $1 M_{\odot}$ up to over $2 M_{\odot}$. Such a mass distribution provides important information on the formation mechanism of neutron stars (i.e. the supernovae), and on the (unknown) behaviour of matter at supranuclear densities.

The compact remnants of massive stars

A neutron star is the compact remnant of a massive star ($M \geq 8 M_{\odot}$) with a central density that can be as high as 5 to 10 times the density of an atomic nucleus. Neutron stars can be detected as radio sources (radio pulsars) or, when they accrete matter coming from a companion star in a binary system, as X-ray sources.

The global structure of a neutron star depends on the equation of state (EOS), i.e. the relation between pressure and density in the neutron star interior (Lattimer and Prakash 2004). So far, the physical properties of matter under these extreme conditions can only be studied on the basis of theoretical models. It is not yet possible to produce the required extremely high density in accelerator experiments. Given an EOS, a mass-radius relation for the neutron star and a corresponding maximum neutron-star mass can be derived. The ‘stiffness’ of the EOS depends e.g. on how many bosons are present in mat-



Visualisation: B. Pounds

ter of such a high density. As bosons do not contribute to the fermi pressure¹, their presence will tend to ‘soften’ the EOS. For a soft EOS, the maximum neutron star mass will be low ($\sim 1.5 M_{\odot}$); for a higher mass, the object would collapse into a black hole. More than 100 candidate equations of state are proposed, but only one EOS can be the correct one. Finding one massive neutron star ($M \geq 2 M_{\odot}$) would rule out the soft equations of state.

The measurement of neutron-star masses is thus important for our understanding of the EOS of matter at supranuclear densities. In practice, this can only be done for neutron stars in binary systems. The most accurate masses have been derived for the binary radio pulsars. Until recently, all of these were consistent with a small mass range near $1.35 M_{\odot}$ (Thorsett and Chakrabarty 1999). An exception is the X-ray pulsar Vela X-1 with a mass of $1.86 \pm 0.16 M_{\odot}$ (Barziv et al. 2001). This important result was obtained following a nine-month spectroscopic monitoring campaign with the ESO *Coudé Auxiliary Telescope* and the CES spectrograph, covering 36 orbits of the binary system. Over the past year a few more massive neutron stars were discovered, e.g. the millisecond radio pulsar J0751+

Figure 1: Artist's impression of a high-mass X-ray binary hosting a massive OB-type star and a compact X-ray source, a neutron star or a black hole.

1807 with a mass of $2.1 \pm 0.2 M_{\odot}$ (Nice et al. 2005). These results favour a stiff EOS.

A neutron star cannot be more massive than $3.2 M_{\odot}$, a limit set by general relativity. It is likely that the maximum neutron-star mass is determined by the stiffness of the EOS, and is expected to be about $2.5 M_{\odot}$. Neutron stars also have a minimum mass limit. The minimum stable neutron-star mass is about $0.1 M_{\odot}$, although a more realistic minimum stems from a neutron star's origin in a supernova. Lepton-rich proto neutron stars are unbound if their masses are less than about $1 M_{\odot}$ (Lattimer and Prakash 2004). Whether or not neutron stars occupy the full available mass range depends on the formation mechanism, i.e. the supernova.

We focus here on the initially most massive binary systems², which consist of a massive OB-supergiant and a neutron star (or a black hole). The main motivation to concentrate on these systems is that they are the most likely hosts of massive neutron stars. About a dozen of these systems are known; five of them

¹ The repelling force that neutrons (fermions) exert on each other so that a neutron star can sustain gravity.

² About 80% of the HMXBs are Be/X-ray binaries, where the (transient) X-ray source accretes material from the equatorial disc around a Be star.

contain an eclipsing X-ray pulsar. The masses of all but one (Vela X-1) are consistent (within their errors) with a value of about $1.4 M_{\odot}$. However, most spectroscopic observations used for these mass determinations were carried out more than 20 years ago, before the advent of sensitive CCD detectors and 8-m-class telescopes, which allow high-resolution spectroscopy of the optical companions. The uncertainties in the earlier radial velocity measurements are too large to measure a significant spread in mass among these neutron stars, if present.

High-mass X-ray binaries

High-mass X-ray binaries (HMXBs) represent an important phase in the evolution of massive binaries. They are composed of a massive OB-type star and a compact object, either a neutron star or a black hole (Figure 1). The X-ray source is powered by accretion of material originating from the OB star, transported by the OB-star wind or by Roche-lobe overflow. About a dozen HMXBs are known to host a massive OB-supergiant companion (about 10 to over $40 M_{\odot}$), in a relatively tight orbit (P_{orb} several days) with an X-ray pulsar or black-hole companion (Table 1). Some of these X-ray binaries include a dense accretion disc and produce relativistic jets. Recently, several new sources have been discovered with the ESA gamma- and hard-X-ray observatory INTEGRAL that show the characteristics of a HMXB with an OB-supergiant companion hidden by large amounts of interstellar dust (e.g. Negueruela et al. 2005); these are not included in the table.

The compact companion is the remnant of the initially most massive star in the system that exploded as a supernova. Due to a phase of mass transfer, the secondary became the most massive star in the system before the primary supernova, so that the system remained bound. A consequence, however, is that HMXBs are runaways due to the kick velocity exerted by the supernova (Blaauw 1961). When they run through space with supersonic velocity, the interaction of the OB-supergiant wind with the interstellar medium can result in the formation of a bow shock (see also The Messenger 89, 28).

The HMXB phase is relatively short for OB-supergiant systems, of the order of 10 000 years. This corresponds to the time required for the secondary to evolve into a supergiant when the hydrogen in the nucleus has been exhausted. As soon as the secondary has become an OB-supergiant it develops a strong stellar wind. The accretion of wind material turns the compact object into an observable X-ray source. Once the supergiant starts to overflow its Roche lobe, the mass transfer rate increases further so that an accretion disc is formed around the compact object, turning it into a very strong X-ray source accreting at the Eddington limit. Soon after, the increasing mass transfer rate causes the system to enter a phase of common-envelope evolution swamping the X-ray source and finally causing the compact object to spiral into the OB-supergiant.

From this stage on the evolution of the system can proceed in different ways, depending on the orbital separation. In the relatively wide Be/X-ray binaries the

spiral-in likely results in the removal of the envelope of the Be companion, and after the (second) supernova a bound (or disrupted) double neutron star remains, like the Hulse-Taylor binary pulsar PSR 1913+16 (or a neutron star – white dwarf system, if the mass of the Be companion is less than $8 M_{\odot}$). In HMXBs with an orbital period less than about a year the compact object will enter the core of the OB companion which will become a Thorne-Zytkow object, a red supergiant with a high mass loss rate. These objects have been predicted on evolutionary grounds, but have so far not been recognised as such.

Table 1 lists the basic properties of the HMXBs with OB-supergiant companions in the Milky Way and the Magellanic Clouds. Most sources contain an X-ray pulsar; the pulse period (i.e. rotation period of the neutron star) is short and the X-ray luminosity high ($L_X \sim 10^{38}$ erg s⁻¹) in systems undergoing Roche-lobe overflow due to the higher mass- and angular-momentum accretion rate. The latter systems also have circular orbits, while the wind-fed systems have eccentricities up to $e = 0.45$ (GX301-2, Kaper et al. 2006) and an X-ray luminosity $L_X \sim 10^{35} - 10^{36}$ erg s⁻¹.

Neutron stars versus black holes

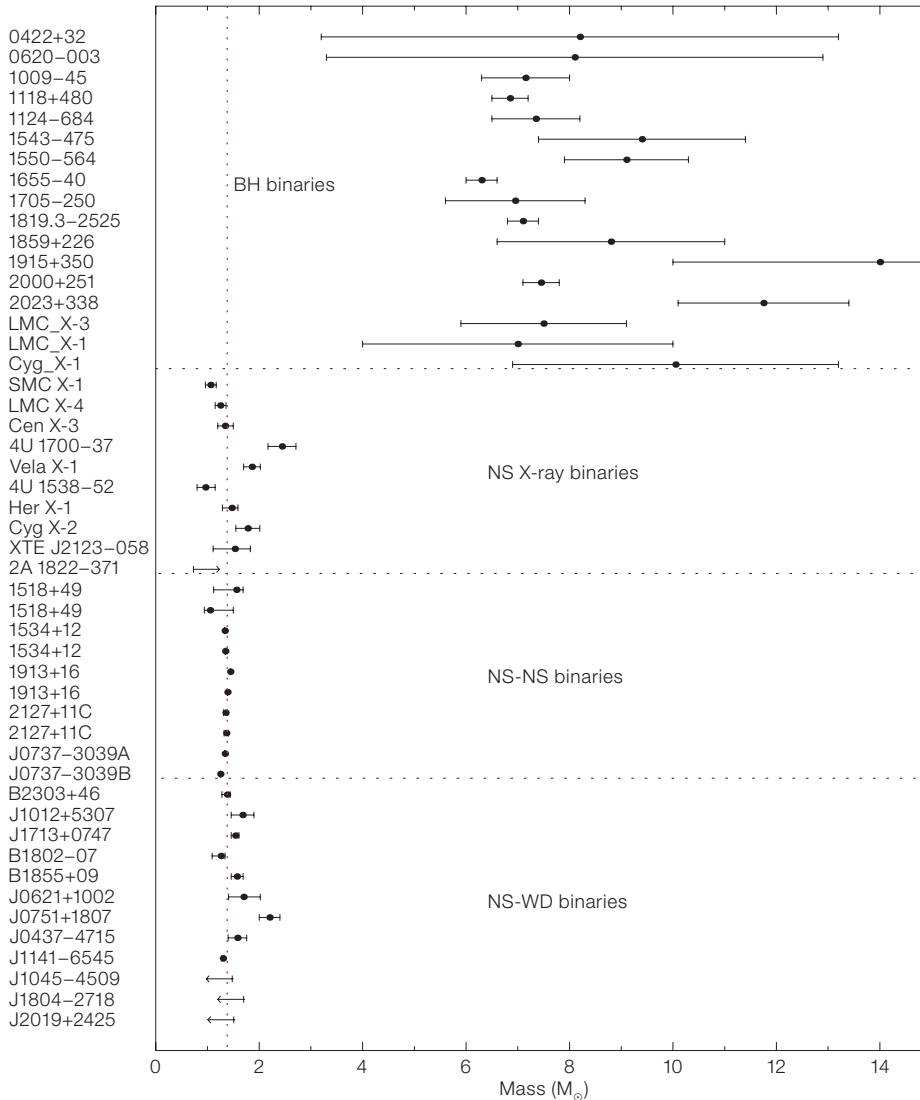
In Figure 2 the mass distribution of neutron stars and black holes is shown, based on measurements collected from the literature (Stairs 2004, McClintock and Remillard 2005). The neutron stars occupy a relatively narrow mass range near $1.4 M_{\odot}$. The most accurate neutron-

Name	Spectral Type	$M_{\text{OB}} (M_{\odot})$	$M_X (M_{\odot})$	$P_{\text{orb}} (d)$	$P_{\text{pulse}} (d)$
2S0114+650	B1 Ia	16 ± 5	1.7 ± 0.5	11.6	860
SMC X-1	B0 Ib	15.7 ± 1.5	1.06 ± 0.11	3.89	0.71
LMC X-4	O7 III–IV	14.5 ± 1.0	1.25 ± 0.11	1.40	13.5
Vela X-1	B0.5 Ib	23.8 ± 2.4	1.86 ± 0.16	8.96	283
Cen X-3	O6.5 II–III	20.2 ± 1.8	1.34 ± 0.16	2.09	4.84
GX301-2	B1.5 Ia+	40 ± 10	1.9 ± 0.6	41.5	696
4U1538-52	B0 Iab	16 ± 5	1.1 ± 0.4	3.73	529
4U1700-37	O6.5 Iaf+	58 ± 11	2.4 ± 0.3	3.41	
4U1907+09	early B I	~ 27	~ 1.4	8.38	438
LMC X-3	B3 ve	~ 6	6–9	1.70	
LMC X-1	O7-9 III	~ 20	4–10	4.22	
LS5039	O6.5 v((f))	20–35	1.4 ± 0.4	4.43	
SS433	A3-7 I	11 ± 3	2.9 ± 0.7	13.08	
Cyg X-1	O9.7 Iab	18 ± 6	10 ± 5	5.60	

Table 1: High-mass X-ray binaries with OB-supergiant companion in the Milky Way and the Magellanic Clouds (ordered according to right ascension). The name corresponds to the X-ray source, the spectral type to the OB-supergiant. For the systems hosting an X-ray pulsar the masses of both binary components can be measured (given an estimate of the inclination of the system). The last five systems most likely contain a black-hole candidate; for the Galactic sources among them relativistic jets have been detected.

Figure 2: Neutron-star and black-hole masses obtained from the literature (Stairs 2004, McClintock and Remillard 2005, and references therein). The neutron stars, especially the binary radio pulsars (at the bottom), occupy a relatively narrow mass range near $1.35 M_{\odot}$. The X-ray pulsars (to the middle)

show a wider spread, including two systems with a neutron-star mass near $2 M_{\odot}$. Such a high neutron-star mass would rule out a soft equation of state. The black-hole candidates (at the top) are significantly more massive, indicative of a different formation mechanism.



star masses have been derived for the binary radio pulsars (NS-NS binaries), with an average mass of $1.35 \pm 0.04 M_{\odot}$ (Thorsett and Chakrabarty 1999). The X-ray pulsars (NS-X-ray binaries) show a somewhat larger mass range, extending both below and above $1.35 M_{\odot}$. Besides Vela X-1, also a high mass is claimed for the system 4U1700-37 ($2.4 \pm 0.3 M_{\odot}$, Clark et al. 2002), although the X-ray source is, contrary to Vela X-1, not an X-ray pulsar (and perhaps a low-mass black hole).

The estimated masses of black-hole candidates are substantially larger ($8.4 \pm 2.0 M_{\odot}$) than those measured for neutron stars. This suggests that neutron stars and black holes are formed in different

ways. If, for example, black holes are the result of 'failed' supernovae in which the stellar mantle is not blown away, but accretes onto the compact remnant, one would expect a significant difference in mass between neutron stars and black holes. However, if the mass of the (proto) neutron star is increased by the fall back of material which was located outside the collapsing degenerate Fe core of the exploding star, one would predict that neutron stars would occupy a range in mass, up to the maximum neutron-star mass allowed by the equation of state. Certainly in the binary radio pulsars such a mass distribution is not observed. With the recent evidence that a black hole may be formed during the collapse of a massive star in a gamma-ray burst (see,

e.g., The Messenger 109, 37, and this issue, page 16) the hypothesis would be that neutron stars are formed in 'ordinary' supernovae, while black holes originate in gamma-ray bursts.

VLT/UVES observations

If the HMXB hosts an X-ray pulsar, its orbit can be very accurately determined through pulse-timing analysis. When the radial-velocity curve of the OB-supergiant is also obtained, the mass of the neutron star and that of the massive star can be derived with precision, given an estimate of the system inclination. In systems showing an X-ray eclipse the inclination must be larger than $i \sim 65^{\circ}$. For Roche-lobe overflow systems a valid assumption is that the OB-supergiant is in corotation with the orbit, which provides a strong constraint on the system inclination.

Van der Meer et al. (2006) have analysed the radial-velocity curves of the three known OB-supergiant systems with an (eclipsing) X-ray pulsar undergoing Roche-lobe overflow. These systems are Cen X-3, the first detected binary X-ray pulsar (Giacconi et al. 1971) in the Milky Way; LMC X-4 in the Large Magellanic Cloud; and SMC X-1 in the Small Magellanic Cloud. The OB-supergiant counterparts to these X-ray pulsars have V magnitudes in the range 13-14. Other properties of these systems are listed in Table 1. High spectral resolution ($R \sim 40000$) and high signal-to-noise spectra of these systems have been obtained with VLT/UVES, covering 12 epochs evenly spread over the (circular) orbit of the system.

To obtain a radial-velocity measurement, often the complete spectra are cross correlated with a template spectrum. This approach has many advantages when using spectra with relatively low spectral resolution and poor signal to noise. In our case the spectra are of such high quality (Figure 3) that the radial-velocity amplitude can be determined for each line separately (Figure 4). The advantage of such a strategy is that it is possible to assess the influence of possible distortions due to e.g. X-ray heating and gravity darkening, as in these systems the



The turbulent region around the ring-shaped nebula DEM L 299 in the Large Magellanic Cloud. Colour composite based on images obtained with the Wide-Field-Imager (WFI) at the ESO/MPG 2.2-m telescope at the La Silla Observatory. (From ESO Press Photo 34a/04)

Good Vibrations: Report from the Commissioning of CRIRES

Hans Ulrich Käufel, Paola Amico, Pascal Ballester, Eduardo Bendek, Peter Biereichel, Paul Bristow, Mark Casali, Bernhard Delabre, Reinhold Dorn, Siegfried Eschbaumer, Raul Esteves, Enrico Fedrigo, Gert Finger, Gerhard Fischer, Gordon Gillet, Domingo Gojak, Gotthard Huster, Yves Jung, Florian Kerber, Jean-Paul Kirchbauer, Jean-Louis Lizon, Enrico Marchetti, Leander Mehrgan, Manfred Meyer, Alan Moorwood, Sylvain Oberti, Jean-François Pirard, Jérôme Paufique, Eszter Pozna, Francesca Primas, Ricardo Schmutzer, Andreas Seifahrt, Ralf Siebenmorgen, Armin Silber, Alain Smette, Barbara Sokar, Jörg Stegmeier, Lowell Tacconi-Garman, Sebastien Tordo, Stefan Uttenthaler, Ueli Weilenmann (all ESO)

CRIRES is a cryogenic, pre-dispersed, infrared echelle spectrograph designed to provide a nominal resolving power $\lambda/\Delta\lambda$ of 10^5 between 1000 and 5000 nm for a nominal slit width of 0.2". The CRIRES installation at the Nasmyth focus A of the 8-m VLT UT1 (Antu) marks the completion of the original instrumentation plan for the VLT. A curvature sensing adaptive optics system feed is used to minimise slit losses and to provide 0.2" spatial resolution along the slit. A mosaic of four Aladdin InSb-arrays packaged on custom-fabricated ceramic boards has been developed. It provides for an effective 4096×512 pixel focal plane array to maximise the free spectral range covered in each exposure. Insertion of gas cells is possible in order to measure radial velocities with high precision. Measurement of circular and linear polarisation in Zeeman sensitive lines for magnetic Doppler imaging is foreseen but not yet implemented. A cryogenic Wollaston prism on a kinematic mount is already incorporated. The retarder devices are located close to the Unit Telescope focal plane. Here we briefly recall the major design features of CRIRES and describe the commissioning of the instrument including a report of extensive laboratory testing and a preview of astronomical results. Thanks to the strong efforts of the CRIRES commissioning team and all other ESO staff involved, it was possible to include the instrument

in the general ESO call for proposals for Period 79.

The CRIRES spectrograph is the last instrument of the first-generation VLT instrumentation plan (D'Odorico et al. 1991). It was included in the very first call for VLT instruments in 1989. Then several options for this instrument were discussed during the Workshop on High Resolution Spectroscopy with the VLT held at ESO in 1992 (Ulrich 1992). By then, however, infrared astronomy had just left behind the era of single-pixel detectors. In fact in those days there was even a strong case to build a Fourier-transform spectrometer, rather than a grating spectrograph. The small detector formats of those days would have left a grating spectrograph with a rather limited spectral coverage. The trade-offs then were analysed in some detail at ESO. By 1997, however, detector formats and the respective performance had developed sufficiently to secure the formal inclusion of CRIRES in the VLT instrumentation plan. The CRIRES instrument is an entirely ESO internal project. The instrument team was advised, as for all other VLT instruments, by a specific science team¹. As there was some competition for the limited resources within ESO, the project proceeded slowly but steadily. Finally the instrument had its real start in 1999. The preliminary design review (PDR) was held in April 2000 and the final design review (FDR) took place in October 2001. Assembly and integration progressed and in January 2005 the team celebrated 'first light' in the laboratory. For the rest of 2005 the team was busy bringing the spectrograph in line with specifications, understanding and fixing many problems. Finally, in December 2005 the two independent subsystems of CRIRES, the vacuum vessel with the cryogenic assembly and the adaptive optics part, were merged and integrated. This marked the start of end-to-end testing. Since then nearly all tests required to pass the Preliminary Acceptance Europe (PAE) review could be performed. CRIRES was then again split and the adaptive optics part sent to Paranal to be commis-

sioned independently (c.f. Käufel et al. 2006). Meanwhile the cryostat underwent last modifications and tests to arrive at a state that also the basic spectrograph was itself ready for the review process. The PAE review meeting was held on 13 April 2006 and the green light for shipping – after completing the essentials from the action item list – was granted on 25 April. Thereafter, in a process which in retrospect resembles a miracle, CRIRES was literally ripped to pieces, packed, collected by the shipper in Garching on 28 April and shipped to Paranal to arrive in record time. Unpacking could commence on 7 May, only nine days later. The cryostat was pre-erected in the laboratory, while the (heavy) instrument support was mounted immediately directly to the Nasmyth platform of UT1. In spite of the extremely fast packing, shipping and unpacking not even minor transport damage was encountered. The instrument was then tested for two weeks in the integration lab of the VLT control building. Laboratory testing ended on 25 May and, after warm-up of CRIRES, a few minor last-minute changes were applied. CRIRES was then transferred to its final location for the foreseeable future, the Nasmyth platform A of UT1 (Figure 1).

Main characteristics

Figure 2 shows the general layout of CRIRES and Figure 3 gives an impression of the cryogenic instrument. The instrument main characteristics are summarised in Table 1. The instrument and its operations concept have been described in some detail by Käufel et al. 2004. For the latest state the reader is referred to the CRIRES User's manual: <http://www.eso.org/instruments/cIRES/>

For calibration a physical model approach has been taken. In spite of the crowded scheme, as shown in Figure 2, CRIRES is from the model point of view rather simple: once the telescope/slit-viewer scale in the slit-plane have been calibrated, the pre-slit optics has no real influence anymore on spectral and spatial calibration. It is thus not part of the model. The pre-disperser can be easily represented by a re-imager with a magnification close to unity and, according to the optical design calculations, negligible distortion. The

¹ The members of the CRIRES science team are: Catherine de Bergh, Meudon; Ewine van Dishoek, Leiden; Bengt Gustafsson (chair), Uppsala; Artie Hatzes, Tautenburg; and Ken Hinkle, Tucson.

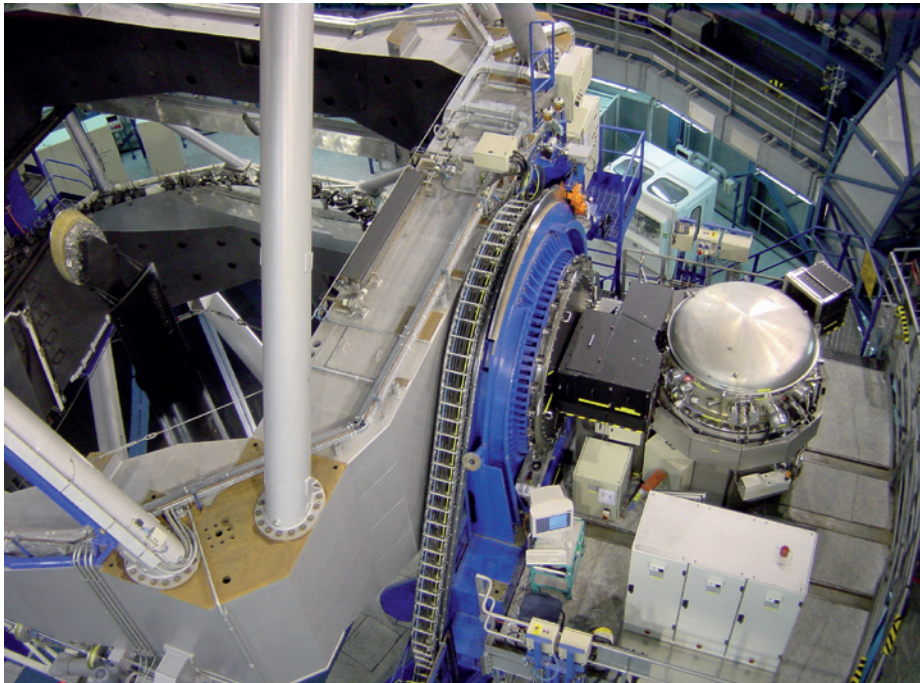


Figure 1: CRiRES at its final destination, the Nasmyth platform A of UT1 (Antu). It is still amazing that even a rather big instrument is literally dwarfed by the VLT. On the right side of the blue Nasmyth adaptor the 'black box' holding the de-rotator and the MACAO adaptive optics system can be seen. Below this box are calibration lamps and an integrating sphere. Inside the box is a motorised linear stage to position the gas cells, the retarder plates and other auxiliary optical elements. The gray cylindrical structure is the vacuum vessel containing the instrument cryogenic opto-mechanical assembly. CRiRES is cooled to ~ 65 K.

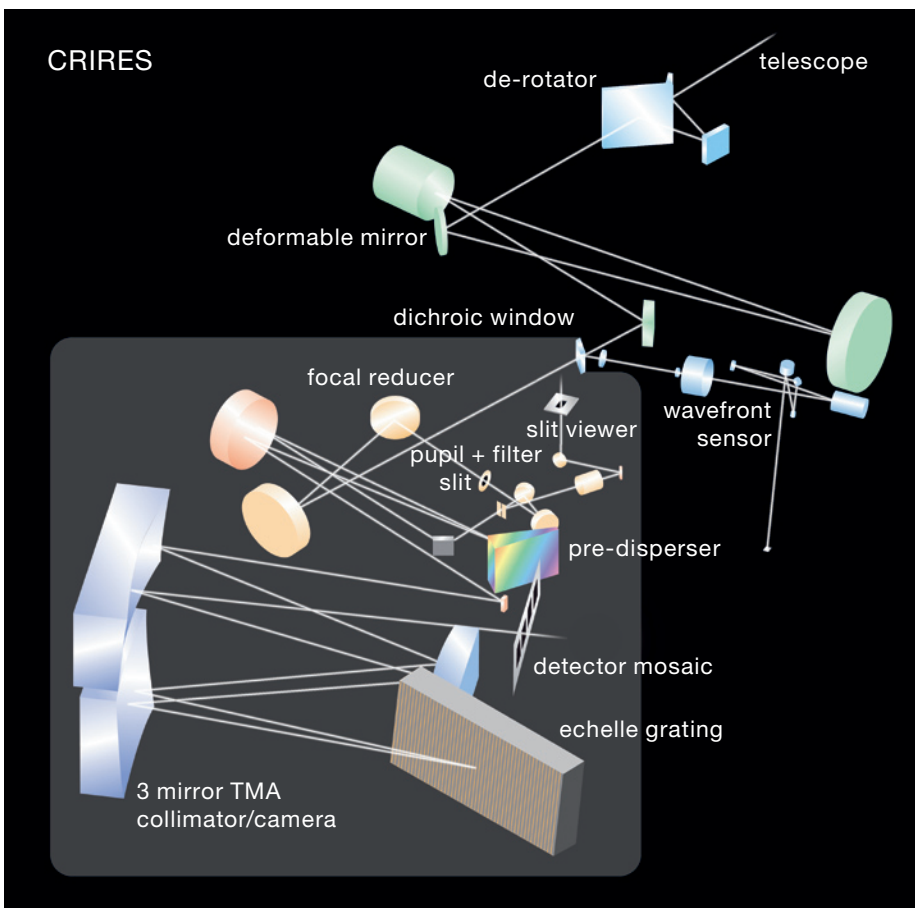


Figure 2: The CRiRES optical design. The VLT Nasmyth focus ($f/15$) is close to the first mirror of the de-rotator assembly. There is a calibration unit (neon arc-lamp, ThAr hollow cathode lamp, a halogen lamp and an infrared glower in combination with an integration sphere) for flat fielding and spectral calibration. In addition, a selection of gas cells can be moved into the beam for calibration and for search for very small radial velocity changes similar to the Iodine-cell technique applied in optical spectrographs. Instead of the gas cells retarders in a motorised mount can be placed to use CRiRES for spectro-polarimetry (see text). The de-rotator is followed by the curvature sensing adaptive optics system with the deformable mirror on a kinematic gimbal mount. The entrance window to the cryostat is a dichroic, separating the visible light with high efficiency for the AO wavefront control. The entire optical bench is cooled by three closed cycle coolers to ~ 65 K. The pre-slit optics of CRiRES consists of an all-reflective re-imager with a cold-pupil stop, reducing the f -ratio to an $\sim f/7.5$. Close to the cold pupil a Wollaston prism (MgF_2) can be inserted, eventually with a linear polariser compensating instrumental polarisation. The slit-viewer has a $\text{BaF}_2/\text{Schott N-SF56}$ doublet as an objective giving a pixel scale of ~ 0.05 arcsec/pixel and an unvignetted field of view of 25×50 arcsec². The main slit is continuously adjustable up to several arcsec with a closed-loop encoder controlling the slit separation. The pre-disperser has a collimated beam diameter of 100 mm and uses a ZnSe prism in retro-reflection. The collimator mirror can be slightly tilted with a piezo for vernier adjustment to compensate for stick-slip effects in the grating and the prism drives. Order selection in the pre-dispersed spectrum is provided by a second intermediate slit located close to the small folding mirror next to the pre-disperser. The main collimator, a three-mirror anastigmat, produces a 200-mm collimated beam which illuminates an R2 Echelle grating (31.6 gr/mm).

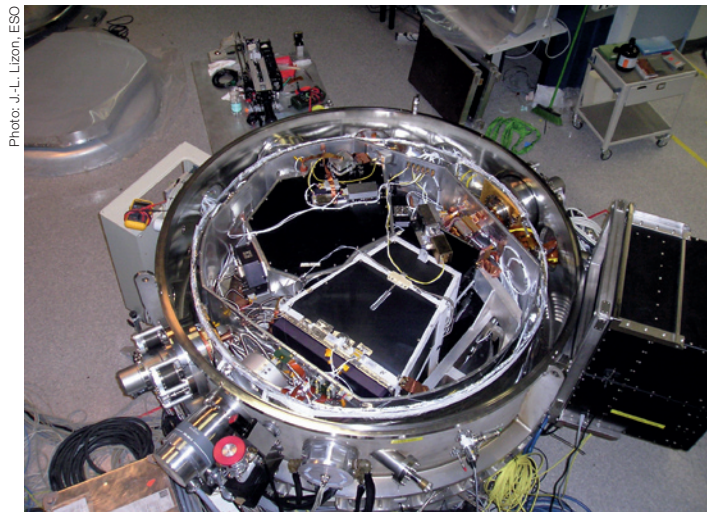


Figure 3: The CRIRES vessel open: a view to the interior of the cyrostat. On the circumference of the vacuum vessel two of the three cryo-coolers can be seen and next to the red safety valve there is the vacuum pump. To achieve the stability goal the instrument support and the radiation shield are thermally stabilised. Inside the radiation shield (round cylindrical shape, covered by 'super-insulation') there is the separate light shield (complex shiny structure). To avoid radiation leaks at the shield level, all cables are fed through with connectors, some of which can be seen on the photo. The optics itself is configured in two sub-assemblies. In the centre of the image there is the trapezoidally shaped 'Three-Mirror-Anastigmat' assembly (TMA), the main spectrograph. The grating is below the TMA structure and hence invisible. On the upper left side to the TMA there is the assembly holding pre-optics and prism pre-disperser. In the state the instrument is shown, all detectors, all sensors and motors are easily accessible. Thus CRIRES is relatively easy to maintain.

ZnSe-prism refractive index is parameterised with a Sellmeier formula. These parameters have been measured at operating temperature using the CHARMS facility at NASA-GSFC. Using (or one might even say abusing) CRIRES, the coefficients have been verified in the range $\sim 60\text{--}80\text{ K}$. To have a sufficient line density, the ThAr infrared spectrum has been explored and a corresponding hollow cathode lamp has been incorporated into the instrument (Figure 4). Using this facility as well as the N_2O gas cell the physical model is being calibrated. This model will soon be available within the instrument pipeline. These modelling efforts are based on established principles developed for Echelle spectrographs and have been applied previously to other ESO instruments (e.g. UVES).

Figure 5 shows the detector mosaic that is the 'eyes' of CRIRES.

Summary of status

At this point CRIRES is provisionally commissioned. While the activities in August 2006 and the first science verification observations were still plagued with alignment and focus problems, all these issues were solved in a final – at least for the moment – intervention to the instrument in September. The major specifications are met and the performance has been re-checked at the telescope. The details are condensed into the CRIRES exposure time calculator. However, already after the second commissioning run in August 2006, which was followed by four nights of early science verification observations, CRIRES and the associated software and documentation had reached a status which made it possible to include the instrument, basically unrestricted, in the regular call for proposals for Period 79. Many thanks go at this point to the colleagues who participated in the two calls for science verification and who have provided the team with valuable feedback. The response from the community to the very first regular call was quite encouraging: more than 60 proposals asking for more than 160 nights!

Table 1: Main characteristics of CRIRES.

Spectral coverage	$\lambda \sim 950\text{--}5300\text{ nm}$ ($\nu \sim 56\text{--}315\text{ THz}$)
Spectral resolution	$\lambda/\Delta\lambda \approx 10^5$ or $\Delta\nu \approx 3\text{ km/s}$ (2 pixel Nyquist sampling)
Array detector mosaic	$4 \times 1024 \times 512$ Aladdin III InSb mosaic, therefore instantaneous λ -coverage $> 2.0\%$ pixel scale $0.1''$ per pixel
Dark current	$0.05\text{--}0.1\text{ e}^-/\text{s}$ per pixel
Infrared slit viewer	Aladdin III InSb with J , H and K -filters 0.05 arcsec/pixel
Precision	for calibration and stability (goal) $\sim 75\text{ m/s}$ i.e. $1/20\text{th}$ of a pixel or 5 mas tracking error
Intrinsic stability goal	spectrograph $\ll 75\text{ m/s}$ preference in design was given to stability therefore gas cells for high-precision radial velocity work
Adaptive optics	curvature sensing ESO-MACAO system 60 sub-apertures, R -band wavefront sensor
Spectro-polarimetry in lines	goal to measure all four Stokes parameter $\lambda/4$ Fresnel rhomb and $\lambda/2$ plate in rotary mounts on the gas-cell slide cold kinematic MgF_2 Wollaston prism in fore-optics
Cryogenic system	three closed-cycle coolers to reach 65 K liquid Nitrogen pre-cooling system

In spite of all the efforts of the team, there is still a long list of action items to be completed. Fortunately, this list does not contain show-stoppers. Moreover, there is some room for improvements to the instrument. In the coming months the team will gradually work on the action item list, and CRIRES users can expect that the instrument performance will slightly improve its use.

Before the start of observations in Period 79 there will be one final commissioning run and a third call for science verification proposals. In parallel with the final commissioning and to the start of operations the polarimetric mode will be implemented, including a calibration module allowing to rigorously calibrate the instrument such that all four Stokes parameters can be measured. This will happen 'invisibly' for operations and first astronomical commissioning of spectropolarimetry is planned around August or September 2007. A detailed description of the polarimetric mode including its scientific potential is given in Käufl et al. 2003.

Figures 6, 7 and 8 give some typical examples of data taken during commissioning and science verification observations.

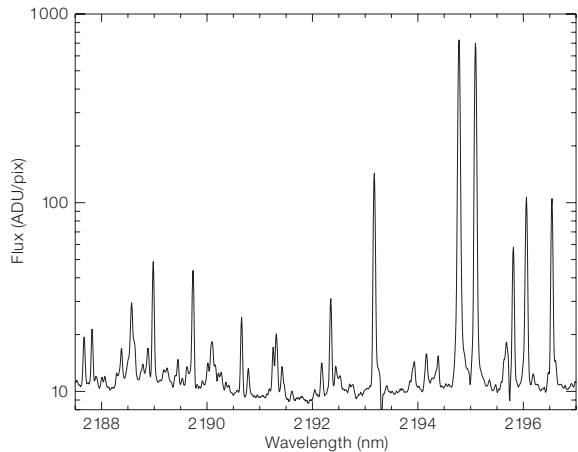


Figure 4: ThAr sample spectrum: The extracted spectrum corresponds to one of the four detectors and is a representative example of the line density. While the frequencies of the strongest lines have been measured with high precision in collaboration with NIST (F. Kerber, catalogue in preparation) the weaker lines will be catalogued with CRILES and ways to measure their frequencies equally precisely have to be explored.

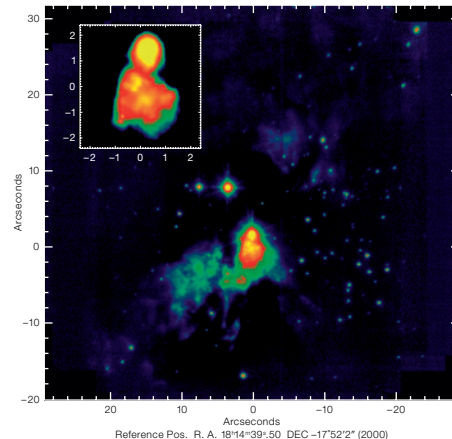


Figure 6: CRILES as an adaptive optics pseudo imager: This K-band image was obtained using the MACAO adaptive optics system and the CRILES slit-viewer camera. At the centre is the galactic H II region W33A (North is up, East to the right). To accommodate the very high dynamic range of this image a logarithmic intensity scale has been chosen. The insert shows the centre region with a different scale. It is remarkable to see in this image a dark lane South of the main source which is aligned with Maser spots reported in literature (data courtesy R. Siebenmorgen, K. Menten and the CRILES science verification team). CRILES is of course not meant to be a competitor to dedicated AO-imagers especially as the spatial sampling is only 0.05" per pixel. However users can expect, if required, this kind of quality imaging to record the exact location of the spectrograph entrance slit.

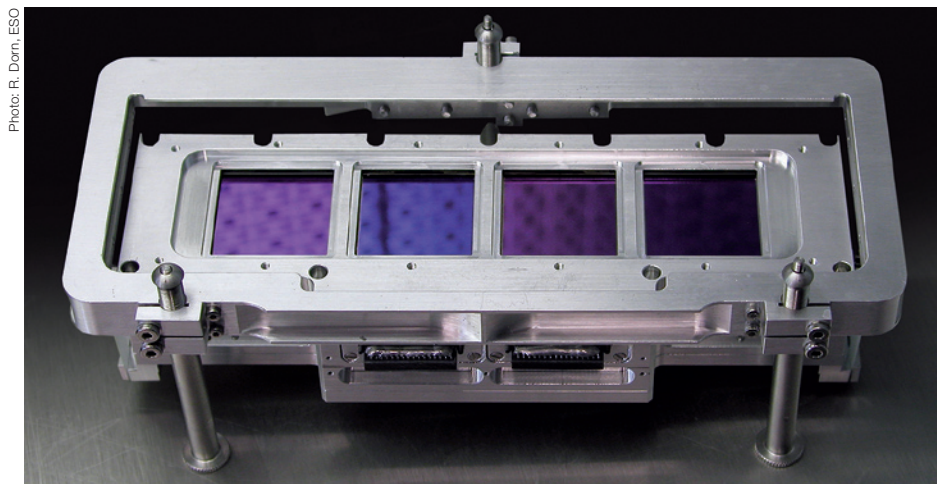


Figure 5: CRILES spectrograph detector assembly: The four Aladdin III detectors comprising the spectrograph focal plane in their mount. The detectors have been taken out of their original sockets and hybridised to custom-made ceramic boards. In this way the requirement of very high mechanical and thermal stability as well as a minimal gap between detectors (nominally 283 pixel) was achieved. While the complete assembly can be adjusted relative to the TMA-housing, the individual detectors – for reasons of stability – have not been mounted with means for relative adjustment. From each of the four

1k x 1k arrays the best two 512 x 512 quadrants are being used. Thus the two central detectors are being read perpendicularly to the dispersion direction while the devices left and right are read parallel to the dispersion direction. The effective useful area of the detector is ~ 5000 x 512 pixel which corresponds to an instantaneous coverage of a wavelength interval ~ 2.5% of the central wavelength. As the detector focus can only be changed by manual intervention it is intrinsically quite stable, but it required an iterative process of thermal cycles for final alignment.

sitions. As many of these lines are seen in absorption while intrinsically quite narrow, the spectral resolution is an absolute must. CRILES has a resolution nearly three times that of the next competing instrument and thus in many cases will be three times more sensitive. Thus many new discoveries can be expected. It should be noted, however, that any infrared observer *volens volens* does high-resolution infrared spectroscopy as the infrared active trace-gases of our atmosphere provide for an extremely high-resolution quasi statistical narrow-band filter (Figure 8). A rigorous calibration of telluric effects is often only possible if the telluric lines are resolved, irrespective of the resolution required for the astrophysical object under study.

Science with CRILES

To have an optimum match between the scientific requirements and the Procrustes' bed of technical constraints, a second scientific workshop was organised in November 2003 at ESO on "High Resolution Infrared Spectroscopy in Astronomy" (Käufl et al. 2005). This workshop confirmed, that CRILES is a long awaited unique observing facility, to which there will be a great demand in astronomy ranging from the inner Solar System to

damped Lyman- α absorption systems. Correspondingly diverse were the many proposals received for science verification, and even new projects have emerged, which were not on the horizon at the time of the workshop in Garching.

While the frequency range accessible to CRILES contains many atomic transitions, which match or complement optical observations very well, the really new features to be observed with CRILES are molecular rotational-vibrational tran-

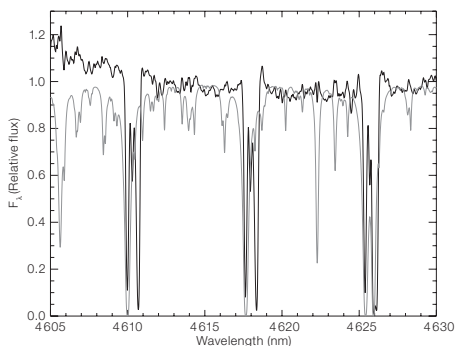


Figure 7: Sample spectrum from W33A: The sample spectrum is taken in the centre of the CO-fundamental band. It corresponds to a fraction of one of the four detectors. The solid line is the spectrum from the compact HII region and the gray line is a reference star to illustrate the telluric absorption. The W33A spectrum has been corrected as well as possible for the telluric absorption. The parabolic shape of the continuum from W33A is due to CO ice. As can be seen from the standard star, our local atmosphere also contains CO, however a bit Doppler-shifted. The local telluric CO is saturated, so that a correction in the centre of the lines is not possible. To be able to get good and useful data, i.e. data which can be calibrated, the CRIRES exposure time calculator has a tool to predict the telluric absorption taking into account the exact circumstances of

the observations. For this sample spectrum, the Doppler shift is approximately 50 km/s. This needs to be compared with the orbital component of the Earth, i.e. the orbital velocity projected on the line of sight to the target which can be as much as ± 30 km/s. In that sense the exact timing of observations matters, and must be part of the planning process when preparing a proposal or observing blocks from P2PP. The CO spectrum will provide for new and extremely detailed constraints on the conditions of the molecular cloud surrounding this HII region (data courtesy R. Siebenmorgen, K. Menten and the CRIRES science verification team). CO, by the way, is the most abundant molecule in the Universe, which can be regularly observed (i.e. it emits dipole radiation).

Conclusion and outlook

With CRIRES the ESO VLT first-generation instrumentation plan has been completed. CRIRES fills a large gap in the parameter map. It complements space astronomy very well, because high-resolution observations from the ground complement satellite observatories such as HST, Spitzer or the planned JWST. While CRIRES was built at ESO, the detector technology has progressed, so that a speedy detector upgrade is being investigated. This, together with other measures, will ensure significant further improvements of performance.

CRIRES will also be very valuable to assess and prepare the science case for a similar instrument for the European Extremely Large Telescope project, which is presently taking its first steps.

Acknowledgements

Special thanks go to all colleagues on both sides of the Atlantic contributing to our project. Hans Ulrich Käuffl feels particularly indebted to all colleagues and their families sometimes enduring a long string of quite extended missions to Paranal.

References

- D’Odorico S., Moorwood A. F. M. and Beckers J. 1991, *Journal of Optics* 22, 85
- Käuffl H. U. et al. 2003, *SPIE proc.* 4843, 223
- Käuffl H. U. et al. 2004, *SPIE proc.* 5492, 1218
- Käuffl H. U. et al. 2006, *The Messenger* 124, 2
- Käuffl H. U., Siebenmorgen R. and Moorwood A. F. M. 2005, proceedings of the ESO Workshop on “High Resolution Infrared Spectroscopy in Astronomy”, Springer-Verlag Berlin/Heidelberg
- Ulrich M. H., proceedings of the ESO Workshop on “High Resolution Spectroscopy with the VLT”, 1992

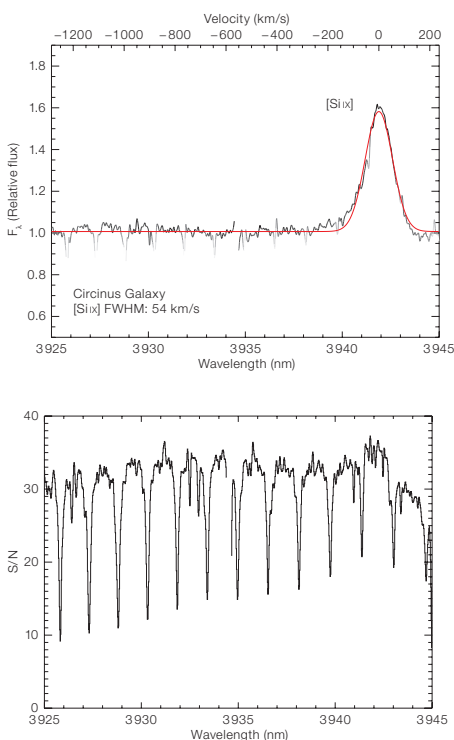


Figure 8: Sample spectrum of an active galaxy: The top spectrum shows a coronal line observed with CRIRES during commissioning originating from eight times ionised Silicon at 3942 nm. This line has an intrinsic width of 54 km/s. One may wonder what could be the ‘added value’ of such an observation with a resolution of 1.5 km/s per pixel. The answer comes from looking at the raw data in the bottom figure, which shows the interfering telluric absorption spectrum. The SiIV line falls into a band of quite narrow telluric molecular absorption features. Only when resolving the telluric lines is it possible to correct for them. In other words, when observing this particular line with ten times lower resolution one would get both the equivalent width and the centre of gravity and thus the redshift wrong.



Figure 9: The happy commissioning team – at least most of them – shortly after first light in the VLT control room.

Enabling Fringe Tracking at the VLTI

Henri Bonnet¹
 Bertrand Bauvir¹
 Anders Wallander¹
 Michael Cantzler¹
 Johan Carstens¹
 Fabio Caruso¹
 Nicola Di Lieto¹
 Stéphane Guisard¹
 Pierre Haguenaer¹
 Nico Housen¹
 Manfred Mornhinweg¹
 Jean-Luc Nicoud¹
 Andres Ramirez¹
 Johannes Sahlmann¹
 Gautam Vasisht^{1,2}
 Stefan Wehner¹
 Juan Zagal¹

¹ ESO

² Jet Propulsion Laboratory, California
 Institute of Technology, Pasadena, USA

Just as adaptive optics reduces the image blur induced by the atmosphere in conventional single telescope observations, Fringe Tracking, or co-phasing, reduces the blur in interferometric observations. We present the status of the VLTI after the deployment by the Interferometer Task Force of new beam quality control tools, which enabled the UTs and ATs to be co-phased, using FINITO as a fringe sensor.

Co-phasing the VLTI consists in canceling the Optical Path Length Difference (OPD) from the observed astronomical source to the instrument detector via the different telescopes of the array and on the observation line of sight and changes with time at a typical rate of 1 cm/sec due the Earth's diurnal rotation. These changes are compensated internally by the Delay Lines, consisting of retro-reflectors mounted on carriages positioned along 60 m long rails and reflecting the collimated beam towards the re-combining laboratory.

In addition to the large and predictable geometric changes, the atmospheric turbulence introduces random OPD perturbations with amplitude of 10 μm , and the telescope infrastructures generate vibrations up to 100 Hz that propagate to

the optics with an amplitude of one micron. Without Fringe Tracking, these perturbations limit the maximum integration time of scientific instruments to a few milliseconds. The purpose of Fringe Tracking is to stabilise the OPD within a fraction of the observing wavelength (goal 100 nm rms) in order to increase the scientific detector integration time and reach dimmer targets.

FINITO is an OPD sensor, operating in the *H*-band (1.65 μm). It generates fringes modulated in time by means of an internal OPD modulation. The synchronous detection of the phase shift between the observed fringe and the applied modulation provides an estimation of the OPD error. As any decent rejection of the atmospheric OPD requires a closed-loop control bandwidth of a few tens of Hz, a modulation frequency of a few hundreds Hz is needed with a typical detector sampling rate of 1 kHz.

FINITO was delivered in 2003 but Fringe Tracking could not be demonstrated at commissioning. In April 2005, an Interferometer Task Force (ITF) was set up at the Paranal Observatory to investigate the feasibility of Fringe Tracking with FINITO. Several failure causes were identified: Delay Line rail alignment errors, pointing errors induced by the internal turbulence downstream of the Adaptive Optics and intermittent explosions of the stellar images caused by saturations of the Adaptive Optics Deformable Mirror (DM). In addition, the impact of vibrations was beyond a mere degradation of the performance as it distorted the modulated fringe to a point that phase estimation was not possible.

ITF developed a beam quality control strategy based on the existing set of hardware, encompassing the pupil alignment and the control of piston, pointing and higher-order aberrations. Fringe tracking was demonstrated in March 2006 on the Auxiliary Telescopes (AT) in nominal atmospheric conditions with performance close to specification (100–150 nm rms). On Unit Telescopes (UT), the first stable closed-loop operations were demonstrated on sky in June 2006 albeit with a degraded performance limited by the telescope vibrations (460 nm rms). Vibration rejection methods were

then developed by ITF and demonstrated their potential to reject 75 % of the residual energy and lower the residual OPD to 230 nm rms.

The next sections present the main features developed by ITF to achieve this performance:

- a Delay Line rail alignment tool making it possible to maintain the attitude error of the cat's eye within the tolerance,
- an Adaptive Optics Deformable Mirror Saturation Management Algorithm aiming at minimising the impact of saturations on the wavefront quality,
- a fast guiding mode based on IRIS, the VLTI laboratory Near Infrared Camera, rejecting the tip-tilt components of the tunnel turbulence,
- an acquisition procedure allowing to reduce the static pointing error to less than 5 mas,
- an open-loop vibration compensation method based on accelerometers mounted to the M1 cell.
- A closed-loop vibration tracking algorithm, rejecting harmonics in tip-tilt and piston beyond the control bandwidth of the Fringe Tracking controller.

Pupil control

A Variable Curvature Mirror (VCM) is mounted at the focal plane of the Delay Line cat's eye and can be adjusted in curvature to image the telescope pupil at the appropriate distance while the carriage moves along the rail. The curvature applied to the VCM increases the sensitivity of the exit pupil lateral displacement to cat's eye attitude errors induced by rail distortions. When ITF started, VCM operations were functionally not possible because the amplitude of the rail distortions were such that the DL laser metrology beam, also reflected by the VCM, would be lost while the DL twisted along the rail. ITF recycled the tools developed for the Delay Line installation and developed DELIRIUM, a rail observer based on capacitive sensors permanently installed on-board the DL carriage, monitoring the position and attitude of the carriage with respect to a mechanical reference. The profile of the guiding rail is then reconstructed and filtered with the calibrated influence functions of the rail supports to generate a vector of corrective com-

mands. After convergence of the rail alignment procedure, the residual carriage jitter is dominated by the contribution of the wobble of the wheels (Figure 1). The analysis of the DELIRIUM data accumulated over six months established that the evolution of the rail profile is driven by its response to temperature changes and that a regular maintenance will allow tracking the seasonal variations and guarantee a continuous operability of the VCM.

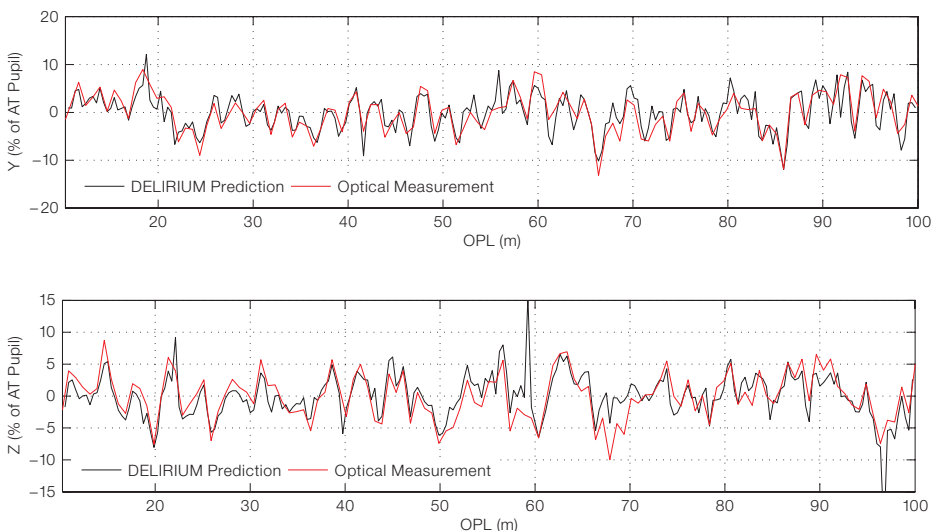
Rejection of atmospheric aberrations

The VLT Coudé Focus Adaptive Optics (AO) System, MACAO has been specified to deliver a mean Strehl ratio of 50% in K in nominal atmospheric conditions, on axis with a bright reference star (R mag < 10), over long integration times (minutes). This requirement has been met and demonstrated at delivery but was unfortunately not sufficient for an application such as FINITO, running at 1 kHz with the task to deliver a reliable measurement of the phase at each cycle.

To maintain the best fringe contrast in the presence of optical aberrations, the beams are spatially filtered at the entrance of FINITO by means of monomode fibres, at the cost of a flux loss in proportion to the instantaneous Strehl ratio. Since fringes are sampled at high frequency, the critical performance parameters for MACAO is not the mean image quality, as in standard imaging AO applications, but the frequency and amplitude of intermittent image 'explosions' caused by uncontrolled Deformable Mirror (DM) saturations.

MACAO relies on a curvature mirror, very efficient at compensating low-order intra pupil aberrations, but quite inefficient at generating a higher-order wavefront with features at the spatial scale of the inter-electrode distances. The atmosphere does not generate a substantial energy in these so-called waffle modes, but the noise propagation in MACAO causes a substantial fraction of the DM stroke budget to be spent along them with hardly any impact on the wavefront quality. This causes the DM command to saturate frequently, even in good seeing conditions. A simple clipping of the command at saturations projects the energy

Figure 1: Lateral motion of the Pupil. Black = prediction based on DELIRIUM. Red: Actual Optical measurement. This performance is compatible with glitchless operations on the UTs and on the AT stations currently offered.



propagated along the waffle modes on more efficient modes. This induces short PSF explosions that result in deep fibre injection dropouts. The Saturation Management Algorithm (SMA) developed by ITF implements a non-linear modal control along the waffle modes, triggered when saturations of the linear command are detected and aiming at minimising the impact of saturations on the wavefront. In addition, an Anti-Windup (AW) module freezes the projection of the controller integrator along the waffle modes during the saturation events, in order to prepare a faster recovery of the control after the event. SMA and AW have been demonstrated on Sky in engineering mode in February 2006 (Figure 2), and operated since then for all UT test sessions, although not yet offered to science operations.

Rejection of the tunnel seeing

Since the Adaptive Optics Wavefront Sensor is located in the Coudé Room, it does not correct aberrations developed downstream by the tunnel turbulence. The amplitude, projected on sky, of the pointing jitter caused by the tunnel turbulence is ~ 50 mas PV, distributed between 0 and ~ 5 Hz. As this amplitude compares to the H -band diffraction limit at the UT (45 mas), the impact of the tunnel tip-tilt turbulence on injection is potentially devastating. ITF has demonstrated on sky the capability of the IRIS Fast Guiding (IFG) mode to reject the tunnel tip-tilt and stabilise the pointing at the entrance of the VLTI instruments. This control tool relies on IRIS, the near infrared fast imager, originally designed by the

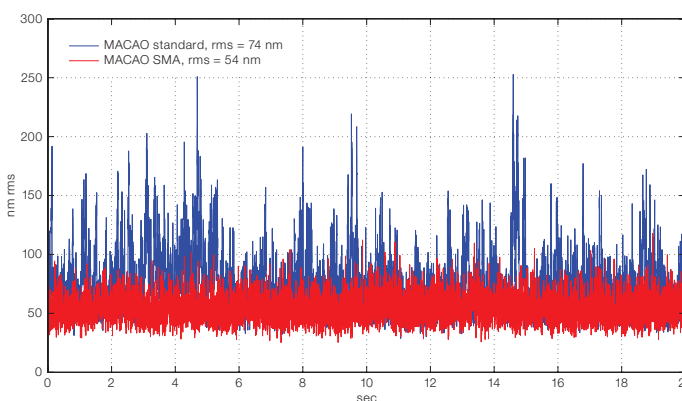


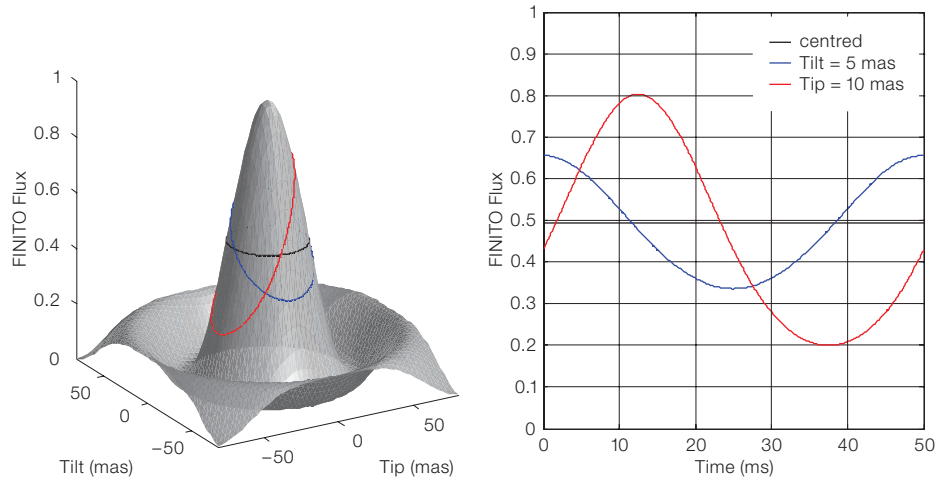
Figure 2: Residual Wavefront Error downstream M9 as reconstructed from MACAO Wavefront Sensor data. Standard MACAO algorithms (blue), Saturation Management Algorithm and Anti-Windup (red). Both sets of data were taken a few minutes apart in similar atmospheric conditions (0.9 arcsec).

thermal variations of the tunnel atmosphere. The controller operates in open loop, addressing the commands to a Tip-Tilt Platform located downstream the dichroic separating the beams fed to FINITO and IRIS. IFG has been demonstrated in K band only with an optical layout allowing FINITO and IRIS to be simultaneously operated but currently incompatible with AMBER operations. A re-organisation of the optical switches on the FINITO table is underway to allow simultaneous FINITO-IFG-AMBER operations.

Minimisation of static pointing error

The injection in the monomode fibre is degrading exponentially with the amplitude of the aberrations. Tip and Tilt are the most energetic atmospheric modes and remain the main residual aberrations downstream of MACAO and IFG, with typical residual amplitude of 10 mas rms per axis. 2σ deviations ($\sim 2\%$ of time) induce an injection loss of 60% that increases dramatically in the presence of a small static pointing error. Minimising the static pointing error is essential to preserve the largest error allocation to the dynamic error. The early alignment strategy proposed for FINITO consisted in scanning the field along a regular grid pattern and recording at each position the mean injection over a user's defined integration time. Short integration times provided results contaminated by dynamic fluctuations and longer integration times led to prohibitive convergence times while results were still potentially biased by e.g. variations of the atmospheric transmission during the calibration. ITF developed an alternative unbiased approach, called Beam Tracking, consisting in minimising the flux fluctuations induced by the coupling between the static error and a circular tip-tilt modulation applied to the Tip-Tilt Platform of IFG (Figure 3). Modulating on a pure harmonic with a frequency selected in a vibration free region (20 Hz) allows extracting the static signal from the dynamic noise distributed over a broad spectrum. The procedure converges within a few tens of seconds to a static residual error estimated to be less than 5 mas.

Figure 3: Beam Tracking principle: the circular modulation of the Tip-Tilt platform induces a periodic walk of the injection fibre around the mean PSF. The amplitude of the induced flux modulation is proportional to the static pointing error and its phase to the error direction.



Rejection of vibrations

The combination of the DM Saturation Management, the IRIS Fast Guiding and the Beam Tracking allows stabilising under typical atmosphere conditions (seeing = 1 arcsec, coherence time = 2.5 ms) the injection of bright stars (H magnitude ~ 5) from the UTs in the FINITO monomode fibres. This was first achieved in May 2006 but the first attempt to close the Fringe Tracking loop was not a success yet. The amplitude of the telescope vibrations not only degraded the performance but also prevented the phase to be correctly estimated due to large phase variations within the period of the FINITO internal modulation cycle.

A new phase reconstruction algorithm was designed to account for the fringe distortion caused by the OPD variations within the modulation cycle. Fringe Tracking was first enabled at 2 kHz with this new phase estimator. Stable but poor performance (~ 450 nm rms) was obtained in July with the UT1-3 baseline and early September with the UT3-4 baseline. The spectral distribution of the residual phase error was mainly found in sharp unresolved peaks distributed between 15 and 100 Hz. Most of the observed frequencies had already been identified by accelerometer measurements carried out at the telescopes and at the Coudé trains. The outstanding features were structural modes of the M1 cell and M3 towers (18 and 24 Hz) excited by the Cryo-Cycle-Coolers of the cold instruments, specially NACO on UT4, and forced vibrations propagated from the telescope

basement equipment to the Coudé optics, e.g. the fans of the MACAO cabinets mounted to the structure of the Coudé room and shaking of M10 and M11 in the 45–50 Hz region.

ITF envisions a tri-therapy to bring the Fringe Tracking performance within the expectations of our future instruments. The first component should be a reduction of the environmental aggression by means of appropriate isolation or damping of vibration sources and propagation paths. The second component of the tri-therapy consists in pre-cleaning the beam delivered to the VLTI by means of accelerometer measurements filtered to estimate the induced OPD via a sensitivity model and fed forwards to the Delay Lines. A flotilla of accelerometers has already had First Vibration at the UT3 and UT4 M3 towers in September and provides a continuous monitoring of the vibration state, featuring a strong correlation with the optical phase seen by FINITO. The aptitude of accelerometers to compensate in open loop the main vibrations was demonstrated on sky in October (Figure 4, green curve and Figure 5). The third component of the tri-therapy, called Vibration Tracking (VTK) was also deployed in September. The idea is to model and compensate stable harmonics beyond the bandwidth of the Fringe Tracking controller by constraining in closed loop their frequency, amplitude and phase. VTK has been implemented in the FINITO controller and has demonstrated on sky its capability to reject about half of the Residual Phase energy

(Figure 4, red curve and Figure 5)¹. This has not only reduced the residual phase to 260 nm rms but also allowed for the first time to close the Fringe Tracking loop at 1 kHz.

The tri-therapy test protocol was tested on 9 October and demonstrated the potential of combining these different approaches. While the vibration controllers were running, the fans of the MACAO electronic cabinets, known to excite the Coudé room optics via acoustic and structural propagations, were shut down. This reduced the amplitude of the dense forest of vibration peaks around 48 Hz that would not be efficiently rejected either by accelerometers feed forward (limited by communication delay at this frequency) or by VTK (limited by spectral resolution). The residual OPD went from 260 to 230 nm rms (Figure 4, cyan curve, Figure 5).

Possible improvements

Fringe Tracking has been demonstrated on bright stars in nominal seeing conditions. The limiting *H*-band magnitude has not been investigated but the experience accumulated in engineering mode indicates that AT operations will be limited by the stability of the photometric injection. The longer wavelength (*K*-band) selected for the PRIMA Fringe Sensor Unit is expected to attenuate the impact of the turbulence but the scientific potential of upgrading the ATs with a low-order Adaptive Optics system may need to be evaluated. On the UT side, the aptitude of the Vibration Tracking and Accelerometer approaches to partially reject the vibrations has been established. The progress demonstrated so far justifies that an intense parallel effort be initiated to improve the dynamical environment of the UTs.

¹ VTK was also successfully tested with MACAO to reject the 18 Hz Tip-Tilt Mode of the M1 cell.

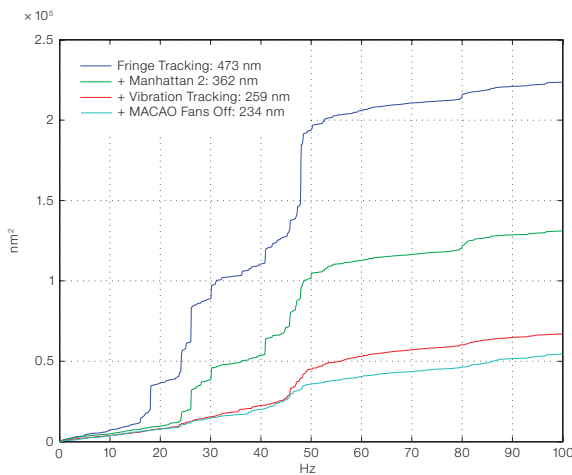


Figure 4: The blue curve shows the cumulative power of the phase (OPD) residual during 'naked' fringe tracking with a residual above 450 nm rms. Accelerometer feed forward to the delay lines is switched on (green) reducing the residual to 362 nm. Vibration tracking (VTK) is added (red) reducing the residual further to 259 nm. Finally MACAO cabinets cooling are switched off (cyan), bringing down the residual to 234 nm.

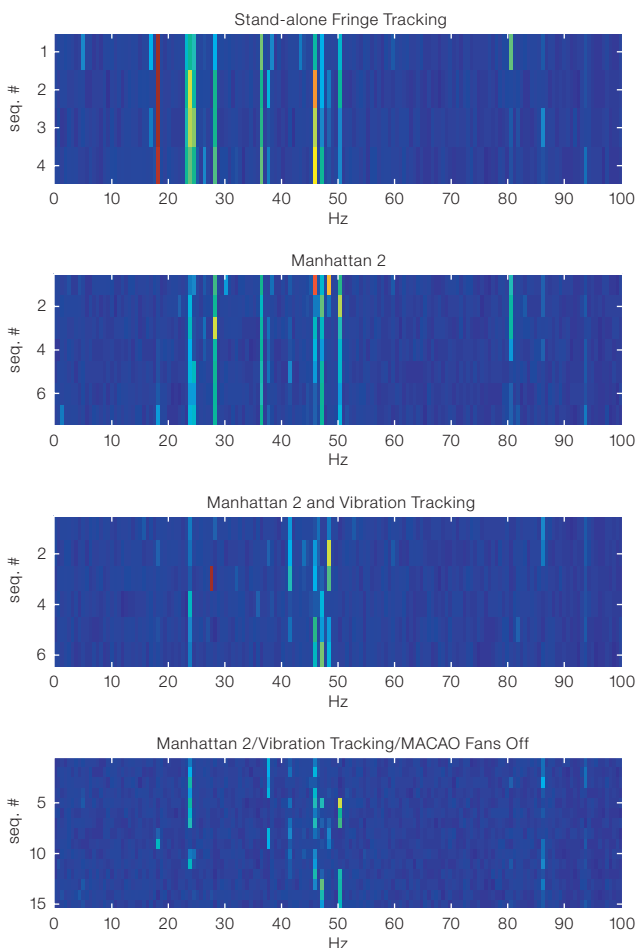


Figure 5: Tri-therapy experiment on the UT3-UT4 baseline. Each line of each plot is a PSD of residual OPD, seen by FINITO, in square root colour scale. The top sub-frame was obtained in stand-alone Fringe Tracking. The atmospheric Piston (< 5 Hz) is correctly rejected but the vibrations are amplified because their frequencies lie in the overshoot region of the controller. On the second frame, the accel-

ometers signal is fed to the Delay Lines. This permitted rejection of frequencies below ~ 30 Hz generated at M3. On the third frame, Vibration Tracking was started and rejected harmonics below 100 Hz. Switching off the fans of MACAO electronics cabinets reduced the residual amplitude in the 45 to 50 Hz region. All these data were acquired within a time window of two hours.

Visible and Infrared Survey Telescope for Astronomy: Progress Report

Jim Emerson¹
Alistair McPherson²
Will Sutherland³

¹ Astronomy Unit, Queen Mary University of London, United Kingdom

² United Kingdom Astronomy Technology Centre, Edinburgh, United Kingdom

³ Institute of Astronomy, Cambridge, United Kingdom

Progress in implementing VISTA is summarised largely through pictures. VISTA's near-IR public surveys are expected to begin in 2007 quarter four.

VISTA (Visible and Infrared Survey Telescope for Astronomy) is a 4-m wide-field survey telescope (1.65° diameter in the IR), equipped with a near-IR (0.85–2.3 μm) camera facility for performing extensive surveys of the southern skies with sensitivity matched to the needs of 8-m-class telescopes. IR imaging surveys particularly target the cold, the obscured, and the high-redshift Universe, to generate science directly and also select objects worthy of further study by the VLT. Details of the design and expected performance of VISTA were given in *The Messenger* 117, page 27, so here we describe, mainly in pictures, progress in implementing VISTA. VISTA's first Public Surveys are expected to begin in late 2007.

Site and enclosure

VISTA lies some 1500 m away from the peak on which the VLT sits (Figure 1).

The enclosure (shown being built in the previous *Messenger* article) is now essentially completed (Figure 2 shows it with the slit open and the windscreen up). The enclosure successfully survived an unplanned water tightness test when ~ 10 cm of rain fell in one 24-hour period – a most unexpected event!

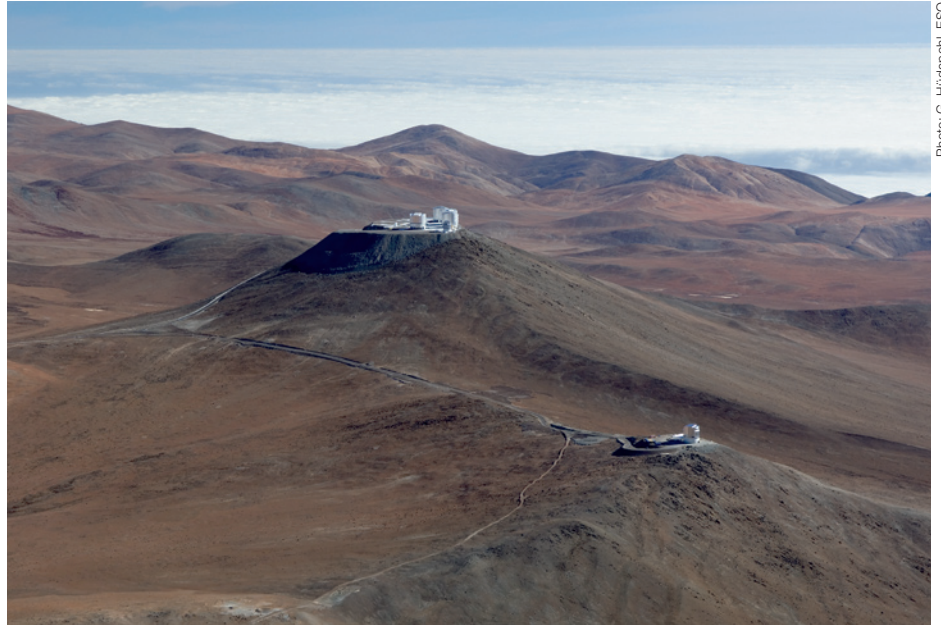


Photo: G. Hudepohl, ESO

Figure 1: VISTA (right) with VLT (left).



Photo: VISTA

Figure 2: Enclosure.

Telescope and mirrors

The telescope, including the primary mirror support and instrument rotator is fully assembled with dummy mirrors, and final cabling and testing is ongoing. Figure 3 (left) shows a side view also showing the dome flat screen in the upper centre, whilst Figure 3 (right) shows a front view with the secondary mirror support structure prominent.

The primary and secondary mirrors are both undergoing final polishing, which is taking longer than originally anticipated (no one has ever polished a 4-m f/1 primary before). Completion of polishing is expected in February 2007. The coating plant, which can coat in either aluminium or in protected silver is already installed in the enclosure annexe.



Photos: M. Cullum, ESO (2)

Figure 3: Telescope: side view (left), front view (right).

IR camera

The camera includes the entrance window, cold baffle tube, lenses, filter wheel and 16 2048 × 2048 IR detectors and is shown in Figure 4 without all its associated electronics boxes and gas lines attached. Note the entrance window, the vacuum vessel which is metallic or black, and that the camera is mounted in its (blue) transport carriage unit in which it will soon be air-freighted to Chile.

Science

VISTA's strength, in addition to its specifications (the exposure time calculator for VISTA may be found through www.vista.ac.uk/observing/etc/), is the dedication of the vast majority of its available time to ambitious, large-scale legacy public surveys (three quarters of VISTA time was envisaged at the start as the baseline fraction for public legacy surveys). At the time of writing the process of deciding which public surveys VISTA will actually undertake over the next few years is drawing to its conclusion. ESO's Public Surveys Panel for VISTA interacted with the original proposers of (12) public surveys to distil/merge these down to six candidate surveys and, following panel feedback and resulting discussions amongst the proposers, their updated submissions underwent review on 31 Oc-

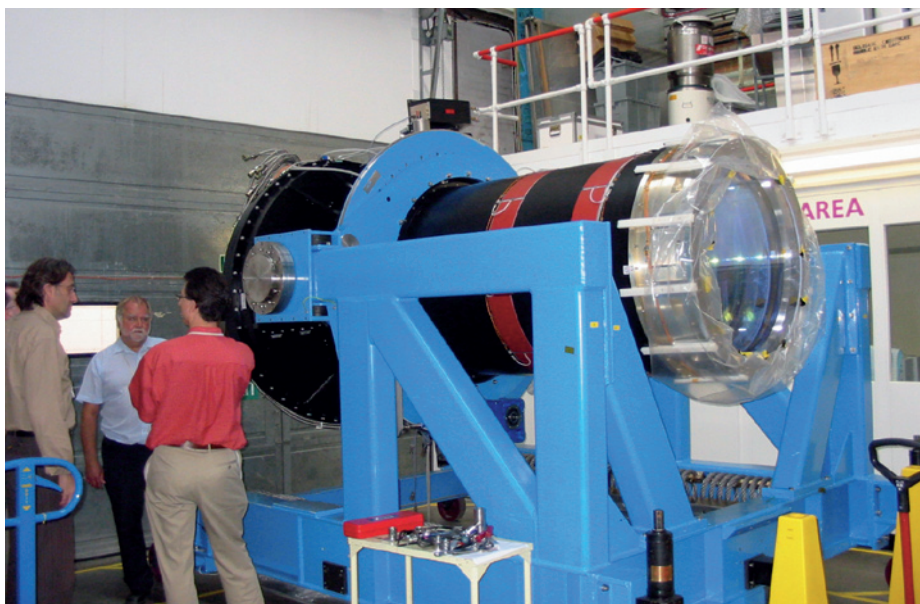


Photo: VISTA

Figure 4: IR camera.

tober 2006. The resulting recommendations of the Public Survey Panel will be put to ESO's Observing Programme Committee in November 2006. The results of this process should be known by the time this article appears in print (and will be posted at www.vista.ac.uk when known), and the surveys themselves are likely to start in 2007 quarter four.

Acknowledgments

The Office of Science and Technology and the Higher Education Funding Council for England funded VISTA through the Joint Infrastructure Fund; and the Particle Physics and Astronomy Research Council (PPARC) provide further funding. Many individuals, companies, and organisations, including ESO, have been crucial to making VISTA but are too numerous to mention here. In particular PPARC's UK Astronomy Technology Centre have organised the realisation of VISTA through their VISTA Project Office, and have skilfully coordinated the work of all those individuals and organisations, including UK ATC, who have contributed.

The European ALMA Regional Centre: User Support for European Astronomers

Paola Andreani, Martin Zwaan (ESO)

What will happen when ALMA is operational? How can an astronomer apply to get observing time with ALMA? What happens when their proposal is approved? Will they be able to process the data, obtain high-quality science products and extract their science from it? Sooner or later each astronomer interested in ALMA science will ask herself or himself these questions. The aim of this article is to describe how the process of proposing for observing time, subsequent execution of the observations, obtaining and processing of the data is going to take place in the ALMA epoch.

From an astronomer's perspective, the basic principles on which the ALMA science operations are based are the following: *every astronomer, including novices to aperture synthesis techniques, should be able to use ALMA; ALMA observations will be carried out in service mode and will be dynamically scheduled to optimally match the weather conditions and array configuration; the calibration shall be reliable and self-consistent, so that data from the archive can be retrieved and reprocessed at any moment; data will be made public in a timely fashion.*

The interface between ALMA and the user communities is formed by the ALMA Regional Centres (ARCs), currently being established in Europe, the US and East Asia. For European users, the European ALMA Regional Centre (EU ARC) is being set up as a cluster of nodes located throughout Europe, with the main centre at the ESO headquarters in Garching. This main centre is part of ESO's Data Management Operations Division (DMO) and serves as the access portal to ALMA for the European user community. In synergy with the distributed network of ARC nodes, the centre's aim is to optimise ALMA's science output and to fully exploit this unique and powerful facility.

The EU ARC will be the point of contact for European ALMA users from the moment of proposal submission to the actual distribution of calibrated data and

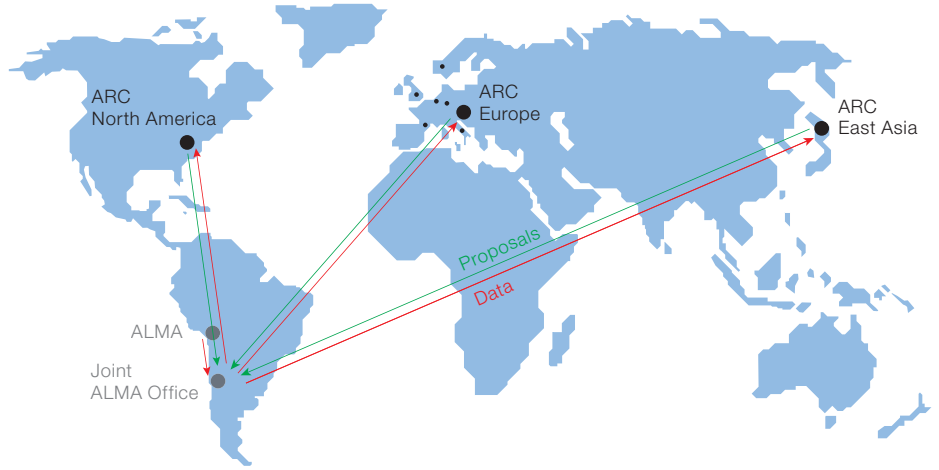
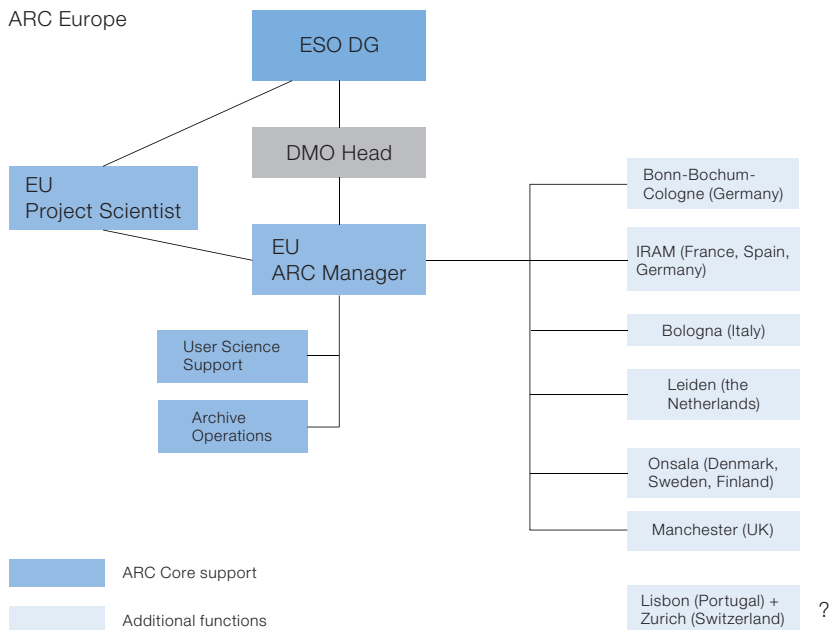


Figure 1 (above): Proposals/Observing files are sent from the ARCs to the Joint ALMA Observatory (JAO) in Santiago (Chile). Data are sent from the JAO to ARCs by reverse route, with complete archives of all data at all four sites.

Figure 2 (below): A schematic sketch of the EU ARC structure, with the ESO central node and the satellite nodes in Europe: Bologna (Italy), Bonn-Bochum-Cologne (Germany), Grenoble (IRAM, France), Leiden (the Netherlands), Manchester (UK), and Onsala (Sweden, Denmark, Finland).



subsequent analysis. The core of the ARC activities will consist of running a help-desk for the proposal submission and submission of observing programmes, the delivery of data to principal investigators, the maintenance and refinement of the ALMA data archive, and the feedback to the data reduction pipeline and the off-line reduction software systems that surround it. The rela-

tionship between the user, the ARC, and the Joint ALMA Observatory (JAO) in Chile, is schematically shown in Figure 1. A sketch of the EU ARC structure is shown in Figure 2. Potential ALMA users may find it interesting to check from time to time the newly set-up EU ARC web page, where more details on the EU ARC tasks will continuously be added (<http://www.eso.org/projects/alma/ARC/>).

Indeed, for day-to-day operations, the three ARCs spread over three continents form an integral part of the overall ALMA operations. The ARC staff serve their regional communities, but also provide products to the entire ALMA observatory, such as improved pipeline heuristics or observing tools. Science staff from the ARCs rotate through Chilean operations, providing the necessary close ties among the sites, and keeping the ARC staff familiar with the realities of observatory operations.

Moreover, fundamental to ALMA's success in Europe are the enhanced services provided by the network of ARC nodes. These are required to fully realise the transformational nature of ALMA and to maximise the scientific return for the European community. Fostering community development and guiding the future evolution of ALMA use are among the nodes' primary tasks. The nodes will provide face-to-face help and additional support, beyond what are called *the ARC core functions*, such as advanced user support for special projects and refinement in the data-reduction process. To achieve these goals, the nodes will conduct a programme of fellowships, user grants, student and postdoctoral programmes, as well as promote the organisation of workshops and schools and any other support facilities for users. The sponsoring of workshops, schools, and events that stimulate the scientific activities around ALMA is very important for ALMA's visibility within the European programmes of education and public outreach.

What does a user have to do to submit an ALMA observing proposal?

Once the Joint ALMA Office (JAO) issues calls for proposals, an astronomer wishing to apply for observing time will have to register on the ALMA web page. After registration, the user will make use of the ALMA Observing tool (AOT) to prepare a proposal. The AOT is a java application and is essentially a complete software package enabling one to construct a so-called *Observing Project*. This Observing Project is the top item that any user will work on and consists of two parts: a *Phase I Observing Proposal* with empha-

sis on the scientific justification of the proposed observations and containing a minimal amount of technical information required to check the feasibility of the proposal, and a *Phase II Observing Programme* submitted only if observing time has been granted. The JAO, with assistance from the ARCs, coordinates the refereeing process. If European astronomers need help with the preparation of their Observing Project, they have to address themselves to the EU ARC, which provides documentation, proposal preparation and submission help. In case the users require face-to-face help, they will be directed to their national or geographically closest ARC node, unless it is a highly specialised issue, which can better be addressed at one of the other nodes.

The EU ARC also helps with the planning of the observations of proposals that successfully pass the scientific and technical evaluation of the time allocation committee. With the use of the AOT the user needs to specify the technical details that control how the observations are to be carried out. The user creates a number of scheduling blocks (SBs) that contain all information necessary to execute a single observation. A scheduling block essentially consists of low-level observation commands to be submitted to the observing queue and will typically take 30 to 60 minutes to execute. It can be thought of as the smallest unit that can be scheduled independently, reminiscent of the VLT observation block (OB). It is self-contained and usually provides scientifically meaningful data as well as a full description of how the science target and the calibration targets are to be observed. Sets of SBs can be combined with a description for the post-processing of the data, ultimately resulting in an image or a data cube.

The AOT provides two different 'Views' that can be used to define an Observing Project: a 'Science View' and a 'System View'. In the Science View, inputs should be provided that relate directly to the science goal, such as the area to be observed for each target, the required sensitivity and frequencies. The amount of technical detail in this view is minimal. Therefore, this view is useful for all astronomers, including those with little experience in aperture synthesis interfer-

ometry, to create full Observing Projects using standard observing modes. For more experienced users who desire more control over the telescope configuration, the AOT provides a 'System View'. In this view, more detailed specifications of each Scheduling Block can be given, such as the frequency setting of the local oscillator, the upper and lower side bands, the correlator parameters and the selection of base-bands and sub-band sets within each base-band. This view can also be used by experienced observers and observatory staff to develop and test new observing modes. Figures 3 and 4 show screen shots of the AOT's Visual Spectral Editor and the Visual Spatial Editor.

In accordance with the statement at the beginning of this article, it is foreseen that for most ALMA projects the Science View provides sufficient detailed information to fully specify the observations. The required SBs will be constructed by the system and the user will only be bothered with system parameters when this is absolutely necessary. All material produced in this phase will be verified by ARC staff, after which it will be certified and released to ALMA operations for scheduling and execution.

What does a user have to do to obtain ALMA data?

In the ALMA era, users will not travel to Chajnantor to carry out the observations. Instead, observations will be dynamically scheduled, depending on weather conditions and the array configuration. Observations will be carried out 24 hours per day. Some projects may require only a single configuration, whereas others may need observations using multiple configurations combined with the ACA (Atacama Compact Array, a Japanese contribution) and total power observations. Such a project may need several months to complete.

Before ALMA data reach the PIs, the data will pass through a multi-tier quality assurance programme. This programme is a combination of on-site duty astronomer checks, a quick-look analysis, system performance checks and feedback from ARC staff. After this stage, the data proceed to the data-reduction pipeline and

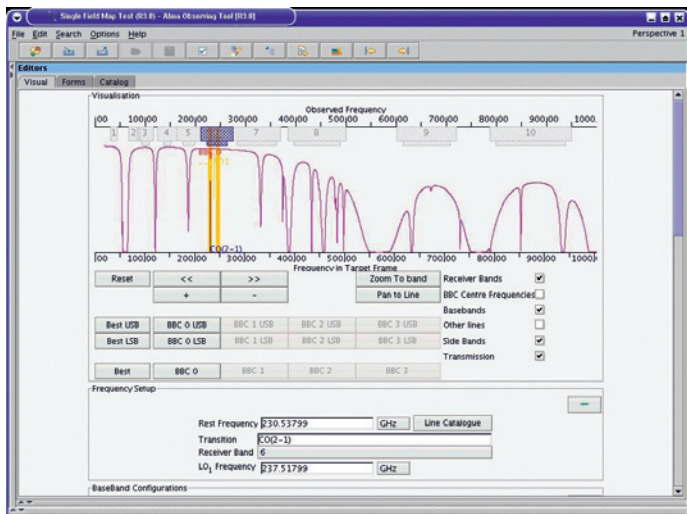


Figure 3: A typical display produced by the ALMA Observing Tool (AOT) using the Visual Spectral Editor. The graphics show the ALMA receiver bands and the user-selected positions for the base-bands and side-bands. Also, the atmospheric transmission curve is displayed.

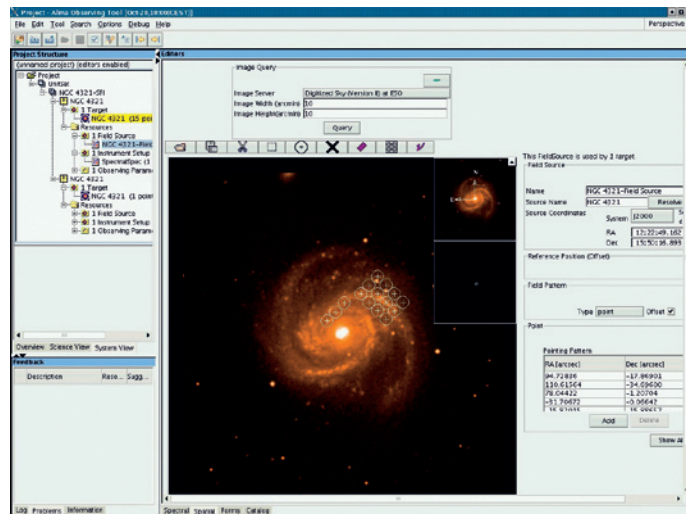


Figure 4: Display of the Visual Spatial Editor of the ALMA Observing Tool for an example single-field interferometry observation of NGC 4321. In the Editors pane the figure shows the image of NGC 4321 as it was retrieved from the ESO image server. The small circles represent the pointing positions for this target observation; the radius shows the size of the primary beam at the observing frequency. On the left the project structure in the System View is visible; on the right is the Field Source form with the Pointing Pattern table of the telescope pointings.

are delivered to the archive. PIs will be notified immediately after their science data become available. The items made available to the PIs are the pipeline products (fully calibrated images or data cubes and calibrated u-v data), raw u-v plane source and calibration data, and off-line data processing software including user support.

It is essential to the success of ALMA that astronomers inexperienced in aperture synthesis imaging techniques are able to obtain science-ready images and data cubes from their ALMA projects. The data-reduction pipeline will therefore produce high-quality science products for most standard observing modes. However, expert hands-on help will be required in many cases, especially when more complicated observing techniques are used. The first point of contact for data reduction help is the ARC main node in Garching, where users can address their questions by telephone or e-mail to a help-desk. Face-to-face help for specialised topics will be available from the nodes spread out over Europe.

Specialised topics that come to mind are for instance high dynamic range imaging, multi-frequency synthesis, mosaicing, high-frequency imaging, self-calibration, advanced data analysis, etc.

The off-line pipeline data-reduction software package responsible for generating science ready data products is CASA (Common Astronomy Software Applications), a C++ code based on aips++ libraries. CASA has recently gone through major changes to optimise its use for ALMA data reduction. One of the most significant modifications is the creation of a completely re-designed python interface. Over the last few years, a series of user tests have been carried out to test the functionality of the data-reduction software and to ensure that the development is adequate for ALMA needs. The tests have concentrated on many data-reduction issues, and essentially covered the full end-to-end process from raw data sets to fully calibrated data cubes. The results from the tests have been very positive and promising, all testers were able to edit, calibrate and image the test data sets.

Concluding remarks

Although full ALMA operations will start in 2012, pre-operation activities have already started. The ARCs are organising the support system, testing the software, writing cookbooks and manuals and preparing the commissioning and science verification phase, which will be starting in 2009. The first call for proposals for Early Science will be issued in early 2010 and the ARCs must be functioning at full speed before that date.

The international community can provide inputs into the ALMA project and operation through their representatives in the ALMA Science Advisory Committee (ASAC) and the European community through the European ALMA Science Advisory Committee (ESAC). Links to these committees can be found in <http://www.eso.org/projects/alma/administration/committees/>.



Photo: H. Botini / ESO



Sunset on Paranal. Unit Telescope 1 (Antu) preparing for observations and three Auxiliary Telescopes of VLTI undergoing tests.

Report on the Workshop on

Deep Impact as a World Observatory Event

held in Brussels, Belgium, 7–10 August 2006

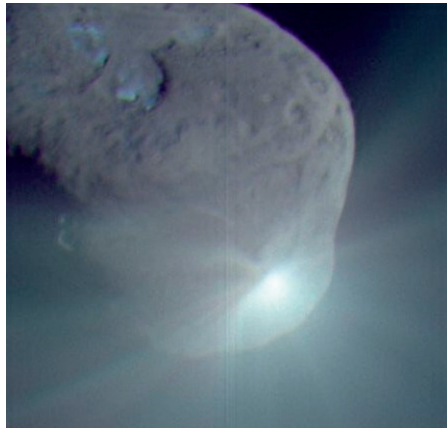
Hans Ulrich Käufel¹
Christiaan Sterken²

¹ ESO

² Vrije Universiteit Brussel, Belgium

In the context of NASA's Deep Impact space mission, Comet 9P/Tempel 1 has been at the focus of an unprecedented worldwide long-term multi-wavelength observation campaign. The comet has been studied through its perihelion passage by various spacecraft including the Deep Impact mission itself, HST, Spitzer, Rosetta, XMM and all major ground-based observatories in basically all wavelength bands used in astronomy, i.e. from radio cm-waves to X-rays. For some 'glossy-print' information please have a look to e.g. ESO's dedicated web-pages (*deepimpact.eso.org*). Due to the dynamical and other technical constraints of the space mission, ESO's telescopes could not observe the moment of impact – the comet was indeed exactly setting on the western horizon. However, the ESO observatory sites, La Silla and Paranal were more or less the worldwide hub of the mid- and long-term ground-based observations for monitoring. Predictions for cometary activity induced by the experiment made before the impact ranged from 'very little' to the instantaneous release of material equivalent to ~ 10 days of normal activity of the comet close to perihelion. In summary, Mike A'Hearn, the PI of Deep Impact, confirmed in his review talk, that the release was at the lower end of expectations and that there was no activity of the impact site induced after the crater had formed. Especially as the long-term signatures after impact were rather subtle, the use of the world's best facilities to document the event was well warranted in retrospect.

The ground-based observing campaign has been described in a recent Science publication by 209 authors from 85 academic institutions all around the world (Meech et al. 2005). Some early results from the ESO observations have been reported earlier in The Messenger (Käufel et al. 2005).



One of the spectacular deconvolved images from the Deep Impact Spacecraft High Resolution Imager shown in the conference (courtesy Mike A'Hearn and the Deep Impact Team). This is a colour composite of an infrared, a green and a violet filter forced to average grey. Note the blueish areas on the surface close to the crater-like structure. Those were entirely unexpected. It is highly interesting to find out if those structures can be correlated with the jets which were meticulously monitored from ground-based observers worldwide. This aspect in the picture – entirely unrelated to the impact plume – illustrates very well how comet research, apart from the impact experiment, will profit from the synergy of spacecraft data and the unprecedented worldwide coordinated observing campaign.

To make full use of the global data set, a workshop bringing together observers across the electromagnetic spectrum and from different sites and projects was considered of great value. Synergy between the different data sets can only be achieved if observers share their data and arrive at a coherent interpretation. Therefore the astronomers participating in the ESO campaign took the lead to organise this workshop on a rather short notice. The workshop was held in Brussels, Belgium from 7 to 10 August. More than 70 colleagues presented 50 oral papers and 18 posters. The proceedings will be published in the ESO Springer conference series.

At the Brussels workshop – 12 months after Deep Impact – all participants had progressed sufficiently in the analysis and understanding of their data sets. The coherent presentation of many diverse results allowed for a synthesis. Thanks to the Deep Impact campaign, many properties from thermal inertia to tensile strength of the cometary nuclear surface are now well constrained. Already at the workshop an intense discussion to arrive at synergies – which will be transcribed for the proceedings – took place. Particularly interesting and exciting, however, are the open questions such as: the chemical composition of the ejecta; the correlation of the complex observed dust fans reported from many weeks of ground-based monitoring of nuclear surface features, as imaged by the spacecraft; and the absence of long-term effects from the impact site. Indeed the nature and physics of jets and active zones of comets appears more enigmatic than ever.

To inspire new ideas, it was very helpful and interesting to have Roberta Olson from the New York Historical Society, author of the book *Fire in the sky* (Olson and Pasachoff 1999), at the workshop delivering a lecture titled *Comets, Charisma, and Celebrity: Reflections on Their Deep Impact*. Comets, like no other class of celestial objects, have spurred intense attention of mankind to watch the skies and to wonder about the underlying principles and messages. For many participants, however, it was new how far reaching the impact of apparitions of bright comets on the general public are and how this manifests itself in many diverse pieces of art.

As with any good research project, the Deep Impact experiment and the associated observation campaign have answered a fair set of questions about comets, but there are still open questions and there is now a full set of new questions. On the other hand, the next generation of spacecraft, especially the ESA-mission ROSETTA, to land in August 2014 on Comet 67P/Churyumov-Gerasimenko and the next generation of optical and radio telescopes, e.g. ALMA and the ELT, will be the keys to solve at least some of the truly enigmatic aspects of comets (and create new questions).

Acknowledgements

Our special thanks go to the sponsoring organisations, ESO, the FWO Research Foundation – Flanders, the Brussels Hoofdstedelijk Gewest, the Ministerie van de Vlaamse Gemeenschap and the host for the workshop, the Royal Academies for Science and the Arts of Belgium.

References

- Meech K. et al. 2005, *Science* 310, 265
Käufel H. U. et al. 2005, *The Messenger* 121, 11
Olson R. and Pasachoff J. M., "Fire in the Sky", ISBN 0521663598. Cambridge, UK: Cambridge University Press, November 1999

The participants to this workshop, in the great hall of the magnificent palace of the Royal Academies for Science and the Arts of Belgium. The very special atmosphere of this historical building was very inspiring for this workshop. During the worldwide ground-based Deep Impact follow-up observing campaign, all observatories were basically linked and exchanging data, views and strategies quasi in real-time. This unique spirit prevailed also during this dedicated workshop.



Photo: T. Tuivikene

Around and about “Europe’s Quest for the Universe”

Jean-Pierre Swings

(Institut d’Astrophysique et de Géophysique, Liège University, Belgium)

Before even starting a review of “Europe’s Quest for the Universe”, I think one should say a few words about its author. A truly impressive characteristic of Professor Lodewijk Woltjer is indeed his vision towards excellence, in particular towards excellence in observational astrophysics in (and for) Europe. One example: almost thirty years ago, he ‘forced’ some fairly conventional European observers to start working on extragalactic astrophysics on the occasion of the erection of ESO’s 3.6-metre telescope, and even more so when the 3.5-m New Technology Telescope became available. As far as my own research group was concerned, this led to the discovery, via these ESO telescopes, of several gravitational lenses. This type of research was in fact made possible because Lo Woltjer put together excellent teams of engineers and scientists at ESO dedicated to

developing innovative and sophisticated telescopes and their auxiliary instruments.

Professor Woltjer, ESO’s Director General for 13 years, was also instrumental in initiating studies towards conceiving and building a European Very Large Telescope (the VLT), and getting the VLT construction started. Having been deeply involved in the VLT advisory structure (which he kindly mentions in his book!) I can testify that Lo Woltjer’s role was incredible: from a European vision to a remarkable ground-based astronomy machine.

In parallel to this, he also had another vision, this one about interesting objects to observe, and at which wave-bands. Here again his role in chairing the groups defining the future of European space astrophysics was really fundamental, so that ESA’s Horizon 2000+ objectives became fantastic challenges.



So, in addition to his skills in theoretical astrophysics, a very interesting characteristic of Lo Woltjer concerns the two complementary facets: ground-based and space-borne astrophysics. In both cases, as briefly outlined above, he played a pivotal role. He is therefore highly qualified to have written the recent 300-page book about the origins and evolution of the European Southern Observatory (ESO) and of the science pro-

gramme of the European Space Agency (ESA): “Europe’s Quest for the Universe”*.

The preface by Philippe Busquin, former European commissioner for research, sets the tone of the book: “Great pride and optimism for European science comes across on reading these pages, all beautifully illustrated. Written to a high scientific level, this book provides the reader with a top quality reference on the subjects covered, and gives us ample reason to believe in a European research environment directed firmly to the future.”

Lo Woltjer has been involved in many, if not most, of the topics he describes in his book. He does this in a factual manner, quoting many actors, including himself, and omitting (purposely?) very few!

* To my knowledge, there exist so far two reviews of this book, one, quite detailed by Françoise Praderie, in the spring 2006 issue of Euroscience News (no. 34, page 9), the other by Giovanni Bignami, published in Nature (441, page 814, 15 June 2006).

Not only does he give us a somewhat ‘historical’ inventory of the telescopes and instruments that were built in the last three decades on the ground and for space, he also presents strong arguments for new sophisticated and ever more challenging developments. The author of “Europe’s Quest for the Universe” gives, probably as good examples to be followed, some interesting details about several of the most important astrophysical results that have been obtained in these last decades, some of which have led to attributing famous prizes (Nobel, Balzan, Gruber, ...) to their ‘prime-investigators’.

In the last sections of his book, Lo Woltjer, in a well-documented way that he shares with the reader, deals with fairly controversial matters such as publications, researchers and funding (“Why fund astronomy?”), and finally he tackles a series of future projects as well as the difficult subjects of international collaborations and organisational issues, the

latter two which, I think, could/should serve as challenges to e.g. the ESO Council and the present and forthcoming ESO Director General, and to their counterparts in the ESA Science and Exploration Directorates!

Let me end this very short review by briefly paraphrasing Philippe Busquin. The Universe is so magnificent that it constantly inspires both scientific and technological developments. Yet, at the same time, it remains a source of wonder and inspiration for our thoughts and dreams: is this not beautiful for all generations, especially the younger ones? Europe is definitely taking advantage of all this, as is so well demonstrated in Lo Woltjer’s book (although here and there a bit critically!). So, let’s continue to follow “Europe’s Quest for the Universe”, showing that our continent is the leader in several aspects of ground-based and space-borne astrophysics, as Lo Woltjer has shown us how to do so successfully.

Open House at the ESO Headquarters

Claus Madsen (ESO)

On 15 October, the ESO Headquarters opened its doors to the public as part of the All-Campus Open House organised in connection with the inauguration of the extension of the underground line U6 from Munich to the Garching campus. The day was blessed with clear skies and plenty of sunshine, and a large number of citizens took advantage of the opportunity to visit the campus. The estimated number of visitors at ESO was close to 3000 people, a record number. Another record was set by the number of ESO staff who, in anticipation of the high number of guests, volunteered to spend their Sunday at work to explain what ESO is doing and why it is important.



Visitors to the Open House learnt about ESO from exhibitions, activities, and presentations throughout the Headquarters in Garching.

Over the last couple of years, we have 'remodelled' the Open House and this time, the activities were organised around 'thematic clusters' called "Welcome to ESO", "The Observatory", "Science", "Technology for Astronomy" and "Astronomy for All". While most staff were assigned to the clusters, some acted as 'roaming astronomers' and as tour guides, accompanying groups of visitors through the house.

As in the past, the programme of the day offered a wide palette of activities and opportunities to learn about ESO: Video presentations and public talks in the auditorium, videoconferences with Paranal, information about employment opportunities at ESO, various technology demonstrations ranging from CAD-based telescope design to AVO, and a dedicated childrens' programme including planetarium shows, quiz and 'passport' games. ESO's amateur astronomy club, AGAPE, had trained their telescopes on the Sun and attracted many interested 'observers'. Also, the ESO Charity Group took part and enjoyed brisk sales from their stand, offering cakes and sandwiches and with the revenue going to, amongst others, the SOS Kinderdorf in Antofagasta. Contests for children (and their parents!) and ESO materials such as posters and T-shirts on sale completed the programme.

Meanwhile, the All-Campus Open House has developed into an activity which is recognised and appreciated beyond the boundaries of Garching or even Munich. This is evident from the fact that ESO, together with three other institutes on the campus, was awarded a special trophy by the initiative "Deutschland – Land der Ideen". This initiative happens under the auspices of the President of the Federal Republic of Germany, Dr. Horst Köhler, and is supported both by the Government and by German industry and commerce.

With this recognition and an end-of-the-day pizza party for the personnel involved in the event, the 60 or so ESO staff members headed for home, tired no doubt, but also with many interesting discussions and encounters behind them – just as the members of the public that had made their way to ESO on the day.

AGAPE, ESO's amateur astronomy club, set up telescopes so that interested visitors could safely observe the Sun while enjoying the good weather.



Photos: H. Hoyer, ESO (4)



Visitors had the chance to see what they looked like in infrared light – and to take home a copy of the results.



Parts of the new VLT instrument HAWK-I, including its steel vessel, were on display in the integration hall.



ESO received a trophy from the "Deutschland – Land der Ideen" programme, in recognition of its contribution to the All Campus Open House event.

Report on the

NEON Observing Schools 2006

Michel Dennefeld¹
Harald Kuntschner²

¹ Institut d'Astrophysique de Paris, France
² ST-ECF

This year has seen the organisation of two NEON summer schools, sponsored by the European Community Marie Curie Actions programme: the Fifth NEON Observing School (23 July–6 August, 2006) at the Observatoire de Haute-Provence, France; and the Second NEON Archive Observing School (30 August–9 September, 2006) at ESO Headquarters, Germany. The purpose of these summer schools is to provide the opportunity for young astronomers to gain practical experience in observational techniques, data reduction and analysis and the use of virtual observatory tools.

The students at both schools carried out small research projects, centred on front-line astrophysical topics, in small groups under the supervision of experienced astronomers. These practical exercises are introduced by lectures on general observational techniques and archival research for both ground- and space-based astronomy, by world-class lecturers also supported by the Opticon Network.

The observing school at the Observatoire de Haute-Provence (OHP) concentrated on the skills required to execute an observing programme at the telescope, from the preparation of targets to data reduction, including the set-up and calibration of the instruments. This school gathered 22 students of 13 different na-



The NEON school participants at OHP.

tionalities, with an exact balance of gender (the selection had been based on purely scientific criteria). The research projects in groups of four or five dealt with the following topics: observation and interpretation of variability at the lower end of the Cepheid instability strip, led by Yves Fremat (Belgium); the Tully-Fisher relation in local clusters, under the direction of Joel Vernet (ESO); spectroscopic and interferometric study of the star χ Cygni, with Hervé Le Coroller (OHP); physical characterisation of selected asteroids, under the supervision of Simone Marchi (Padova); and the study of stellar populations in elliptical galaxies, led by Santos Pedraz from the Calar Alto Observatory (Spain). The students could use four different telescopes with either CCD-photometry or spectroscopy, the smallest but not least interesting being an 80-cm telescope with a mirror polished by André Couder himself; this one was used for visual observations and some technical

tests, in particular the Foucault knife-edge test which probably only the oldest of the presently active astronomers still remember how to perform.

The school saw intensive days and nights in a very pleasant setting. The instrument development laboratories and the geophysical research activity on the site provided other topics of interest as distractions!

The Archive Observing School at ESO focused more on the use of existing data and the multi-wavelength research possible with high-quality archival data combining ground and space observations. The first step, instead of acquiring the data at the telescope, consisted of the archive retrieval and quality appraisal of the data. In the case of HST data, often a science-ready product can be retrieved while for other data the typical data-reduction steps have to be performed. Twenty students (13 female and 7 male) coming from 12 different European countries attended. A full record of the school, including the final presentations of the research projects can be found at <http://www.eso.org/neon-2006>. The research projects, conducted in groups of four, were focused on the multi-wavelength analysis of archival data spanning a wide range of astrophysical topics: VLT/FLAMES-GIRAFFE spectroscopy of stars in the open cluster NGC 2506 to determine radial velocities and abundances, under the lead of Frédéric Royer (Paris); searching for a galaxy at redshift 10 us-



The NEON school participants at ESO Headquarters.

Photo: E. Janssen, ESO

ing ultra-deep ISAAC and FORS imaging, guided by Michael Schirmer (ING, La Palma); calculating the ionising flux of O-stars in dusty embedded star clusters using VLT/VISIR and HST images, introduced by Margrethe Wold (ESO); the search for ultra-compact dwarf galaxies in Abell 1689 with the help of HST images and spectroscopic confirmation with VLT/FORS, led by Steffen Mieske (ESO); and last but not least, the study of globular clusters and low-mass X-ray binaries in a Virgo elliptical by combining HST imaging with Chandra data, under the supervision of Andrés Jordan (ESO). Besides the usual series of lectures introducing basic photometric and spectroscopic techniques, special attention was given to the presentation of the available archives and archival research techniques. Taking advantage of ESO's strong involvement in instrumentation and telescope design, further lectures dealt with

the diversity of instrumentation covering a large wavelength range and the history and future of telescope design.

The feedback from the school indicated a high satisfaction rate of the students and, what is more important, a notable increase in interest to make use of archival data and the need to learn more about the relevant research tools including Virtual Observatory developments. It is clear that the multi-wavelength approach is becoming the best way to do good research in astrophysics.

A common feature of both schools was the very positive impact of gathering students from various origins and nationalities, which is seen as a good start for future, pan-European collaborations. This was complemented by open discussions on the situation of jobs in astronomy and career strategies. Various job

possibilities at individual universities and laboratories were presented as well as the more general exchange programmes offered by the European Union.

It is clear that the success of these schools calls for more such events in the future. We are pleased to announce the next NEON Observing School which will take place in Asiago Observatory (Italy), 4–18 September 2007. More detailed information on programme and registration will be announced later this year on the EAS web pages and through the usual communication channels. A further two NEON schools are planned for 2008: one will take place in La Palma using the ING and NOT telescopes, and the other one at ESO Headquarters, Garching, once more focusing on the use of Archival Data.

Report on the Meeting on

Science with ALMA: a New Era for Astrophysics

held in Madrid, Spain, 13–18 November 2006

**Paola Andreani, Martin Zwaan,
Robert Laing (ESO)**

Three hundred scientists from all over the world met during a warm November week in Madrid to discuss the scientific revolution (or, according to one speaker, evolution) that we expect from ALMA. The large number of participants, the richness of the science and the wider community's increasing interest in ALMA made this meeting an optimistic and exciting one. The talks and posters covered almost all of the science areas relevant to ALMA including its main drivers: the formation and evolution of galaxies, the physics and chemistry of the interstellar medium, and the processes of star and planet formation. We heard about new results from the current generation of millimetre and sub-millimetre arrays such as the SMA and the recently up-

graded Plateau de Bure Interferometer, as well as related observations at other wavelengths (especially from the Spitzer Space Telescope). The anticipated performance of ALMA and the current status of the project were both described, and many speakers presented ambitious plans for observing with the array once it becomes fully operational. It would be impossible even to list all of the contributors in a short article; instead, we briefly summarise some of the key topics, concentrating on star and galaxy formation.

Our present picture of low- and high-mass star formation is based on indirect evidence. Although the formation sites have been identified, the processes cannot be followed in detail. Stars form in the central cores of molecular clouds, mostly in multiple systems and coherent clusters. Observations show that the mass function of the molecular condensations

is similar to the initial mass function for stars and that the fraction of the cloud in the condensed phase corresponds to the expected star-formation efficiency, but we do not know which physical processes govern the mass fragmentation of molecular clouds and hence shape the initial mass function. We do not understand in detail the kinematics and dynamics of accretion onto protostellar cores, the formation and collimation of outflows and the eventual evolution of circumstellar discs to form planetary systems, asteroids and comets. Still less do we comprehend the role of magnetic fields.

ALMA will be able to see the collapse of the central regions in pre-stellar cores and in young stellar objects, image the complex structures of infalling, outflowing and accreting material and follow the formation and evolution of discs. These processes will be studied not only with

high-resolution continuum observations but also spectroscopically. Molecular abundances vary with evolutionary state, as different species appear and disappear, for example by depletion onto dust grains. A plethora of molecular species can be used as tracers of the complex physics and chemistry and the ability to model these processes with high spatial resolution was identified as an essential complement to ALMA observations.

Precision measurements of the spectral energy distributions of dust formation sites will give an indication of the grain size distribution in circumstellar discs. The evolution of dust can be followed as dusty particles around young stars collide and grow from sub-micron sizes to pebbles, boulders, planetesimals and eventually planets. The gaps predicted to occur in circumstellar discs as a result of planetary formation can be imaged directly by ALMA.

ALMA will enable a comparable series of advances in the field of galaxy formation and evolution, particularly at early epochs. Galaxy number counts will be extended to the faintest sources in every ALMA band. The spatial and redshift

distribution of these sources, as well as their luminosity functions will become measurable, as ALMA will not be confusion limited in any of its bands. It will excel as a follow-up instrument for large-area surveys with bolometer arrays, both in resolving continuum emission and in measuring redshifts from molecular lines. Very deep, but narrow-field surveys will also be carried out with ALMA alone. CO will be the molecule of choice for redshift measurement except for the earliest galaxies ($z > 6$), for which singly ionised carbon may be more appropriate. The reason is that the energy output in this line is likely to be much higher than in the very high order CO transitions redshifted to ALMA frequencies. Continuum observations of the dust emission from the very first galaxies, as well as spectroscopy of their molecular and atomic lines, will allow us to probe the epoch of re-ionisation for the first time. The measurement of molecular absorption lines towards quasars will probe more tenuous regions along the line of sight as well as placing strong limits on the variation of fundamental physical constants, such the fine-structure constant α .

The dynamics of mass assembly in galaxies at $z \approx 3$ is just beginning to be resolved using ground-based near-infrared observations. ALMA will extend this to fainter, more typical and obscured objects. Indeed one of its top-level science requirements is to be able to resolve a galaxy like the Milky Way at $z = 3$ in CO or CII. On larger physical scales, imaging of the Sunyaev-Zel'dovich effect will provide a unique probe of substructure in the intracluster medium. The detailed chemistry of star formation in nearby galaxies will be a major topic for ALMA, as will the relationship between active galactic nuclei and starbursts.

The meeting took place at the Consejo Superior de Investigaciones Científicas (CSIC) in Madrid and was financed by CSIC, Observatorio Astronómico Nacional, the ALMA project, ESO, NRAO, NAOJ, RadioNet and Astrocam. It was the second world-wide meeting on "Science with the Atacama Large Millimeter Array" (the first took place in Washington, D.C., in October 1999). The proceedings will be published in a special edition of *Astrophysics and Space Science* and the majority of presentations will be made available linked to <http://www.oan.es/alma2006>.

Prestigious NASA Award for ST-ECF (ESO/ESA) Scientists

A team of scientists from the Space Telescope European Coordinating Facility (ST-ECF) and the United States National Institute of Standards and Technology (NIST) has received one of the most prestigious honours issued by NASA: a Public Service Group Achievement Award: "In recognition of painstaking efforts to provide maximum scientific value to HST data using precision laboratory spectral measurements and physical instrument modelling techniques."

In this transatlantic cooperation which earned this recognition, the European group (Michael Rosa, Florian Kerber and Paul Bristow; Figure 1) joined forces with their US colleagues (Joseph Reader, Gillian Nave, Craig Sansonetti; Figure 2)

with the aim of improving the calibration of Hubble Space Telescope (HST) spectrographs.

In their effort the team combined advanced modelling techniques, to describe the physical properties of a scientific instrument, with high-quality laboratory measurements of the spectral lines emitted by a Pt/Cr-Ne hollow cathode lamp used as calibration source onboard HST. The measurements performed in the laboratory of the NIST Atomic Spectroscopy Group filled a significant gap in our understanding of the output of such lamps and added about 5 000 lines as wavelength standards now usable for calibration purposes. These enhanced line lists were used as input for the instru-



The European part of the NASA award winning team, the group at ST-ECF: Florian Kerber, Michael Rosa, Paul Bristow (left to right).

ment models of two HST spectrographs, a technique that replaces empirical fitting routines with the knowledge of the physical properties of the instrument. A physical instrument model is based on the optical and mechanical design of the spectrograph but will also take into account environmental conditions such as temperature. Group Leader Michael Rosa said: "Calibration based on instrument models has been demonstrated to provide better accuracy than empirical methods but in addition it also provides a real understanding of the instrument which enables one to maintain it at maximum performance and quickly diagnose any deviations."

The NASA award specifically acknowledged that the instrument modelling approach and its success is not specific to any instrument but can be applied to a large variety of astronomical instruments. It is no surprise that instrument modelling, originally developed for ESO's high-resolution spectrograph UVES, and having been 'to space' is coming full circle. Two members of the team (Florian Kerber and Paul Bristow), now with ESO's Instrumentation Division, are applying the NASA award-winning methods – instrument modelling combined with state-of-the-art laboratory measurements in a collaboration with ST-ECF and NIST – to the calibration of the latest spectrographs for the VLT, the Cryogenic IR Echelle Spectrometer (CRIRES) (see page 32 of this issue) and X-shooter. With the development of extremely demanding future instruments for a European ELT, new challenges await.



The US part of the NASA award winning team, the group at NIST: Joseph Reader, Gillian Nave and Craig Sanonetti (left to right).

Fellows at ESO

Dominique Naef

I completed my PhD thesis in the Geneva extra-solar planets search group late 2003. During my PhD years, I participated in so many observing runs at the Swiss telescope at La Silla that making a post doc in Chile became quite an obvious choice. In spring 2004, I moved to ESO-Chile with a Swiss grant. During my first post doc year, I worked in the La Silla Science Operations team where I was mostly involved in the support of the HARPS spectrograph. Later in 2004, I applied successfully for an ESO fellowship.

I started this second post doc in spring 2005 at the Paranal Observatory. At Paranal, I mostly work with the UT2-Kueyen telescope and I am attached to the FLAMES support team. A large part of the fellows' duties consist in executing service-mode observations. I really enjoy it since it gives me the possibility to

learn a lot about fields in astronomy that are very far from my favorite ones. Supporting visiting astronomers during their observing runs at Paranal is also a task I really appreciate because it gives me a unique opportunity to get direct feedback from ESO users. Moreover, very stimulating scientific discussions are not rare during these visitor runs.

My main scientific interests are the detection and characterisation of extra-solar planets and brown dwarfs. I am involved in several planet search programmes using various ESO and non-ESO facilities: HARPS at the 3.6-m telescope, CORALIE at the Swiss 1.2-m Telescope, FLAMES at VLT-UT2 or NACO at VLT-UT4. I also participate in programmes aiming at the characterisation of transiting exoplanets using ground-based facilities (e.g. FORS1 at VLT-UT2) and space-based telescopes (e.g. HST or XMM). The main goal of all these research activities is to understand how planets form around stars.



Dominique Naef

Helping to Build ASTRONET Science Vision: A Unique Opportunity to Contribute to the European Astronomical Scientific Strategy for the Next 20 Years

Guy Monnet (ESO)

In the very short period of two months only (December 2006 and January 2007), every European astronomer is invited to add her/his stone for the building of a common European astronomical "Science Vision" for the next 20 years. You are strongly encouraged to register immediately to the 23–25 January 2007 Science Vision Symposium, and as of 1 December 2006 to contribute to a web-based forum on future scientific challenges in astronomy. Please do not miss this unique opportunity to steer European astronomy towards a vibrant future!

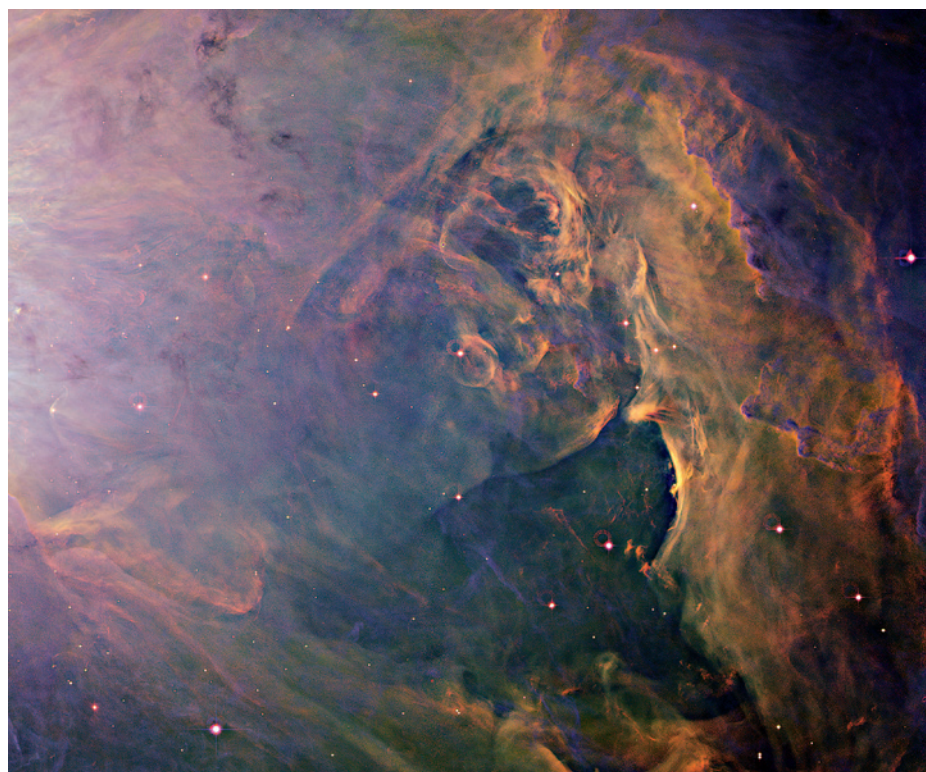


Establishing a Science Vision is the first crucial segment of a whole process conducted by ASTRONET (<http://www.astronet-eu.org/>), the consortium created by a group of European funding agencies, and financed by the European Commission, in order to establish a comprehensive long-term planning for the development of European astronomy. The Science Vision (<http://www.astronet-eu.org/-Science-Vision->) will cover all wavelengths and observing means from ground and space and is currently being distilled by thematic panels drawn from the astronomical community. On 1 December 2006 a discussion forum on "Future Scientific Challenges in Astronomy" will be opened on the ASTRONET web site. Your input will be incorporated by the relevant panels for the presentation of their preliminary conclusions at the 23–25 January 2007 Science Vision Symposium in Poitiers, France (<http://www.eso.org/gen-fac/meetings/SciChall07>). At registration you will be required to sign for the thematic panel closest to your scientific area, and the preliminary conclusions of each panel (including the inputs from the web-based discussion forum) will be re-discussed at the Symposium



venue by these much-enlarged panels. A special general discussion is also organised to bring forward any missing or overlapping science themes. Through this process, for which your advice is absolutely essential, ASTRONET will then deliver its final Science Vision report to the Commission by the end of March 2007.

The next crucial phase will be the building of a detailed "Infrastructure Roadmap" to attain the scientific goals as defined in the "Science Vision". This process is now just starting (<http://www.astronet-eu.org/-Infrastructure-Roadmap->), again from thematic panels soon to be installed. Active participation from the whole community in a rather similar setting will again be actively sought, most probably in a year or so: please bookmark the ASTRONET home page and stay tuned!



A less well-known region of the famous Orion Nebula HII region (M42, NGC 1976) is shown in this image obtained with the WFI instrument on the 2.2-m telescope at La Silla. The ionising star cluster ('The Trapezium') is to the east (left) of the area shown. The combination of three narrow band filters, centred on the strong emission lines of [O III], H α and [S II], provides the colour image and the impression of depth to the picture. The orange and red (low ionisation) regions trace a great bay where the gas and dust of the local cloud has been sculpted by the ionising radiation of the hot young stars. A haze of blue filaments (high ionisation gas) wash over the image from the left and are between the molecular cloud and the observer. The original observations were taken by Massimo Roberto and colleagues in December 2001 and the image was reduced by Benoît Vandame (ESO). The cover picture on The Messenger 122 (December 2005) derives from another region of the same image.

ESO Workshop on

Observing Planetary Systems

5–8 March 2007, Santiago de Chile, Chile

This workshop aims to bring together both communities of Solar System and extra-planetary systems scientists to discuss, mostly from an observational standpoint, our understanding of the formation of our Solar System and its early chemistry, and how it fits with recent observations and current knowledge of the formation of planetary systems at large.

We invite you to join this workshop that will be held at the ESO premises in Vitacura, Santiago de Chile, from 5–8 March 2007. The meeting will be organised in four sessions approached both from the Solar System and extra-solar system perspectives. Each session will host invited talks and contributed presentations. Space will be made available for poster display. The total number of participants will be limited to about 80 people.

Sessions and invited speakers are: *Discs*: François Ménard “Observations and models of circumstellar discs”, Charles Telesco, “Observing planetesimal collisions in discs”, Alessandro Morbidelli “Dynamical processes in the early Solar System”; *Search for planets*: Didier Queloz “Status and prospects of radial velocity searches”, Olivier Hainaut “Finding the big outer Solar System bodies”, David Mouillet “Direct detection of exoplanets”; *Planet’s chemistry*: David Charbonneau “Probing the atmosphere of transiting exoplanets”, Inga Kamp “Astrochemistry: From discs to protoplanets”, Michael Mumma “Comets as messengers from the early Solar System”; *Finding other Earths*: Chas Beichman “Roadmap to other Earths”, Lisa Kaltenegger “Biomarkers of other Earths”, Malcolm Fridlund “Expected results from COROT and Darwin”.

Important deadlines and contact information:

Submission of abstracts: 15 December 2006 (late submission will be considered depending availability of space)
Final selection: 15 January 2007
Conference e-mail: ops_ws07@eso.org
Web page: <http://www.sc.eso.org/santiago/science/OPSWorkshop>

Scientific Organising Committee: Isabelle Baraffe, Antonella Barucci, Hermann Bönnhardt, Dale Cruikshank, Christophe Dumas (Co-chair), Wolfgang Gieren, Anne-Marie Lagrange, Dante Minniti, Andreas Quirrenbach, Michael Sterzik (Co-chair), Stéphane Udry, Benjamin Zuckerman

Local Organising Committee: <http://www.sc.eso.org/santiago/science/PlanetaryGroup>

Conference on

Obscured AGN Across Cosmic Time

5–7 June 2007, Seeon, Bavaria, Germany

Current deep surveys, notably in X-rays and the mid-IR, are making it possible to carry out a census of essentially all the luminous AGN in the Universe. By penetrating the obscuration that, in Type 2 sources, hides the nuclear regions in the UV to the near-IR spectrum, these new surveys are finding the radio quiet counterparts of the powerful radio galaxies.

The completion of such a census has substantial cosmological significance since it will provide the foundation for identifying the role of AGN feedback in the galaxy-formation process. The Type 2 sources are of particular value here since, by acting as their own coronagraphs, they facilitate the study of the star-formation activity and the investigation of the correlated growth of the black hole and the host galaxy.

While radio galaxies – which are being used to trace the massive galaxy population at all epochs – have been studied intensively for the past 40 years, their radio quiet counterparts beyond the local Universe are only now being discovered in substantial numbers. The workshop aims to bring together the established radio galaxy community with the students of the radio quiet sources and so help to elucidate the effects of the (possibly) different host galaxies and environment and those of the powerful radio jets.

The conference will be held at Kloster Seeon, a recently renovated 10th-century benedictine monastery near lake Chiemsee. This state-of-the-art conference centre includes a three-star hotel with 88 rooms and a restaurant proposing excellent cuisine with regional speciali-

ties. Seeon is located halfway between Munich and Salzburg at the foothills of the southern Bavarian Alps. The conference will be limited to 120 participants. We foresee no proceedings and no poster session.

For further information, see <http://www.eso.org/agnii2007>

Contact: agnii2007@eso.org

ESO Workshop on

Science with the VLT in the ELT Era

8–12 October 2007, ESO Headquarters, Garching near Munich, Germany

The first of the ELTs (Extremely Large Telescopes) now under study could see first light in around 10 years when the ESO VLT will still be fully operational and receiving new second-generation instrumentation and upgrades. Even before then we will also have entered the ALMA (and JWST) era. This Workshop will provide a forum for the ESO community to debate and provide valuable feedback on how it expects the scientific use of the VLT and VLTI to evolve over this period and the priorities to be set in the next Call for Instrument Proposals expected to be issued in 2008.

Amongst the topics envisaged are: Science highlights illustrating unique VLT and VLTI capabilities; New science op-

portunities created by instruments becoming available in 2008–2012 (HAWK-I, X-Shooter, KMOS, SPHERE, MUSE, PRIMA, and possible second-generation VLTI instruments); Research priorities identified by ASTRONET, Radionet, ESA/ESO WGs; VLT and VLTI synergies with ELT, ALMA, JWST; ELT science priorities and possible first-light instruments; VLT and VLTI science priorities beyond 2012 and possible consequences for specialisation of telescopes and changes in operational models; Resources and concepts for new second-generation VLT instruments to be installed beyond 2012.

It is intended to invite review/overview talks to introduce these topics; to complement them with contributed papers and posters and to include ample time for discussion.

For more details please consult the web page <http://www.eso.org/vlt07> or e-mail vlt07@eso.org or contact the

Scientific Organising Committee: Alan Moorwood (Chair), Tom Herbst (Co-chair), Willy Benz, Mark Casali, Bruno Leibundgut, Yannick Mellier, Jorge Melnick

Local Organising Committee: Markus Kissler-Patig, Christina Stoffer, Iris Bronnert, Pamela Bristow



ESO
European Organisation
for Astronomical
Research in the
Southern Hemisphere

ESO is opening the following position of

International Cooperation Scientist

The successful candidate will support and assist the Director General in establishing agreements, and represent ESO in various international fora on the European and the international scene. Involvement is expected in the area of international cooperations and in European initiatives in astronomy, such as OPTICON, ASTRONET and RadioNet. Furthermore, she/he will be active in the cooperation with the Board of Directors of the journal *Astronomy and Astrophysics* and with the Forum of European Intergovernmental Research Organisations (EIROForum).

As an astronomer and member of the ESO Science Faculty the successful candidate will be expected and encouraged to conduct astronomical research up to 50 % of the time and participate actively in the scientific life of ESO. Research in areas directed towards effective use of the ESO facilities will be strongly encouraged.

The position requires a PhD in astronomy, physics, or equivalent. Candidates should have worked in astronomical research for several years and should be familiar with the European astronomy scene. A very good scientific publication record, excellent communication and interpersonal skills, the ability to work in a team, managerial abilities, and a good command of the English language are essential.

For details and to download an application form, please consult our home-page: <http://www.eso.org>. If you are interested in working in a stimulating international research environment and in areas of frontline science and technology, please send us your application in English to:

ESO Personnel Department
Karl-Schwarzschild-Straße 2
85748 Garching near Munich, Germany
e-mail: vacancy@eso.org

*ESO is an equal opportunity employer.
Qualified female candidates are invited to apply.*

ESO. Astronomy made in Europe



Personnel Movements

1 October–31 December 2006

Arrivals

Europe

Allouche, Fatmé (LB)	Student
Boutsia, Konstantina (GR)	Student
Brunner, Renate (D)	Accountant
Chéreau, Fabien (F)	Software Engineer
Erdman, Christopher (USA)	Librarian
Felber, Nina (D)	Secretary/Assistant
Galametz, Audrey (F)	Student
Granato, Francesca (GB)	Student
Grillo, Claudio (I)	Student
Hatziminaoglou, Evanthia (GR)	Astronomer
Klein Gebbinck, Maurice (NL)	Software Engineer
Laurini, Silvia (I)	Fellow
Liske, Jochen (D)	Astronomer
Madrid Pariente, Silvia (E)	Secretary/Assistant
Schuhler, Nicolas (F)	Optical Engineer
Sforna, Diego (I)	Software Engineer
Shen, Zhi-Xia (CN)	Student
Sommariva, Veronica (I)	Student
Stanke, Thomas (D)	Fellow
Vargas, Aitana (E)	Student
Zech, Gabriele (D)	Software Engineer
Zilio, Davide (I)	Student
Zwaan, Martin A. (NL)	Astronomer

Chile

Beletsky, Yuri (BY)	Fellow
Blanchard, Guillaume (F)	Optical Engineer
Carry, Benoît (F)	Student
Cesetti, Mary (I)	Student
Gieles, Mark (NL)	Fellow
Papadaki, Christina (GR)	Student
Pinto Moreira, Olga (P)	Student
Snodgrass, Colin (GB)	Fellow
Valenti, Elena (I)	Fellow

Departures

Europe

Corbett, Ian (GB)	Deputy Director General
Döllinger, Michaela (D)	Student
Gandhi, Poshak (IND)	Fellow
Huelamo, Nuria (E)	Fellow
Kotak, Rubina (EAK)	Fellow
Nilsson, Kim (S)	Student
Péroux, Céline (F)	Fellow
Seifahrt, Andreas (D)	Student
Shaver, Peter (CDN)	Senior Astronomer
Shida, Raquel Yumi (BR)	Student
Strazzullo, Veronica (I)	Student
Treumann, Angelika (D)	Librarian Assistant
Uttenthaler, Stefan (A)	Student
Vandame, Benoît (F)	Software Engineer
Wold, Margrethe (N)	Fellow
Wolf, Nadja (D)	Student

Chile

Hibon, Pascale (F)	Student
Nicoud, Jean-Luc (CH)	Mechanical Engineer

New Editor

Jeremy Walsh will become the new editor of *The Messenger* as of 1 December 2006, following my retirement at that time. I have greatly enjoyed serving as editor over the last several years, and working together with Kurt Kjaer, Henri Boffin and Jutta Boxheimer in this endeavour. I am very pleased that the editorship will pass into Jeremy's capable hands, and wish him well in his new role.

Peter Shaver



Peter Shaver pictured at his farewell party at ESO Headquarters on 24 November with the ESO Director General Dr. Catherine Cesarsky in the foreground. He holds a poster which was presented to him featuring Messenger covers.

ESO is the European Organisation for Astronomical Research in the Southern Hemisphere. Whilst the Headquarters (comprising the scientific, technical and administrative centre of the organisation) are located in Garching near Munich, Germany, ESO operates three observational sites in the Chilean Atacama desert. The Very Large Telescope (VLT), is located on Paranal, a 2 600 m high mountain south of Antofagasta. At La Silla, 600 km north of Santiago de Chile at 2 400 m altitude, ESO operates several medium-sized optical telescopes. The third site is the 5 000 m high Llano de Chajnantor, near San Pedro de Atacama. Here a new submillimetre telescope (APEX) is in operation, and a giant array of 12-m submillimetre antennas (ALMA) is under development. Over 1600 proposals are made each year for the use of the ESO telescopes.

The ESO Messenger is published four times a year: normally in March, June, September and December. ESO also publishes Conference Proceedings and other material connected to its activities. Press Releases inform the media about particular events. For further information, contact the ESO Public Affairs Department at the following address:

ESO Headquarters
Karl-Schwarzschild-Straße 2
85748 Garching bei München
Germany
Phone +49 89 320 06-0
Fax +49 89 320 23 62
information@eso.org
www.eso.org

The ESO Messenger:
Editor: Peter Shaver
Technical editor: Jutta Boxheimer
www.eso.org/messenger/

Printed by
Peschke Druck
Schatzbogen 35
81805 München
Germany

© ESO 2006
ISSN 0722-6691

Contents

Reports from Observers

J. Gerssen et al. – Mapping the Properties of SDSS Galaxies with the VIMOS IFU	2
C. Evans et al. – The ARAUCARIA Project – First Observations of Blue Supergiants in NGC 3109	5
S. Warren et al. – Early Science Results from the UKIDSS ESO Public Survey	7
P. P. van der Werf et al. – Starburst Galaxies Under the Microscope: High-Resolution Observations with VISIR and SINFONI	11
J. Hjorth et al. – The Short Gamma-Ray Burst Revolution	16
M. Hettterscheidt et al. – Probing the Universe Using a Mostly Virtual Survey: The Garching-Bonn Deep Survey	19
A. Richichi et al. – Burst or Bust: ISAAC at Antu Sets New Standards with Lunar Occultations	24
L. Kaper et al. – Measuring the Masses of Neutron Stars	27

Telescopes and Instrumentation

H. U. Käufl et al. – Good Vibrations: Report from the Commissioning of CRIFES	32
H. Bonnet et al. – Enabling Fringe Tracking at the VLTI	37
J. Emerson, A. McPherson, W. Sutherland – Visible and Infrared Survey Telescope for Astronomy: Progress Report	41
P. Andreani, M. Zwaan – The European ALMA Regional Centre: User Support for European Astronomers	43

Other Astronomical News

H. U. Käufl, C. Sterken – Deep Impact as a World Observatory Event	48
J.-P. Swings – Around and about “Europe’s Quest for the Universe”	49
C. Madsen – Open House at the ESO Headquarters	50
M. Dennefeld, H. Kuntschner – Report on the NEON Observing Schools 2006	52
P. Andreani, M. Zwaan, R. Laing – Report on the Meeting on Science with ALMA: a New Era for Astrophysics	53
Prestigious NASA Award for ST-ECF (ESO/ESA) Scientists	54
Fellows at ESO – D. Naef	55

Announcements

G. Monnet – Helping to Build ASTRONET Science Vision	56
ESO Workshop on Observing Planetary Systems	57
Conference on Obscured AGN Across Cosmic Time	57
ESO Workshop on Science with the VLT in the ELT Era	58
Vacancy notice	58
Personnel Movements	59
New Editor	59

Front Cover Picture: Tarantula Nebula

This image of the Tarantula Nebula in the Large Magellanic Cloud was obtained during the commissioning of FORS2 on the VLT Unit Telescope KUEYEN in early 2000. It is a composite of three exposures, using *B*, *V* and *R* filters.